

**FOSSIL FUEL  
RESEARCH**

DOE/BC/13407-1

**GASEOUS DETONATION FRACTION OF POROUS MATERIALS  
FOR ENHANCED FOSSIL FUEL UTILIZATION AND RECOVERY**

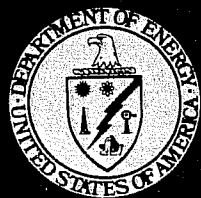
Work Performed for the Department of Energy  
Under Grant No. DE-FG19-80BC13407

Date Published—August 1982

University of Michigan  
Ann Arbor, Michigan

---

**U. S. DEPARTMENT OF ENERGY**



## DISCLAIMER

"This book was prepared as an account of work sponsored by an agency of the United States Government. Neither the United States Government nor any agency thereof, nor any of their employees, makes any warranty, express or implied, or assumes any legal liability or responsibility for the accuracy, completeness, or usefulness of any information, apparatus, product, or process disclosed, or represents that its use would not infringe privately owned rights. Reference herein to any specific commercial product, process, or service by trade name, trademark, manufacturer, or otherwise, does not necessarily constitute or imply its endorsement, recommendation, or favoring by the United States Government or any agency thereof. The views and opinions of authors expressed herein do not necessarily state or reflect those of the United States Government or any agency thereof."

Available from the National Technical Information Service, U.S. Department of Commerce, Springfield, Virginia 22161.

### NTIS price codes

Paper copy: \$12.00

Microfiche copy: \$4.00

**GASEOUS DETONATION FRACTION OF POROUS MATERIALS  
FOR ENHANCED FOSSIL FUEL UTILIZATION AND RECOVERY**

By

C. W. Kauffman  
Chuanjun Yan  
J. A. Nicholls

Gas Dynamics Laboratories  
Department of Aerospace Engineering  
University of Michigan  
Ann Arbor, Michigan 48109

Herbert B. Carroll, Jr., *Technical Project Officer*  
Bartlesville Energy Technology Center  
P.O. Box 1398  
Bartlesville, Oklahoma 74005

Work Performed for the Department of Energy  
Under Grant No. DE-FG19-80BC13407

*Work Sponsored By:*  
University Projects in Fossil Energy Research  
U.S. Department of Energy  
Washington, D.C. 20545

Date Published—August 1982

## FOREWORD

This report represents the final report on DOE Grant DE-FG19-80BC-13407. The research was directed by Dr. C.W. Kauffman, Associate Research Scientist, Department of Aerospace Engineering, The University of Michigan and covered the two-year period September 1, 1978 through August 31, 1980. The Program Officer was Dr. Robert M. Wellek, Office of Fossil Energy, Department of Energy.

## TABLE OF CONTENTS

|   |    |
|---|----|
| Foreword . . . . .  | ii |
| List of Tables . . . . .                                    | iv |
| List of Figures . . . . .                                   | v  |
| Abstract . . . . .  | ix |
| Introduction . . . . .                                      | 1  |
| Experimental Effort. . . . .                                | 3  |
| Test System   |    |
| Detonation Velocities                                       |    |
| Detonation Pressures  |    |
| Dynamic Strain of the Detonation Tube                       |    |
| Discussion  |    |
| Fracture of Coal Pile                                       |    |
| Analytical Model . . . . .                                  | 11 |
| Comparison of Experimental and Analytical Results . . . . . | 20 |
| Conclusions . . . . .                                       | 21 |
| Nomenclature . . . . .                                      | 22 |
| References . . . . .  | 24 |

## LIST OF TABLES

|          |  |     |
|----------|--|-----|
| Table 1. | Minimum Diameter of Spheres in Terms of Friction Losses . . . . .  | .25 |
| Table 2. | Minimum Diameter of Spheres in Terms of Quenching Distance. . . . .  | .25 |
| Table 3. | Comparison of Analytical and Experimental Detonation<br>Velocity Ratios ( $H_2/O_2$ , $\phi = 1$ ) . . . . .   | .26 |
| Table 4. | Comparison of Analytical and Experimental Detonation<br>Velocity Ratios ( $CH_4/O_2$ , $\phi = 1$ ) . . . . .  | .26 |
| Table 5. | Comparison of Analytical and Experimental Detonation<br>Velocity Ratios ( $C_3H_8/O_2$ , $\phi = 1$ ). . . . . | .27 |
| Table 6. | Comparison of Analytical and Experimental Pressure Ratios<br>( $H_2/O_2$ , $\phi = 1$ ). . . . .               | .27 |
| Table 7. | Comparison of Analytical and Experimental Pressure Ratios<br>( $CH_4/O_2$ , $\phi = 1$ ) . . . . .             | .28 |
| Table 8. | Comparison of Analytical and Experimental Pressure Ratios<br>( $C_3H_8/O_2$ , $\phi = 1$ ). . . . .            | .28 |
| Table 9. | Comparison of Analytical and Experimental Maximum Dynamic<br>Stress . . . . .                                  | .29 |

## LIST OF FIGURES

|            |   |    |
|------------|---|----|
| Figure 1.  | Schematic of the test system  | 30 |
| Figure 2.  | Photograph of porous bed  | 31 |
| Figure 3.  | Photograph of spheres   | 32 |
| Figure 4.  | Steady detonation history   | 34 |
| Figure 5.  | Oscilloscope traces of detonation waves   | 35 |
| Figure 6.  | Detonation velocity versus equivalence ratio for various initial pressures: $H_2/O_2$ , 19.05 mm steel spheres.                         | 36 |
| Figure 7.  | Detonation velocity versus equivalence ratio for various initial pressures: $CH_4/O_2$ , 19.05 mm steel spheres.                        | 37 |
| Figure 8.  | Detonation velocity versus equivalence ratio for various initial pressures: $C_3H_8/O_2$ , 19.05 mm steel spheres.                      | 38 |
| Figure 9.  | Detonation velocity versus equivalence ratio for various initial pressures; $H_2/O_2$ , 38.10 mm steel spheres.                         | 39 |
| Figure 10. | Detonation velocity versus equivalence ratio for various initial pressures: $CH_4/O_2$ , 38.10 mm steel spheres.                        | 40 |
| Figure 11. | Detonation velocity versus equivalence ratio for various initial pressures: $C_3H_8/O_2$ , 38.10 mm steel spheres.                      | 41 |
| Figure 12. | Detonation velocity versus equivalence ratio for various initial pressures: $H_2/O_2$ , 38.10 mm ceramic spheres.                       | 42 |
| Figure 13. | Detonation velocity versus equivalence ratio for various initial pressures: $CH_4/O_2$ , 38.10 mm ceramic spheres.                      | 43 |
| Figure 14. | Detonation velocity versus equivalence ratio for various initial pressures: $C_3H_8/O_2$ , 38.10 mm ceramic spheres.                    | 44 |
| Figure 15. | Detonation velocity versus equivalence ratio for different sphere diameters: $H_2/O_2$ , 19.05 mm and 38.10 mm steel spheres, 2 atm.    | 45 |
| Figure 16. | Detonation velocity versus equivalence ratio for different sphere diameters: $C_3H_8/O_2$ , 19.05 mm and 38.10 mm steel spheres, 5 atm. | 46 |
| Figure 17. | Detonation velocity versus sphere diameter: stoichiometric $H_2/O_2$ , 1 atm.   | 47 |
| Figure 18. | Detonation velocity versus equivalence ratio for different material of spheres: $H_2/O_2$ , steel and ceramic spheres, 1 atm.           | 48 |

|            |   |    |
|------------|---|----|
| Figure 19. | Detonation velocity versus equivalence ratio for different material of spheres: $\text{CH}_4/\text{O}_2$ , steel and ceramic spheres, 1 atm.            | 49 |
| Figure 20. | Detonation velocity versus equivalence ratio for different material of spheres: $\text{C}_3\text{H}_8/\text{O}_2$ , steel and ceramic spheres, 2 atm.   | 50 |
| Figure 21. | Oscilloscope traces of detonation pressures.  | 51 |
| Figure 22. | Pressure ratio versus equivalence ratio for various initial pressures: $\text{H}_2/\text{O}_2$ , 19.05 mm steel spheres.                                | 52 |
| Figure 23. | Pressure ratio versus equivalence ratio for various initial pressures: $\text{CH}_4/\text{O}_2$ , 19.05 mm steel spheres.                               | 53 |
| Figure 24. | Pressure ratio versus equivalence ratio for various initial pressures: $\text{C}_3\text{H}_8/\text{O}_2$ , 19.05 mm steel spheres.                      | 54 |
| Figure 25. | Pressure ratio versus equivalence ratio for various initial pressures: $\text{H}_2/\text{O}_2$ , 38.10 mm steel spheres.                                | 55 |
| Figure 26. | Pressure ratio versus equivalence ratio for various initial pressures: $\text{CH}_4/\text{O}_2$ , 38.10 mm steel spheres.                               | 56 |
| Figure 27. | Pressure ratio versus equivalence ratio for various initial pressures: $\text{C}_3\text{H}_8/\text{O}_2$ , 38.10 mm steel spheres.                      | 57 |
| Figure 28. | Pressure ratio versus equivalence ratio for various initial pressures: $\text{H}_2/\text{O}_2$ , 38.10 mm ceramic spheres.                              | 58 |
| Figure 29. | Pressure ratio versus equivalence ratio for various initial pressures: $\text{CH}_4/\text{O}_2$ , 38.10 mm ceramic spheres.                             | 59 |
| Figure 30. | Pressure ratio versus equivalence ratio for various initial pressures: $\text{C}_3\text{H}_8/\text{O}_2$ , 38.10 mm ceramic spheres.                    | 60 |
| Figure 31. | Pressure ratio versus equivalence ratio for different sphere diameters: $\text{H}_2/\text{O}_2$ , 19.05 mm and 38.10 mm steel spheres, 2 atm.           | 61 |
| Figure 32. | Pressure ratio versus equivalence ratio for different sphere diameters: $\text{CH}_4/\text{O}_2$ , 19.05 mm and 38.10 mm steel spheres, 2 atm.          | 62 |
| Figure 33. | Pressure ratio versus equivalence ratio for different sphere diameters: $\text{C}_3\text{H}_8/\text{O}_2$ , 19.05 mm and 38.10 mm steel spheres, 1 atm. | 63 |
| Figure 34. | Pressure ratio versus equivalence ratio for different sphere materials: $\text{H}_2/\text{O}_2$ , steel and ceramic spheres, 1 atm.                     | 64 |
| Figure 35. | Pressure ratio versus equivalence ratio for different sphere materials: $\text{CH}_4/\text{O}_2$ , steel and ceramic spheres, 1 atm.                    | 65 |

|            |  |    |
|------------|--|----|
| Figure 36. | Pressure ratio versus equivalence ratio for different sphere materials: $C_3H_8/O_2$ , steel and ceramic spheres, 1 atm. | 66 |
| Figure 37. | Typical oscilloscope trace of dynamic strain.  | 67 |
| Figure 38. | Dynamic stress versus equivalence ratio for various initial pressures: $H_2/O_2$ , 19.05 mm steel spheres.               | 68 |
| Figure 39. | Dynamic stress versus equivalence ratio for various initial pressures: $CH_4/O_2$ , 19.05 mm, steel spheres.             | 69 |
| Figure 40. | Dynamic stress versus equivalence ratio for various initial pressures: $C_3H_8/O_2$ , 19.05 mm steel spheres.            | 70 |
| Figure 41. | Dynamic stress versus equivalence ratio for various initial pressures: $H_2/O_2$ , 38.10 mm steel spheres.               | 71 |
| Figure 42. | Dynamic stress versus equivalence ratio for various initial pressures: $CH_4/O_2$ , 38.10 mm steel spheres.              | 72 |
| Figure 43. | Dynamic stress versus equivalence ratio for various initial pressures: $C_3H_8/O_2$ , 38.10 mm steel spheres.            | 73 |
| Figure 44. | Normalized velocities versus equivalence ratio for various initial pressures: $H_2/O_2$ , 19.05 mm steel spheres.        | 74 |
| Figure 45. | Normalized velocities versus equivalence ratio for various initial pressures: $CH_4/O_2$ , 19.05 mm steel spheres.       | 75 |
| Figure 46. | Normalized velocities versus equivalence ratio for various initial pressures: $C_3H_8/O_2$ , 19.05 mm steel spheres.     | 76 |
| Figure 47. | Normalized velocities versus equivalence ratio for various initial pressures: $H_2/O_2$ , 38.10 mm steel spheres.        | 77 |
| Figure 48. | Normalized velocities versus equivalence ratio for various initial pressures: $CH_4/O_2$ , 38.10 mm steel spheres.       | 78 |
| Figure 49. | Normalized velocities versus equivalence ratio for various initial pressures: $C_3H_8/O_2$ , 38.10 mm steel spheres.     | 79 |
| Figure 50. | Normalized velocities versus equivalence ratio for various initial pressures: $H_2/O_2$ , 38.10 mm ceramic spheres.      | 80 |
| Figure 51. | Normalized velocities versus equivalence ratio for various initial pressures: $CH_4/O_2$ , 38.10 mm ceramic spheres.     | 81 |
| Figure 52. | Normalized velocities versus equivalence ratio for various initial pressures: $C_3H_8/O_2$ , 38.10 mm ceramic spheres.   | 82 |
| Figure 53. | Normalized pressure ratios versus equivalence ratio for various initial pressures: $H_2/O_2$ , 19.05 mm steel spheres.   | 83 |

|            |  |    |
|------------|--|----|
| Figure 54. | Normalized pressure ratios versus equivalence ratio for various initial pressures: $\text{CH}_4/\text{O}_2$ , 19.05 mm steel spheres.            | 84 |
| Figure 55. | Normalized pressure ratios versus equivalence ratio for various initial pressures: $\text{C}_3\text{H}_8/\text{O}_2$ , 19.05 mm steel spheres.   | 85 |
| Figure 56. | Normalized pressure ratios versus equivalence ratio for various initial pressures: $\text{H}_2/\text{O}_2$ , 38.10 mm steel spheres.             | 86 |
| Figure 57. | Normalized pressure ratios versus equivalence ratio for various initial pressures: $\text{CH}_4/\text{O}_2$ , 38.10 mm steel spheres.            | 87 |
| Figure 58. | Normalized pressure ratios versus equivalence ratio for various initial pressures: $\text{C}_3\text{H}_8/\text{O}_2$ , 38.10 mm steel spheres.   | 88 |
| Figure 59. | Normalized pressure ratios versus equivalence ratio for various initial pressures: $\text{H}_2/\text{O}_2$ , 38.10 mm ceramic spheres.           | 89 |
| Figure 60. | Normalized pressure ratios versus equivalence ratio for various initial pressures: $\text{CH}_4/\text{O}_2$ , 38.10 mm ceramic spheres.          | 90 |
| Figure 61. | Normalized pressure ratios versus equivalence ratio for various initial pressures: $\text{C}_3\text{H}_8/\text{O}_2$ , 38.10 mm ceramic spheres. | 91 |
| Figure 62. | Coal pile  | 92 |
| Figure 63. | Fractured coal pile  | 94 |
| Figure 64. | Control volume and coordinate system for the one-dimensional model.  | 95 |
| Figure 65. | Theoretical curve of normalized velocity versus sphere diameter for different initial pressures of the mixture.                                  | 96 |
| Figure 66. | Theoretical curve of normalized pressure ratio versus sphere diameter for different initial pressures of the mixture.                            | 97 |

## ABSTRACT

There are many applications with pronounced energy implications where it is desirable to increase the permeability of a porous bed. Such applications include "in situ" coal gasification and shale oil retorting and enhanced oil and gas recovery. A closely related problem is that of the breakup of a frozen mass of coal while being transported in open railroad hopper cars. This study was directed to the feasibility of using gaseous detonation to effect the increase in porosity. Towards that end, a heavy walled pipe (1.829 m long, 0.124 m I.D., and 0.168 m O.D.) was filled with solid spheres. In separate experiments, steel spheres of 19.05 mm and 38.1 mm and ceramic spheres of 38.1 mm were used. The gaseous combustible mixtures tested included hydrogen, methane, and propane, all with oxygen as the oxidizer. A range of elevated initial pressures and mixture equivalence ratios were tested. In each case, the variation of wave velocity and pressure along the tube, as well as the strain (stress) on the outside of the tube, were determined. The spheres caused the detonation velocity to be lower than the theoretical Chapman-Jouguet (CJ) velocity, which would be expected in an open tube of that size. Increase of the initial pressure, diameter of the spheres, and equivalence ratio from lean towards stoichiometric resulted in an increase in detonation velocity (and hence pressure and stress). The material of the sphere had a slight effect; the steel spheres resulted in the higher velocities. The measured velocities and pressures were compared with the calculated CJ values. An approximate one-dimensional steady analytical model, which included energy losses in the reaction zone, was developed. This expression was used to calculate the critical condition wherein the detonation

would no longer propagate through the packed bed, thus predicting the minimum sphere diameter required for quenching. Finally, some experiments were conducted wherein a large container was filled with coal, sprayed with water, and allowed to freeze outside. Propane-oxygen was blown through the pile and then detonated. Considerable fracturing was experienced.

## INTRODUCTION

It is well known that a gaseous detonation wave is capable of generating a large pressure increase; its magnitude is determined by the gaseous mixture composition and initial pressure. Some previous investigations<sup>1,2</sup> have shown that gaseous detonations are able to propagate, with only slight modification, through a porous medium with as little as a 25% void fraction. Some even more recent work<sup>3,4</sup> has shown that detonations can propagate through crushed stone and, for energetic reactants, even through sand. Considerable mechanical forces are exerted on the solid matrix because of intense local overpressures produced by the detonation waves. If these pressures are large enough to fracture the bonds between the larger particles, the overall structural rigidity of the material will be destroyed and the material may collapse, or become less resistant to deforming forces. If the overpressures are not sufficient to fracture the major structural bonds, they may rupture secondary diaphragms and thereby increase the porosity. Since the gaseous combustibles may be initially dispersed homogeneously through the entire matrix, a uniform treatment at each location is assured, thus causing a uniform modification of structural and fluid mechanical properties. Condensed (liquid or solid) explosives are not attractive from this standpoint in that the extreme pressures create a void at the location of the explosion but highly compress the material away from that point.

This phenomenon of detonative fracturing could have several applications in enhanced fossil fuel utilization and recovery efforts. In underground gasification or enhanced petroleum recovery, it may be necessary to increase the porosity of the strata to assist the passage of various gases and fluids. When pulverized solid fuels freeze together in the process of being shipped or stored, the ice bonds between particles and their containers must be broken. In addition to these applications, the propagation characteristics of detonation waves through porous beds is also of interest for hazard suppression in the chemical and petroleum industries.

This investigation was initiated in order to determine the effect of variations of some important factors upon the characteristics of detonation waves in a porous bed. These factors were initial pressure, different gaseous fuels, equivalence ratio, and the material and diameter of spheres which comprised the porous bed. The measured parameters were detonation velocities, pressures behind the detonation waves, and the dynamic strain of the detonation tube.

These parameters were also calculated for Chapman Jouguet detonation so that velocity and pressure deficits in the porous bed could be ascertained and a mechanism for propagation developed.

Further, it was desired to vividly demonstrate the concept by conducting tests wherein a container of coal was frozen and then fractured by a gaseous detonation.

## EXPERIMENTAL EFFORT

### Test System

Figure 1 is a schematic of the test system, which consists of a detonation tube, combustible gaseous mixture supply, detonation initiation tube, evacuation system, and instrumentation system. The detonation tube was a cylindrical steel chamber with an inside diameter of 0.124 m, an outer diameter of 0.168 m, and overall length of 1.829 m. The detonation tube was completely filled with solid spheres, and the ends of the tube were closed. Figure 2a shows an end view of the tube partially filled with large diameter spheres. A closer view is given in Fig. 2b and shows large ceramic spheres after the passage of numerous detonations. The white unused sphere is shown for comparison. Detailed views of the spheres constituting the porous bed are in Fig. 3. In Fig. 3a, new spheres consisting of 19.05 mm steel, 38.1 mm steel, and 38.1 mm ceramic are shown. After the passage of numerous detonations, these spheres are as shown in Fig. 3b. It is possible to see regions on the spheres where they were in contact with each other. Figure 3c shows the surface detail for all spheres, both new and used.

The detonating gas, a mixture of the gaseous fuel and oxygen, was fed into the detonation tube through stainless steel pressure tubing and solenoid valves. The mixture ratio of the two gases was measured by two flow meters. Before each run, high-pressure air heated by an electrical heater was bled into the chamber to evaporate the combustion products remaining from the preceding run. After removing the residual

gases from the chamber and recharging it with a combustible gaseous mixture to a given pressure (measured by a mercury manometer at low initial pressure or a pressure gauge at high initial pressure) the detonation was initiated at one end of the chamber by using a glow plug in a small initiator tube.

The parameters to be measured were the detonation velocity, the pressure trace of the detonation, and the dynamic strain trace for the test chamber, caused by the detonation wave.

Ionization gauges were used to measure the detonation velocities. Five ionization gauges were positioned along the tube at intervals of 0.4 m. The output from the first ionization gauge was used only to trigger the oscilloscope sweep. The output from each subsequent ionization gauge was connected via an amplifier circuit to a raster display oscilloscope with a camera.

Two pressure transducers were installed in the test chamber wall, 0.8 m apart and 0.112 m from the initiating end. The output from each of the two transducers was connected via an amplifier to one of the beams of a dual-beam oscilloscope with a camera.

The strain gauges were attached on the outer surface of the detonation tube, as shown in Fig. 1. An oscilloscope with a camera was used to record the dynamic strain trace.

The first tests were made using ceramic spheres with a diameter of 38.1 mm. Next, steel spheres with a diameter of 38.1 mm and 19.05 mm were used. The initial pressures of the detonatable mixtures were 1 atm, 2 atm, 5 atm, and 9 atm. The gaseous fuels were hydrogen, methane, and propane. The equivalence ratios were 0.5, 0.6, 0.7, 0.8, 0.9, 1.0, 1.1, 1.2, 1.3, 1.4, and 1.5.

## Detonation Velocities

The detonation velocities were computed using time-versus-distance plots, as shown in Fig. 4. Here,  $d = A_0 + A_1 t$  and DEV is the sum of the squares of the deviations. The time versus distance plots were obtained from the raster oscilloscope traces of detonation waves, as shown in Fig. 5. A straight line on the distance-time plot indicates a constant wave velocity, while concave downward and concave upward lines indicate decaying and accelerating waves, respectively. The local slope gives the local detonation velocity. A close examination of all time-versus-distance plots obtained shows that most of the plots are straight lines, although a few showed decaying behavior. The velocity reported herein is the rate at which the overall detonation front moves along the axis of the test chamber, and not to the velocity of propagation through any given void. Presumably, this latter velocity is greater.

Representative curves of detonation velocities versus equivalence ratio for different initial pressures are shown for a given fuel, material, and diameter of spheres in Figs. 6 through 14. As can be seen, there is appreciable scatter and the resultant shape of the curve is questionable, in some cases. It is believed that this scatter is attributable to uncertainties in the mixture composition and in the response of the ion gauges. Even so, certain trends can be recognized. Higher initial pressures result in higher detonation velocities if all other conditions are held constant. It has been found that the detonation velocity is very close to the calculated Chapman Jouguet value of the detonation through unpacked beds when the initial pressure reaches 5 atm or more.

The effect of the diameter of the spheres upon detonation velocities is shown in Figs. 15 through 17, where Fig. 17 incorporates some data

from Ref. 2. The following trend is found: an increase in the diameter of the spheres results in a higher detonation velocity.

The results as shown in Figs. 18 through 20 are somewhat surprising in that the detonation velocity is slightly higher for 38.10 mm steel spheres than it is for 38.10 mm ceramic spheres. A similar phenomenon was found by Giere<sup>2</sup>, where the propagation velocity was higher for the copper-coated 8 mm sphere than for the same size sphere with no coating.

### Detonation Pressures

Typical oscilloscope traces showing detonation pressure time history are given in Fig. 21 for the two differently located transducers; they are the bottom two traces in each photograph. These photographs indicate that the pressure rapidly rises to its peak value which, however, is not nearly as fast as in a typical detonation. It then falls within a few microseconds to a lower value. Thereafter, the pressure decays in an exponential manner from the Chapman Jouguet value, leveling off at a pressure of about one-third of the Chapman Jouguet value. The Von Neumann pressures, i.e., those immediately behind the shock, are commonly about twice the CJ pressure. However, they are not usually resolved in gaseous detonation. Because of the location of the transducer at the wall with its finite size sensing element behind or under a sphere, it is not clear what pressure the transducer would see. This made it difficult to accurately determine overpressures.

Representative curves of the detonation pressure ratio versus equivalence ratio were obtained at the three or four different initial pressures for a fixed fuel and oxidizer combination, material, and diameter of spheres, as shown in Figs. 22 through 30. It can be seen that the pressure ratios increase with initial pressure and equivalence ratio (at least on the lean side as the mixture is enriched).

Figures 31 through 33 show the effect of the diameter of the sphere on the pressure ratio. The following trend can be recognized: larger diameter spheres will result in higher pressure ratios. Figures 34 through 36 show the effect of the material of the spheres upon the pressure ratio. It is found that the pressure ratios are slightly higher for the steel spheres than for the ceramic spheres of the same size.

### Dynamic Strain of the Detonation Tube

Oscilloscope traces showing the strain gauge output as a function of the time were employed to determine the dynamic strain when the test chamber was subjected to dynamic loading by the detonation wave passing through the porous bed. Some typical data is shown by the upper trace in Fig. 37. The signal oscillation forms an envelope and appears to vibrate about a mean that is above the datum line. These large oscillatory vibrations were considered to be the result of the "overshoot" created by the detonation force. Using the microstrain read from the oscilloscope, the dynamic stress was calculated by means of using the ratio of Young's modulus of elasticity for dynamic loading to that for static loading as being 1.22 (Ref. 5).

Representative curves of dynamic stress versus equivalence ratio at the different initial pressures are given in Figs. 38 through 43 for a given fuel and oxidizer combination, material, and diameter of spheres. The trend is recognized, not surprisingly, that the stress increases with initial pressure, equivalence ratio, and diameter of the spheres.

### Discussion

For convenience in analytical work, both the detonation velocities and pressure ratios in a porous bed have been non-dimensionalized using the Chapman Jouquet values (denoted by the subscript "0"). These were calculated by means of the computational program developed by Gordon and McBride.<sup>6</sup>

Figures 44 through 52 present the effect of variations in the initial pressure, equivalence ratio, and diameter and type of spheres on the velocity ratio,  $u_s/u_{s0}$ . It is seen that  $u_s/u_{s0}$  varies from about 0.65 to 0.85 at the initial pressure of 1 atm. The velocity ratio,  $u_s/u_{s0}$ , increases with increasing initial pressure, equivalence ratio, and diameter of the spheres. When the initial pressure reaches 5 atm or more,  $u_s/u_{s0}$  is near unity. These results indicate that a porous bed decreases detonation velocities, especially at low initial pressure. As shown later, this is because of the drag forces between the hot gas and the surface of spheres and the wall of the tube. However, when the initial pressure increases, these losses will decrease.

Figures 53 through 61 present the effect of variations in the initial pressure, equivalence ratio, and diameter of the spheres on the normalized pressure ratios,  $p/p_i/(p/p_i)_0$ , for a fixed fuel and oxidizer combination and material of the spheres. It can be recognized that the overpressures in porous beds at an initial pressure of 1 atm are about 27% to 35% less

than Chapman Jouguet. The pressure ratio,  $p/p_i/(p/p_i)_0$ , increases slightly with the initial pressure. When the initial pressure reaches 5 atm or more, the overpressure in porous beds is about 15% to 20% less than Chapman Jouguet, even though  $u_s/u_{s0}$  is near unity.

### Fracture of Coal Pile

At the initiation of the program, it was thought to be desirable to measure the shear and tension forces between adjacent spheres in the porous bed. This would have provided information regarding the fracturing potential of detonation waves in porous media. It was found, however, that an appropriate strain gauge system could not be sufficiently miniaturized. Analytically, at least in concept, similar data could be obtained by integrating the pressure field as it passed through such a matrix.

However, in lieu of such data, a small experiment was performed. A quantity of bituminous coal, consisting on the average of irregular 40 mm cubes, was placed in a heavy (5 mm thick) cylindrical container having a diameter of 750 mm and height of 450 mm. The container and coal are shown in Fig. 62, a and b. During the process of filling the container, snow and cracked dry ice were mixed with the coal. The container was insulated and allowed to stand outside overnight in below freezing weather. Subsequently, the entire mass froze solid into one large mass. The container is shown outside in Fig. 62c.

The center of the container bottom had an opening through which metered combustible gases could be fed. A glow plug was located in the fuel system near the container. A stoichiometric mixture of propane and oxygen was allowed to flow into the vessel for a period of time, during which it was judged that the air in the voids of the frozen coal mass

would be replaced. The top of the container was covered with a rope mat, and the combustible gases were ignited. A dull thud was heard, and the rope mat lifted slightly. The previously frozen coal mass was inspected, and it was found that fracturing indeed had occurred. The entire coal container is shown in Fig. 63 a. The coal was easily dumped from the container, and the resulting individual pieces of coal and ice and coal only are shown in Fig. 63 b. These pieces are of such a size that they could be handled easily.

Apparently, a propane oxygen detonation generates sufficient inter-particle forces to rupture the ice bonds between frozen coal particles.

## ANALYTICAL MODEL

The propagation of a gaseous detonation wave through a porous bed is a three-dimensional process involving friction and heat transfer between the hot gas and the surface of solid spheres and the wall of the tube. Both mechanical and thermal losses would result in a decrease in the effective heat of a reaction and would consequently decrease the detonation velocity and overpressure. From the experimental results with two different sphere materials, it is clear that thermal losses, in comparison with the friction losses, do not play a significant role. In fact, the results are the inverse of what would be expected. The intense turbulence caused by the spheres can strengthen the burning velocity and decrease the non-uniform distribution of some important quantities with respect to cross section. The experimental results obtained are comparable, to some extent, with the calculated Chapman Jouguet values of one-dimensional detonation.

With the aid of the experimental data, it seems reasonable to make the following simplifying, but physically admissible, assumptions according to the analysis of Ragland.<sup>7</sup>

The detonation front is planar and steady. The flow in the region where the chemical reaction takes place is assumed to be one-dimensional. The drag and heat transfer which actually occur at the boundaries surrounding the spheres are distributed uniformly across the cross section. The distribution of the spheres in the tube is uniform. The spheres fill the tube in a hexagonal closely packed arrangement. Each void is the same.

For the control volume and the coordinate system shown in Fig. 64, the equations of conservation of mass, momentum, and energy have the form:

$$\rho_3 \bar{u}_3 - \rho_1 \bar{u}_1 = 0, \quad (1)$$

$$\rho_3 \bar{u}_3^2 - \rho_1 \bar{u}_1^2 = p_1 - p_3 + \frac{1}{A_c} \int_2^3 \tau b_w d\bar{x}, \quad (2)$$

and

$$\begin{aligned} \rho_3 \left( e_3 + \frac{\bar{u}_3^2}{2} \right) \bar{u}_3 - \rho_1 \left( e_1 + \frac{\bar{u}_1^2}{2} \right) \bar{u}_1 \\ = p_1 \bar{u}_1 - p_3 \bar{u}_3 + \frac{1}{A_c} \int_2^3 (Q - q + \tau u_s) b_w d\bar{x}. \end{aligned} \quad (3)$$

Now assume:

1.  $u_1 = 0$ , i.e. the gas is initially at rest.
2. The Chapman Jouguet condition holds at position  $\bar{x}_3$ , i.e.  $\bar{u}_3 = a_3$ .
3. The gases are calorically and thermally perfect, i.e.,

$$h = c_p T = \frac{a^2}{\gamma - 1}$$

$$a^2 = \gamma \frac{p}{\rho} = \gamma RT.$$

Also, define non-dimensional drag and heat transfer coefficients:

$$C_d = \int_2^3 \tau b_w d\bar{x} / \frac{1}{2} A_s \rho_2 u_2^2 \quad (4)$$

$$C_h = \int_2^3 q b_w d\bar{x} / A_s \rho_2 u_s \left( h_2 + \frac{u_2^2}{2} - h_w \right). \quad (5)$$

And, for convenience, replace the integrals in the momentum and energy equations by:

$$B = \frac{1}{A_c} \int_2^3 \tau b_w d\bar{x} = \frac{A_s}{A_c} \frac{u_2^2}{u_s \bar{u}_2} \frac{C_d}{2} \rho_1 u_s^2 \quad (6)$$

$$C = \frac{1}{A_c} \int_2^3 (Q - q) b_w d\bar{x} = \Delta H - C_h (h_i + u_s u_2 - h_w) \\ \times \frac{A_s}{A_c} \frac{u_2}{\bar{u}_2} \rho_1 u_s \quad (7)$$

Using these relations (4) to (7), the conservation equations become

$$\rho_3 a_3 - \rho_1 u_s = 0 \quad (8)$$

$$\rho_3 a_3^2 \left( \frac{\gamma_3 + 1}{\gamma_3} \right) - \rho_1 \left( u_s^2 + \frac{a_1^2}{\gamma_1} \right) = B \quad (9)$$

and

$$\rho_3 a_3^2 \left( \frac{\gamma_3 + 1}{\gamma_3 - 1} \right) - \rho_1 u_s \left( \frac{2a_1^2}{\gamma_1 - 1} + u_s^2 \right) = 2u_s B + 2C \quad (10)$$

Using Eqs. (6) through (9) and the relation  $p = (\rho a^2) / \gamma$ , the expressions for the ratios of several flow properties across the detonations can be derived:

$$\frac{p_3}{p_1} = \frac{1 + \gamma_1 M_s^2 \left( 1 + \frac{C_d A_s u_2^2}{2A_c u_s \bar{u}_2} \right)}{1 + \gamma_3} \quad (11)$$

$$\frac{a_3}{a_1} = \frac{\gamma_3 M_s^2}{1 + \gamma_3} \left( 1 + \frac{1}{\gamma_1 M_s^2} + \frac{C_d A_s u_2^2}{2A_c u_s \bar{u}_2} \right) \quad (12)$$

$$\frac{\rho_3}{\rho_1} = \frac{1 + \gamma_3}{\gamma_3 \left( 1 + \frac{1}{\gamma_1 M_s^2} + \frac{C_d^A u_2^2}{2A_c u_s \bar{u}_2} \right)} \quad (13)$$

$$\frac{T_3}{T_1} = \frac{m_3}{m_1} \frac{\left\{ 1 + \gamma_1 M_s^2 \left( 1 + \frac{C_d^A u_2^2}{2A_c u_s \bar{u}_2} \right) \right\} \gamma_3 \left( 1 + \frac{1}{\gamma_1 M_s^2} + \frac{C_d^A u_2^2}{2A_c u_s \bar{u}_2} \right)}{(1 - \gamma_3)^2} \quad (14)$$

$$M_s^2 = \frac{2(\gamma_3^2 - 1) \phi \Delta H / a_1^2}{1 + \frac{C_d^A u_2^2}{A_c u_s \bar{u}_2} + \frac{2(\gamma_3^2 - 1) C_h^A u_2^2}{A_c u_s \bar{u}_2}} \quad (15)$$

$$\frac{u_s}{(u_s)_0} = \left\{ 1 + \left[ C_d + 2(\gamma_3^2 - 1) C_h \right] \frac{A_s}{A_c} \frac{u_2^2}{u_s \bar{u}_2} \right\}^{-\frac{1}{2}} \quad (16)$$

For a face-centered cubic unit cell:

$$\frac{A_s}{A_c} = \frac{\frac{\sqrt{2}}{d} \pi X_3}{1 - \frac{\sqrt{2}}{6} \pi} = 17.15 \frac{X_3}{d} \quad (17)$$

Substituting Eq. (17) into (16), the following expression can be obtained:

$$\frac{u_s}{(u_s)_0} = \left\{ 1 + [C_d + 2(\gamma_3^2 - 1) C_h] 17.15 \frac{X_3}{d} \frac{u_2^2}{u_s \bar{u}_2} \right\}^{-1/2} \quad (18)$$

The value for  $(u_s)_0$  and for  $\gamma_3$  and  $M_s$  are available as functions of equivalence ratio and initial pressure from the computer program developed by Gordon and McBride<sup>6</sup>. Knowing  $C_d$ ,  $C_h$ , and the reaction zone length,  $u_s/(u_s)_0$  can be calculated after several iterations. Initially, Chapman Jouguet values are used for the required parameters on the right hand side of the equation.

The total drag coefficient is the sum of the shear drag coefficient and the form drag coefficient, as given by

$$C_d = C_{ds} + C_{df} \quad (19)$$

However, the shear drag is only about 1% of the total drag, so the shear drag can be neglected. Tallmadge<sup>8</sup> suggests that a useful analogy can be drawn between the form drag and the Reynolds number in a porous bed, i.e.,

$$C_{df} = \frac{0.98}{\eta} Re_d^{-0.14} \quad (20)$$

where  $\eta$  is the bed porosity (the fraction of volume not occupied by spheres) and  $Re_d$  is the Reynolds number based on the sphere diameter, i.e.,

$$Re_d = \frac{\rho_2 u_2 d}{\mu_2} \quad (21)$$

For the face-centered cubic packing, the porosity has a value of 0.259.

In the case being studied, when the Prandtl number is unity, the Reynolds analogy may be used to relate the shear drag and heat transfer, i.e.,

$$C_{ds} = 2C_h \quad (22)$$

Since  $C_{ds}$  is ignored,  $C_h$  is also neglected.

Additionally, the characteristic time for heat transfer to the spheres can be approximately calculated. Consider the spheres to be represented by a cylinder of radius  $d$  and length  $d$ , which is conducting heat along its length. The thermal energy of this volume of hot gas is:

$$Q_1 = \rho C_p (T_g - T_o) \frac{\pi}{4} d^2 d \quad (23)$$

The heat conducted to the cylinder is:

$$Q_2 = \frac{\lambda}{d} (T_g - T_w) \pi d^2 \quad (24)$$

The characteristic time for heat loss is defined as:

$$\tau = \frac{Q_1}{Q_2} = \frac{\rho C_p d^2}{4\lambda} \quad (25)$$

For the 38.1-mm spheres and a stoichiometric hydrogen-oxygen detonation, the characteristic times calculated for ceramic and steel spheres are  $10^{-2}$  and  $10^{-3}$  sec, respectively. The calculated characteristic times for

the spheres seem to be much too long, compared to the characteristic time for the reaction zone,  $10^{-6}$  sec, again justifying the neglect of heat transfer. Indeed, one would expect that on the basis of heat transfer alone that the detonation would show a greater velocity deficit while propagating through steel spheres. However, the inverse was found experimentally.

For detonations, it is known that increasing the initial pressure will result in a decrease of the reaction-zone length. From Eqs. (18), (20), and (21), it is clear that increasing initial pressure and diameter of the spheres will result in a decrease of the form drag coefficient  $C_{df}$ . Therefore, the  $u_s/(u_s)_0$  will increase with initial pressure. The theoretical curves of  $u_s/(u_s)_0$  versus sphere diameter and initial pressure are given for a stoichiometric mixture of hydrogen and oxygen in Fig. 65.

The pressure ratios can also be calculated, and theoretical curves of  $[p/p_i]/[(p/p_i)_0]$  versus the initial pressure and the diameter of spheres are given for a stoichiometric mixture of hydrogen and oxygen in Fig. 66.

These values, however, reflect a modification of Chapman Jouquet values. In much of the detonation data collected to date<sup>9</sup>, while the velocities are frequently found close to Chapman Jouquet values, the pressures seem consistently low. This may be explained by considering that, for unsupported detonations, the state point at the end of the reaction zone is on the weak branch of the detonation Hugoniot curve. Most measurements of detonation velocity, pressure, density, and final Mach number are consistent with the hypothesis. In White's work<sup>10</sup>, the measured pressure and density are 10% to 15% below the calculated Chapman

Jouguet value. The detonation velocities are 0.5% to 1.0% above the Chapman-Jouguet value. Therefore, the calculated Chapman-Jouguet values for pressure were decreased by 15%.

This pressure may also be used to calculate the dynamic strain in the confining tube. For a thick-wall tube having an inner diameter of  $r_1$  and an outer diameter of  $r_2$ , the tangential stress is given by

$$\sigma = \frac{r_2^2 + r_1^2}{r_2^2 - r_1^2} p \quad (26)$$

with the strain, of course, being obtained through

$$\epsilon = \sigma/E \quad (27)$$

with the previously mentioned appropriate correction being made to relate dynamic and static quantities.

One effect which was not included in the analysis was catalytic wall reactions. This would effectively appear as modification in the heat of reaction. In a porous-bed arrangement, there is certainly a large surface area. The experimental data consistently indicated that, especially for hydrogen and oxygen at lower pressures, the detonation waves propagating through the ceramic spheres showed larger deficits than those propagating through steel spheres. The ceramic spheres were alumina grinding balls furnished by Coors Porcelain Company.

In work reported by Fujiwara<sup>11</sup>, oxygen/hydrogen detonations were allowed to propagate through small-diameter tubing of different material—steel, glass, alumina—with different roughness. Lower velocities, 4 to 6%, were consistently measured for alumina walls. Analytically, this could be predicted by considering the reaction,  $H + OH \rightarrow H_2O$ , occurring at the wall with 100% efficiency. This would appear to offer a

satisfactory explanation for the velocity differences observed for the two different materials used in the porous bed.

From Fig. 65, it is clear that  $u_s/(u_s)_0$  decreases with decreasing diameter of the spheres. Obviously, there should exist a minimum diameter of a sphere below which the detonation wave could not travel through the porous bed. Assuming the minimum detonation velocity through a packed bed is equal to the speed of sound (probably too conservative), the following expression for the minimum diameter of the spheres may be derived:

$$d_{\min} = \left[ \frac{0.98}{\eta_1 \left( \frac{\rho_2 u_2}{\mu_2} \right)^{0.14} \frac{(M_{so}^2 - 1)}}{\left( \frac{17.15 \chi_3 u_2^2}{u_s \bar{u}_2} \right)} \right]^{1/1.14} \quad (28)$$

where

$$\frac{u_2^2}{u_s \bar{u}_2} = \frac{4 (M_{so}^2 - 1)^2}{(\gamma_1 + 1) (\gamma_1 M_{so}^2 - M_{so}^2 + 2) M_{so}^2} \quad (29)$$

The theoretical minimum diameter of spheres for successful detonation propagation at the initial pressures of 1, 2, 5, and 10 atm are given for stoichiometric mixtures of  $H_2/O_2$ ,  $CH_4/O_2$ , and  $C_3H_8/O_2$  in Table 1. This is, of course, based solely on drag losses. The failure of the detonation to propagate through the porous bed may also be based on interstitial quenching. The critical diameters of spheres, calculated on the basis of a minimum quenching distance corresponding to the different fuels, are given in Table 2. The quenching criterion requires a much smaller sphere in order to prevent the propagation of a detonation.

## COMPARISON OF EXPERIMENTAL AND ANALYTICAL RESULTS

A comparison of analytical and experimental detonation velocity ratios for the four different initial pressures, the three kinds of fuel, the two different materials of spheres, and the two different diameters of the spheres is given in Tables 3 through 5. The results show that the average accuracy of prediction is within 6%.

A comparison of analytical and experimental detonation pressure ratios is given in Tables 6 through 8. The predicted results follow the trend of experimental results. They are, on the average, accurate to 5%.

A comparison of the analytical and experimental maximum stress of the test chamber is given in Table 9. It can be found that the experimental results, on the average, agree with those predicted by the analytical model, with an error of 8%.

The departure from experimental values becomes less puzzling, considering that there are several effects which make the comparisons only approximate. First, the observed flow is neither exactly steady nor exactly one-dimensional. The one-dimensional, steady model can apply at best, only in an average sense. Second, the measurements are not made at the center of the tube. The pressure and detonation velocity are measured at the wall of the tube and are thus affected by the boundary layer flow. Third, the measurements have a certain scatter caused by the instrumentation system and the operator. While there is some disagreement between the experiments and the predictions, the results are encouraging.

## CONCLUSIONS

Experiments have shown that under certain conditions gaseous detonation waves are able to propagate through porous beds. The detonation velocities, overpressures, and dynamic stress of the detonation tube depend mainly on the fuel and oxidizer, initial pressure, equivalence ratio, and diameter of the spheres. They are, of course, reduced from their Chapman Jouguet values. Increasing the initial pressure and diameter of the spheres will cause an increase in the detonation velocity, pressure ratio, and dynamic stress of the detonation tube. Changing the material of the spheres will cause some change in the detonation velocity, overpressure, and dynamic stress, with the velocity and overpressure slightly higher for 38.1-mm steel spheres than for the ceramic spheres of the same size. The propagation of the detonation is most affected by low initial pressure and by small spheres. Experimental results indicate that the forces exerted on the bed by the detonation are sufficient to rupture the cohesive forces in frozen coal.

## NOMENCLATURE

|          |   |
|----------|---|
| $a_1$    | sound speed of the combustible mixture                              |
| $a_3$    | sound speed of the combustion products at the Chapman-Jouguet plane |
| $A_c$    | average unoccupied cross-sectional area                             |
| $A_s$    | surface area of the spheres in reaction zone                        |
| $b_w$    | perimeter   |
| $C_d$    | drag coefficient of the spheres                                     |
| $C_{df}$ | form drag coefficient of the spheres                                |
| $C_{ds}$ | shear drag coefficient of the spheres                               |
| $C_h$    | heat transfer coefficient   |
| CJ       | Chapman-Jouguet point   |
| $C_p$    | constant pressure specific heat of mixture                          |
| $d$      | diameter of the spheres   |
| $e_1$    | internal energy of the combustible mixture                          |
| $e_3$    | internal energy of the combustion products                          |
| $h$      | specific enthalpy   |
| $m_1$    | molecular weight of the mixture                                     |
| $m_3$    | molecular weight of the products                                    |
| $M_s$    | Mach number of the detonation wave                                  |
| $p_1$    | pressure of the mixture   |
| $p_3$    | pressure of the products at the Chapman-Jouguet plane               |
| $q$      | heat dissipation  |
| $Q$      | heat liberated due to chemical reaction                             |
| $r_1$    | inside radius   |
| $r_2$    | outside radius  |
| $T_1$    | temperature of the mixture  |
| $T_3$    | temperature of products at the Chapman-Jouguet plane                |
| $u_1$    | velocity of the combustible mixture                                 |
| $u_2$    | velocity of the mixture behind the shock wave                       |
| $u_3$    | velocity of the combustion products at Chapman-Jouguet plane        |
| $u_s$    | detonation velocity   |
| $X_3$    | reaction zone length  |

|            |  |
|------------|--|
| $\gamma_1$ | specific heat ratio of the mixture                               |
| $\gamma_3$ | specific heat ratio of the products at the Chapman-Jouguet plane |
| $\Delta H$ | heat of combustion   |
| $\epsilon$ | strain   |
| $\eta$     | bed porosity   |
| $\mu$      | viscosity coefficient  |
| $\rho_1$   | density of the mixture   |
| $\rho_3$   | density of the products at the Chapman-Jouguet plane             |
| $\sigma$   | stress   |
| $\tau$     | shear stress of the spheres                                      |
| $\phi$     | equivalence ratio  |

## REFERENCES

1. Glass, D.R., Hays, P.O., and Nicholls, J.A., "Reaction Velocity and Pressures Related to the Chemotronics Reticulation Process for Polyurethane Foam," Report 08223-1-T, Dept. of Aerospace Engineering, The University of Michigan, December 1966.
2. Giere, D.F., "A Study of High Speed Flow Through Close Packed Beds," Unpublished report, Department of Aerospace Engineering, The University of Michigan, January 1968.
3. Almstrom, H. and Berglund, S., "Hydrogen Behavior in the Filtra Filtered-Vertical Containment System," National Defense Research Institute, Stockholm, Sweden, January 1981.
4. Lee, J.H., "Propagation of Detonations in Packed Beds and Capillary Tubes," Department of Mechanical Engineering, McGill University, Montreal, Canada, January 1981.
5. Lucker, J.A. and Mosier, S.A., "Dynamic Loading of Thin-Walled Cylinders with Detonation Waves," Ind. & Eng. Chem 51, 1959.
6. Gordon, S. and McBride, B.J., "Computer Program for Calculation of Complex Chemical Equilibrium Compositions, Rocket Performance, Incident and Reflected Shocks, and Chapman-Jouguet Detonations," NASA SP-273, 1971.
7. Ragland, K.W., "The Propagation and Structure of Two-Phase Detonations," Ph.D. Thesis, The University of Michigan, 1967.
8. Tallmadge, "Three Turbulent Drag Coefficients for Closely Packed Spheres," AICHE 13, May 1967.
9. Fickett, W. and Davis, W.D., Detonation, University of California Press, 1979.
10. White, D.R., "Turbulent Structure Gaseous Detonation," Phys. Fluids 4, 1961.
11. Fujiwara, T., "Slowdown of Oxyhydrogen Detonation by Surface Catalysis," 16th International Symposium on Combustion, The Combustion Institute, 1977.

TABLE 1. MINIMUM DIAMETER OF SPHERES IN TERMS OF FRICTION LOSSES

| $\phi = 1$<br>Mixtures                        | $d_{min}$ (mm) |      |       |       |
|---|----------------|------|-------|-------|
|   | $P_1$ (atm)    |      |       |       |
|   | 1              | 2    | 5     | 10    |
| H <sub>2</sub> /O <sub>2</sub>                | 1.04           | 0.52 | 0.20  | 0.09  |
| CH <sub>4</sub> /O <sub>2</sub>               | 0.69           | 0.34 | 0.13  | 0.06  |
| C <sub>3</sub> H <sub>8</sub> /O <sub>2</sub> | 0.35           | 0.17 | 0.066 | 0.033 |

TABLE 2. MINIMUM DIAMETER OF SPHERES IN TERMS OF QUENCHING DISTANCE

| $\phi = 1$<br>Mixtures                        | $d_{min}$ (mm) |      |       |       |
|---|----------------|------|-------|-------|
|   | $P_1$ (atm)    |      |       |       |
|   | 1              | 2    | 5     | 10    |
| H <sub>2</sub> /O <sub>2</sub>                | 0.22           | 0.11 | 0.043 | 0.022 |
| CH <sub>4</sub> /O <sub>2</sub>               | 0.26           | 0.13 | 0.052 | 0.026 |
| C <sub>3</sub> H <sub>8</sub> /O <sub>2</sub> | 0.21           | 0.10 | 0.050 | 0.021 |

TABLE 3. COMPARISON OF ANALYTICAL AND EXPERIMENTAL  
 DETONATION VELOCITY RATIOS  
 ( $H_2/O_2$ ,  $\phi = 1$ )

| Sphere<br>mm       | $P_1$<br>(atm) | $u_s/u_{so}$<br>Analytical | $u_s/u_{so}$<br>Experi-<br>mental | Relative<br>Error<br>% |
|--------------------|----------------|----------------------------|-----------------------------------|------------------------|
| 19.05 <sup>1</sup> | 1              | 0.71                       | 0.78                              | - 9.9                  |
| 19.05 <sup>1</sup> | 2              | 0.85                       | 0.90                              | - 5.9                  |
| 19.05 <sup>1</sup> | 5              | 0.93                       | 0.97                              | 4.3                    |
| 19.05 <sup>1</sup> | 9              | 0.97                       | 0.98                              | - 1.0                  |
| 38.10 <sup>1</sup> | 1              | 0.84                       | 0.87                              | - 3.6                  |
| 38.10 <sup>1</sup> | 2              | 0.91                       | 1.00                              | - 9.9                  |
| 38.10 <sup>1</sup> | 5              | 0.97                       | 1.00                              | - 3.1                  |
| 38.10 <sup>2</sup> | 1              | 0.84                       | 0.81                              | 3.6                    |
| 38.10 <sup>2</sup> | 2              | 0.91                       | 0.89                              | 2.2                    |
| 38.10 <sup>2</sup> | 5              | 0.97                       | 0.98                              | - 1.0                  |

<sup>1</sup>Steel

<sup>2</sup>Ceramic

TABLE 4.

COMPARISON OF ANALYTICAL AND EXPERIMENTAL  
 DETONATION VELOCITY RATIOS  
 ( $CH_4/O_2$ ,  $\phi = 1$ )

| Sphere<br>mm       | $P_1$<br>(atm) | $u_s/u_{so}$<br>Analytical | $u_s/u_{so}$<br>Experi-<br>mental | Relative<br>Error<br>% |
|--------------------|----------------|----------------------------|-----------------------------------|------------------------|
| 19.05 <sup>1</sup> | 1              | 0.69                       | 0.75                              | - 8.4                  |
| 19.05 <sup>1</sup> | 2              | 0.83                       | 0.88                              | - 6.0                  |
| 19.05 <sup>1</sup> | 5              | 0.91                       | 0.97                              | - 3.0                  |
| 19.05 <sup>1</sup> | 9              | 0.96                       | 0.01                              | - 5.2                  |
| 38.10 <sup>1</sup> | 1              | 0.82                       | 0.82                              | 0.0                    |
| 38.10 <sup>1</sup> | 2              | 0.91                       | 0.92                              | - 1.0                  |
| 38.10 <sup>1</sup> | 5              | 0.96                       | 0.99                              | - 3.1                  |
| 38.10 <sup>2</sup> | 1              | 0.82                       | 0.75                              | 8.5                    |
| 38.10 <sup>2</sup> | 2              | 0.91                       | 0.86                              | 5.5                    |
| 38.10 <sup>2</sup> | 5              | 0.96                       | 0.97                              | - 1.0                  |

<sup>1</sup>Steel

<sup>2</sup>Ceramic

TABLE 5. COMPARISON OF ANALYTICAL AND EXPERIMENTAL  
 DETONATION VELOCITY RATIOS

$$(C_3H_8/O_2, \phi = 1)$$

| Sphere<br>mm       | $P_1$<br>(atm) | $u_s/u_{so}$<br>Analytical | $u_s/u_{so}$<br>Experi-<br>mental | Relative<br>Error<br>% |
|--------------------|----------------|----------------------------|-----------------------------------|------------------------|
| 19.05 <sup>1</sup> | 1              | 0.79                       | 0.95                              | - 20.0                 |
| 19.05 <sup>1</sup> | 2              | 0.89                       | 0.98                              | - 10.0                 |
| 19.05 <sup>1</sup> | 5              | 0.96                       | 1.02                              | - 6.0                  |
| 19.05 <sup>1</sup> | 9              | 0.98                       | 1.00                              | - 2.0                  |
| 38.10 <sup>1</sup> | 1              | 0.89                       | 1.00                              | - 12.0                 |
| 38.10 <sup>1</sup> | 2              | 0.95                       | 1.04                              | - 9.5                  |
| 38.10 <sup>1</sup> | 5              | 0.98                       | 1.03                              | - 5.1                  |
| 38.10 <sup>2</sup> | 1              | 0.89                       | 0.99                              | - 11.0                 |
| 38.10 <sup>2</sup> | 2              | 0.95                       | 1.03                              | - 8.4                  |
| 38.10 <sup>2</sup> | 5              | 0.98                       | 1.08                              | - 10.2                 |

<sup>1</sup>Steel

<sup>2</sup>Ceramic

TABLE 6. COMPARISON OF ANALYTICAL AND EXPERIMENTAL  
 PRESSURE RATIO

$$(H_2/O_2, \phi = 1)$$

| Sphere<br>mm       | $P_1$<br>(atm) | $p/p_1$<br>$\frac{p/p_1}{(p/p_1)_0}$<br>Analytical | $p/p_1$<br>$\frac{p/p_1}{(p/p_1)_0}$<br>Experi-<br>mental | Relative<br>Error<br>% |
|--------------------|----------------|--|---|------------------------|
| 19.05 <sup>1</sup> | 1              | 0.65   | 0.62  | 4.6                    |
| 19.05 <sup>1</sup> | 2              | 0.73   | 0.70  | 4.1                    |
| 19.05 <sup>1</sup> | 5              | 0.79   | 0.73  | 7.6                    |
| 19.05 <sup>1</sup> | 9              | 0.82   | 0.77  | 5.0                    |
| 38.10 <sup>1</sup> | 1              | 0.73   | 0.68  | 6.8                    |
| 38.10 <sup>1</sup> | 2              | 0.78   | 0.74  | 5.1                    |
| 38.10 <sup>1</sup> | 5              | 0.82   | 0.79  | 3.6                    |
| 38.10 <sup>2</sup> | 1              | 0.73   | 0.65  | 10.9                   |
| 38.10 <sup>2</sup> | 2              | 0.78   | 0.73  | 6.4                    |
| 38.10 <sup>2</sup> | 5              | 0.82   | 0.78  | 4.9                    |

<sup>1</sup>Steel

<sup>2</sup>Ceramic

TABLE 7. COMPARISON OF ANALYTICAL AND EXPERIMENTAL PRESSURE RATIOS  
(CH<sub>4</sub>/O<sub>2</sub>, φ = 1)

| Sphere<br>mm       | P <sub>1</sub><br>(atm) | $\frac{p/p_1}{(p/p_1)_0}$<br>Analytical | $\frac{p/p_1}{(p/p_1)_0}$<br>Experimental | Relative<br>Error<br>% |
|--------------------|-------------------------|---|---|------------------------|
| 19.05 <sup>1</sup> | 1                       | 0.63                                    | 0.65                                      | - 3.2                  |
| 19.05 <sup>1</sup> | 2                       | 0.71                                    | 0.72                                      | - 1.4                  |
| 19.05 <sup>1</sup> | 5                       | 0.77                                    | 0.76                                      | 1.3                    |
| 19.05 <sup>1</sup> | 9                       | 0.82                                    | 0.89                                      | - 8.5                  |
| 38.10 <sup>1</sup> | 1                       | 0.71                                    | 0.75                                      | - 5.6                  |
| 38.10 <sup>1</sup> | 2                       | 0.78                                    | 0.76                                      | 2.6                    |
| 38.10 <sup>1</sup> | 5                       | 0.82                                    | 0.85                                      | - 3.7                  |
| 38.10 <sup>2</sup> | 1                       | 0.71                                    | 0.69                                      | 8.5                    |
| 38.10 <sup>2</sup> | 2                       | 0.78                                    | 0.74                                      | 5.1                    |
| 38.10 <sup>2</sup> | 5                       | 0.82                                    | 0.73                                      | 10.9                   |

<sup>1</sup>Steel

<sup>2</sup>Ceramic

TABLE 8. COMPARISON OF ANALYTICAL AND EXPERIMENTAL PRESSURE RATIOS  
(C<sub>3</sub>H<sub>8</sub>/O<sub>2</sub>, φ = 1)

| Sphere<br>mm       | P <sub>1</sub><br>(atm) | $\frac{p/p_1}{(p/p_1)_0}$<br>Analytical | $\frac{p/p_1}{(p/p_1)_0}$<br>Experimental | Relative<br>Error<br>% |
|--------------------|-------------------------|---|---|------------------------|
| 19.05 <sup>1</sup> | 1                       | 0.69                                    | 0.71                                      | 2.9                    |
| 19.05 <sup>1</sup> | 2                       | 0.77                                    | 0.73                                      | 5.2                    |
| 19.05 <sup>1</sup> | 5                       | 0.82                                    | 0.79                                      | 3.7                    |
| 19.05 <sup>1</sup> | 9                       | 0.82                                    | 0.80                                      | 2.4                    |
| 38.10 <sup>1</sup> | 1                       | 0.77                                    | 0.77                                      | 0.0                    |
| 38.10 <sup>1</sup> | 2                       | 0.81                                    | 0.76                                      | 6.1                    |
| 38.10 <sup>1</sup> | 5                       | 0.84                                    | 0.79                                      | 5.9                    |
| 38.10 <sup>2</sup> | 1                       | 0.77                                    | 0.72                                      | 6.5                    |
| 38.10 <sup>2</sup> | 2                       | 0.81                                    | 0.78                                      | 3.7                    |
| 38.10 <sup>2</sup> | 5                       | 0.84                                    | 0.78                                      | 6.0                    |

<sup>1</sup>Steel

<sup>2</sup>Ceramic

TABLE 9. COMPARISON OF ANALYTICAL AND EXPERIMENTAL  
MAXIMUM DYNAMIC STRESS

| Mixture<br>$\phi = 1$ | Sphere<br>mm   | $P_1$<br>(atm) | $\sigma$<br>(kg/cm <sup>2</sup> )<br>Analytical | $\sigma$<br>(kg/cm <sup>2</sup> )<br>Experi-<br>mental | Relative<br>Error<br>% |
|-----------------------|----------------|----------------|---|--|------------------------|
| $H_2/O_2$             | 19.05<br>Steel | 1              | 41.5  | 37.6   | 9.4                    |
|                       |                | 2              | 94.6  | 87.9   | 8.8                    |
|                       |                | 5              | 269.8   | 251.0  | 6.9                    |
|                       | 38.10<br>Steel | 1              | 47.0  | 50.2   | - 6.8                  |
|                       |                | 2              | 102.8   | 100.4  | 2.3                    |
|                       |                | 5              | 279.1   | 301.2  | - 7.9                  |
| $CH_4/O_2$            | 19.05<br>Steel | 1              | 63.2  | 62.8   | 0.7                    |
|                       |                | 2              | 145.9   | 150.6  | - 3.2                  |
|                       |                | 5              | 407.7   | 351.4  | 13.8                   |
|                       | 38.10<br>Steel | 1              | 71.2  | 75.3   | - 5.6                  |
|                       |                | 2              | 160.3   | 163.1  | - 4.5                  |
|                       |                | 5              | 434.2   | 376.9  | 13.3                   |
| $C_3H_8/O_2$          | 19.05<br>Steel | 1              | 84.2  | 87.9   | - 4.4                  |
|                       |                | 2              | 195.4   | 163.1  | 16.5                   |
|                       |                | 5              | 536.6   | 401.6  | 25.1                   |
|                       | 38.10<br>Steel | 1              | 95.3  | 100.4  | - 5.3                  |
|                       |                | 2              | 205.5   | 201.1  | 2.2                    |
|                       |                | 5              | 549.7   | 502.0  | 8.7                    |

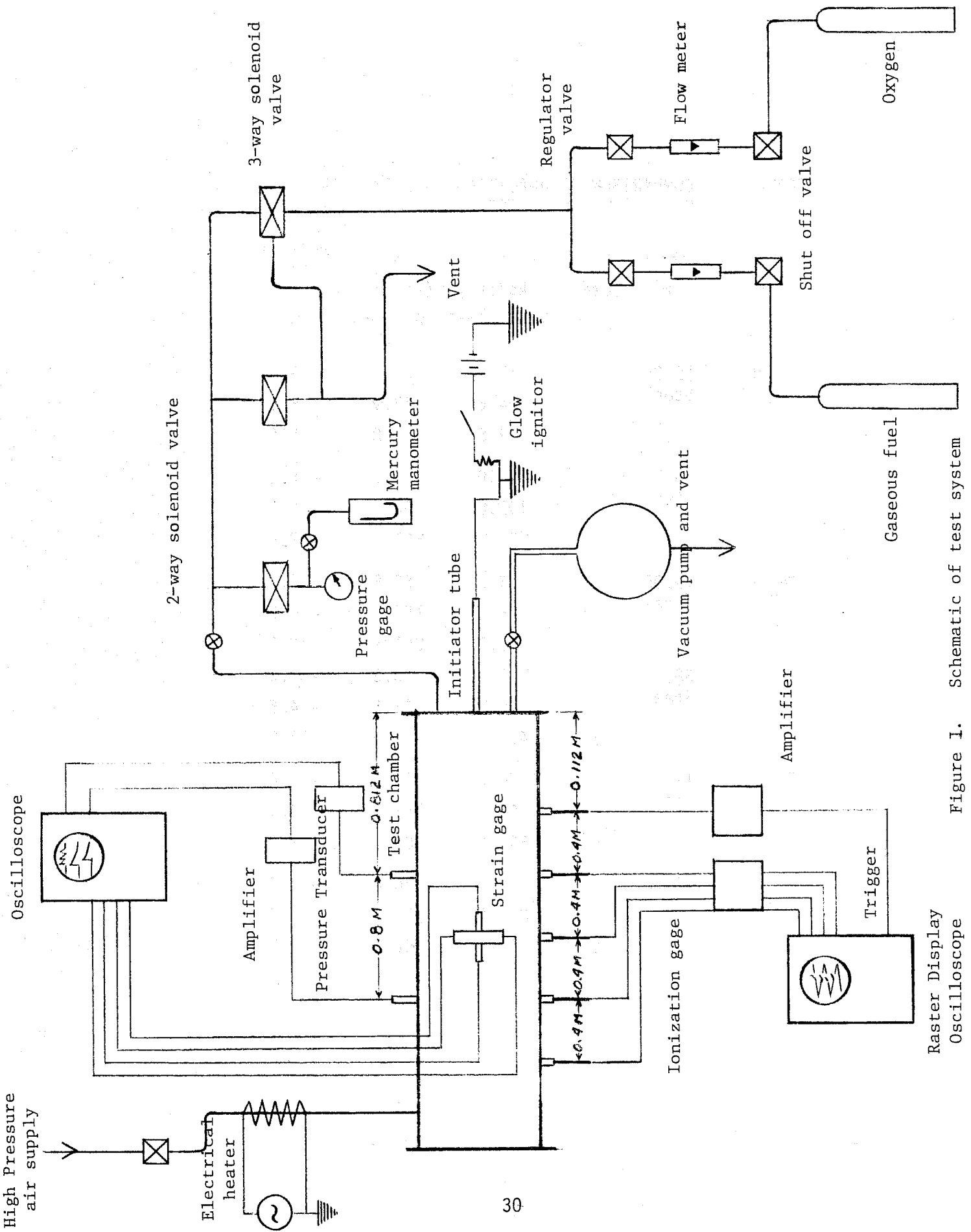
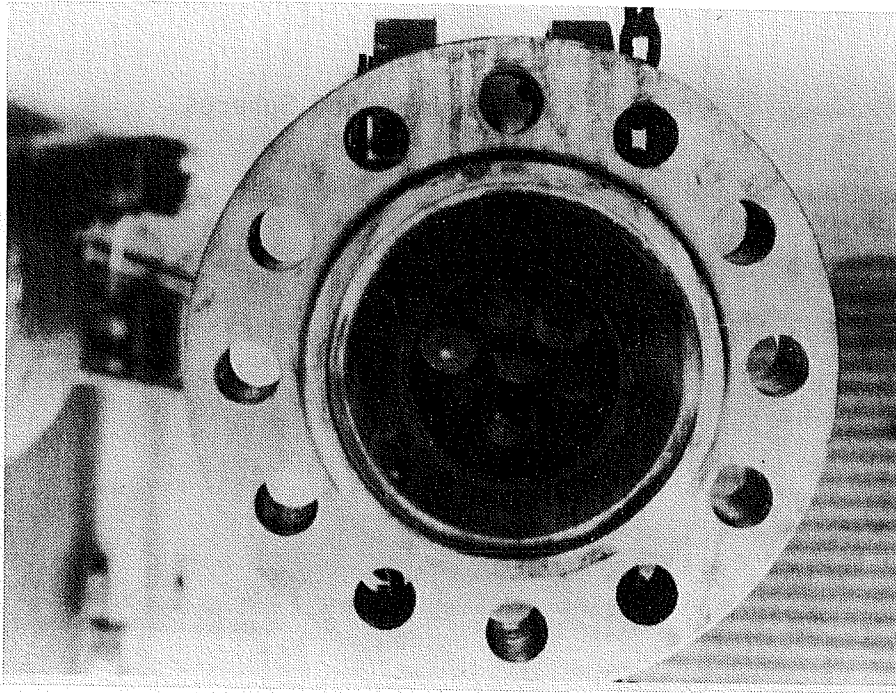
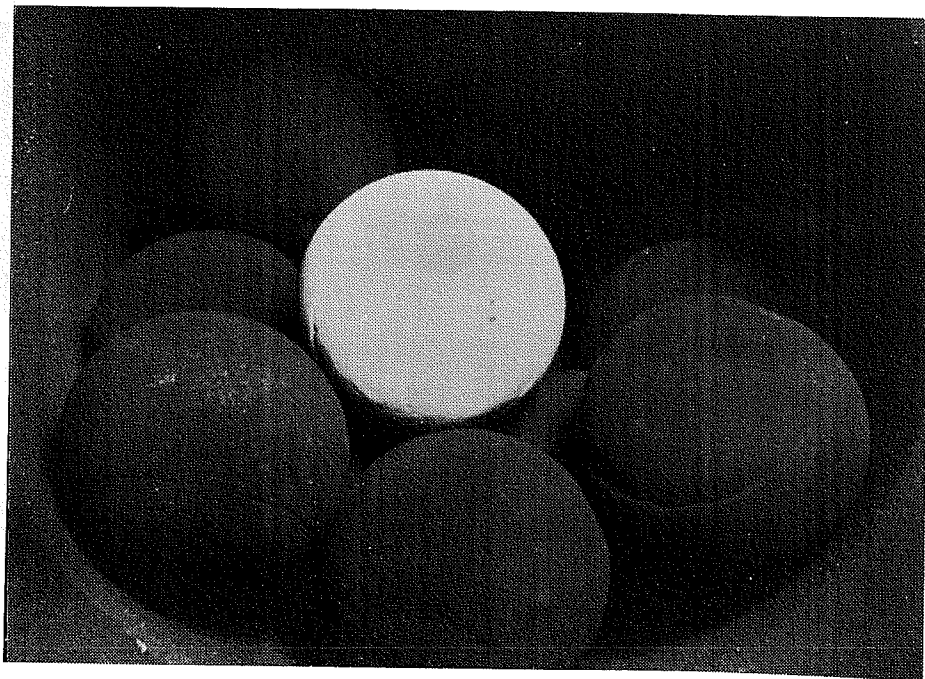


Figure 1. Schematic of test system



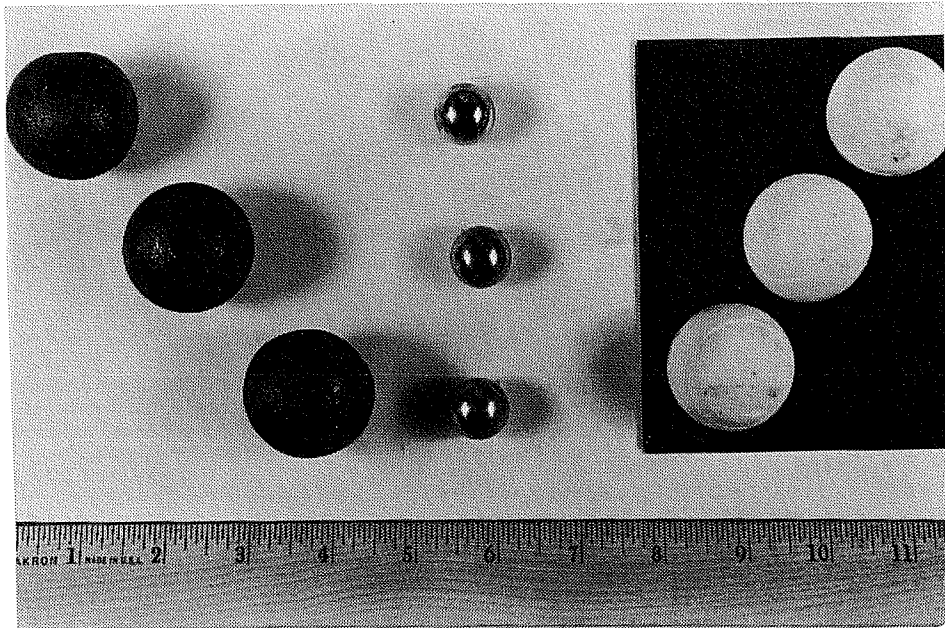
a. End of Detonation Tube



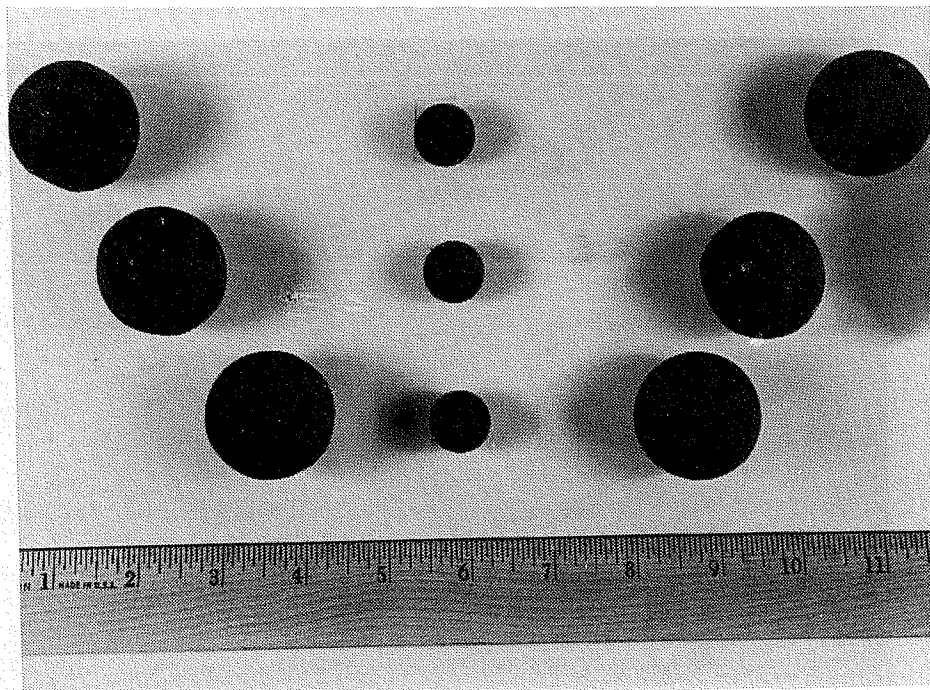
b. Ceramic Spheres in Detonation Tube

Figure 2. Photograph of Porous Bed

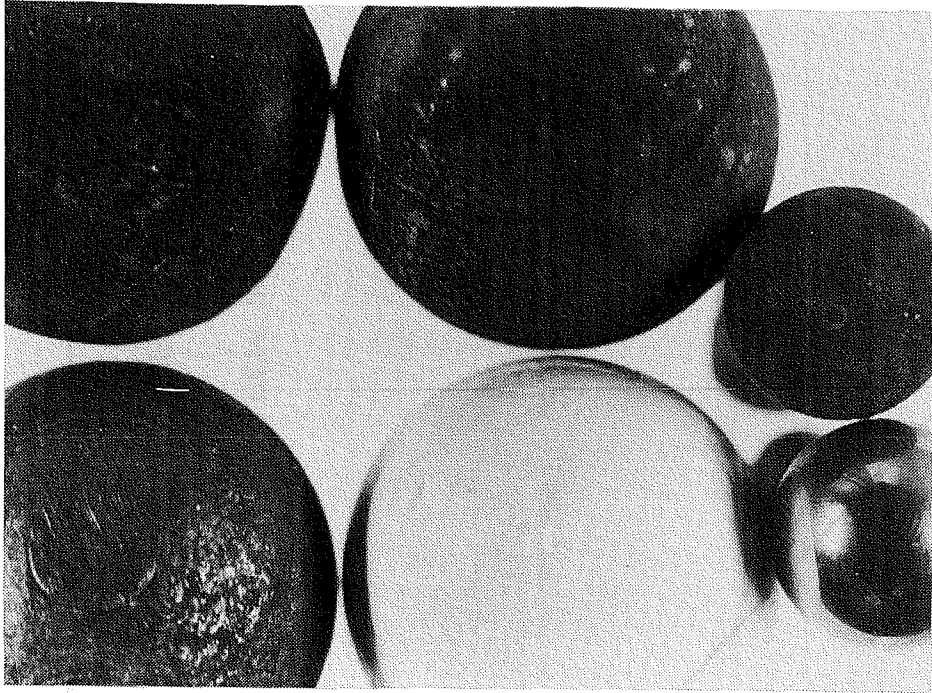
Figure 3. Photograph of Spheres



a. New Spheres



b. Used Spheres



c. Surface of Spheres

H2/O2

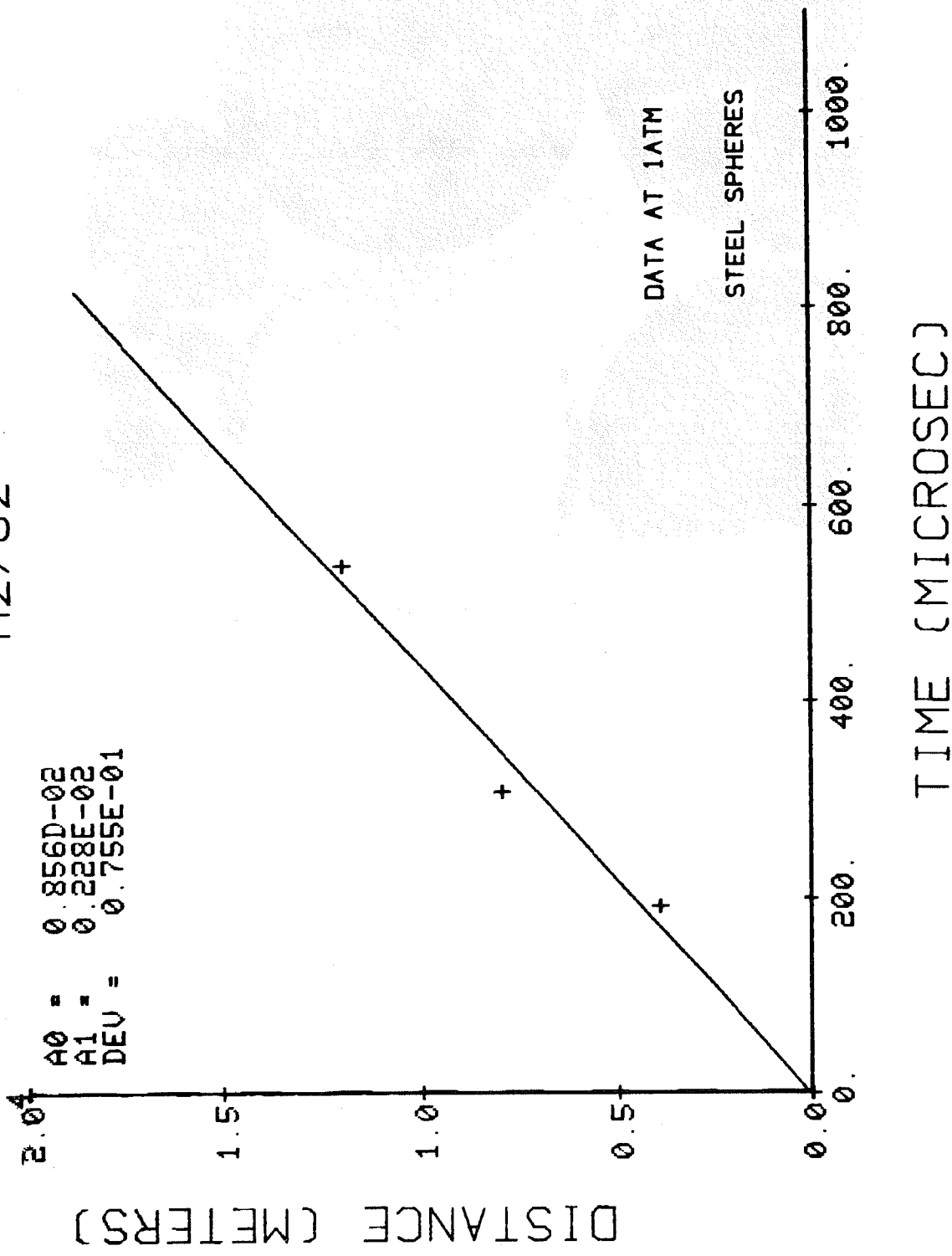
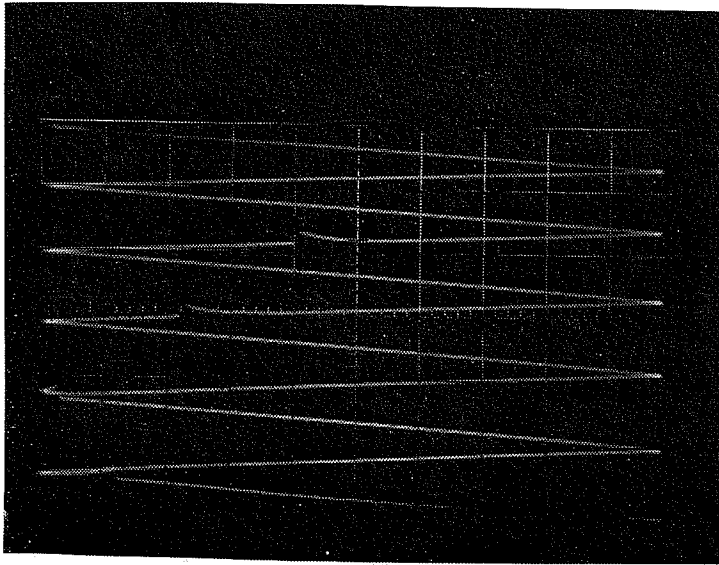


Figure 4. Steady detonation history.

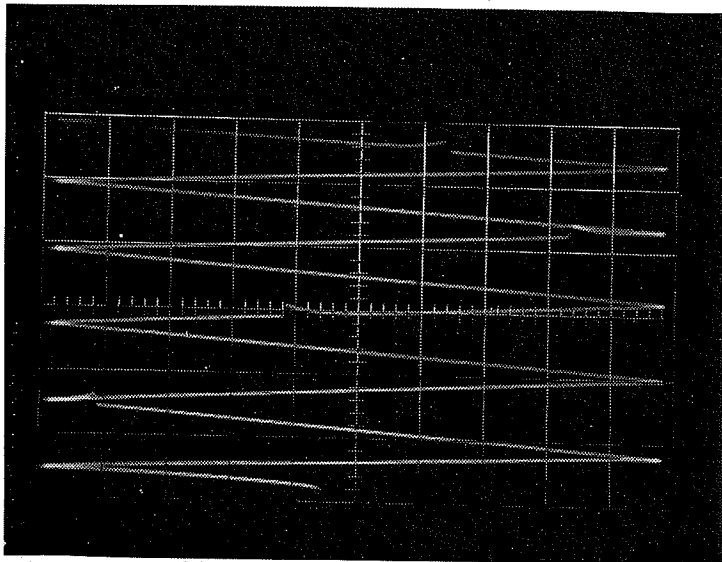


$H_2/O_2, \phi = 0.7$

$p_1 = 1 \text{ atm}$

19.05 mm steel sphere

sweep  $10^{-5} \text{ sec/div.}$

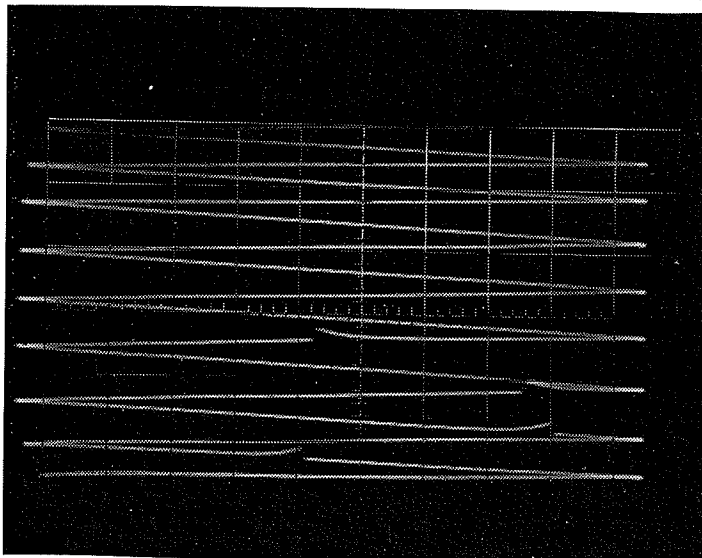


$CH_4/O_2, \phi = 0.6$

$p_1 = 1 \text{ atm}$

19.05 mm steel sphere

sweep  $10^{-5} \text{ sec/div.}$



$C_3H_8/O_2, \phi = 0.9$

$p_1 = 5 \text{ atm}$

19.05 mm steel sphere

sweep  $10^{-5} \text{ sec/div.}$

Figure 5. Oscilloscope traces of detonation waves.

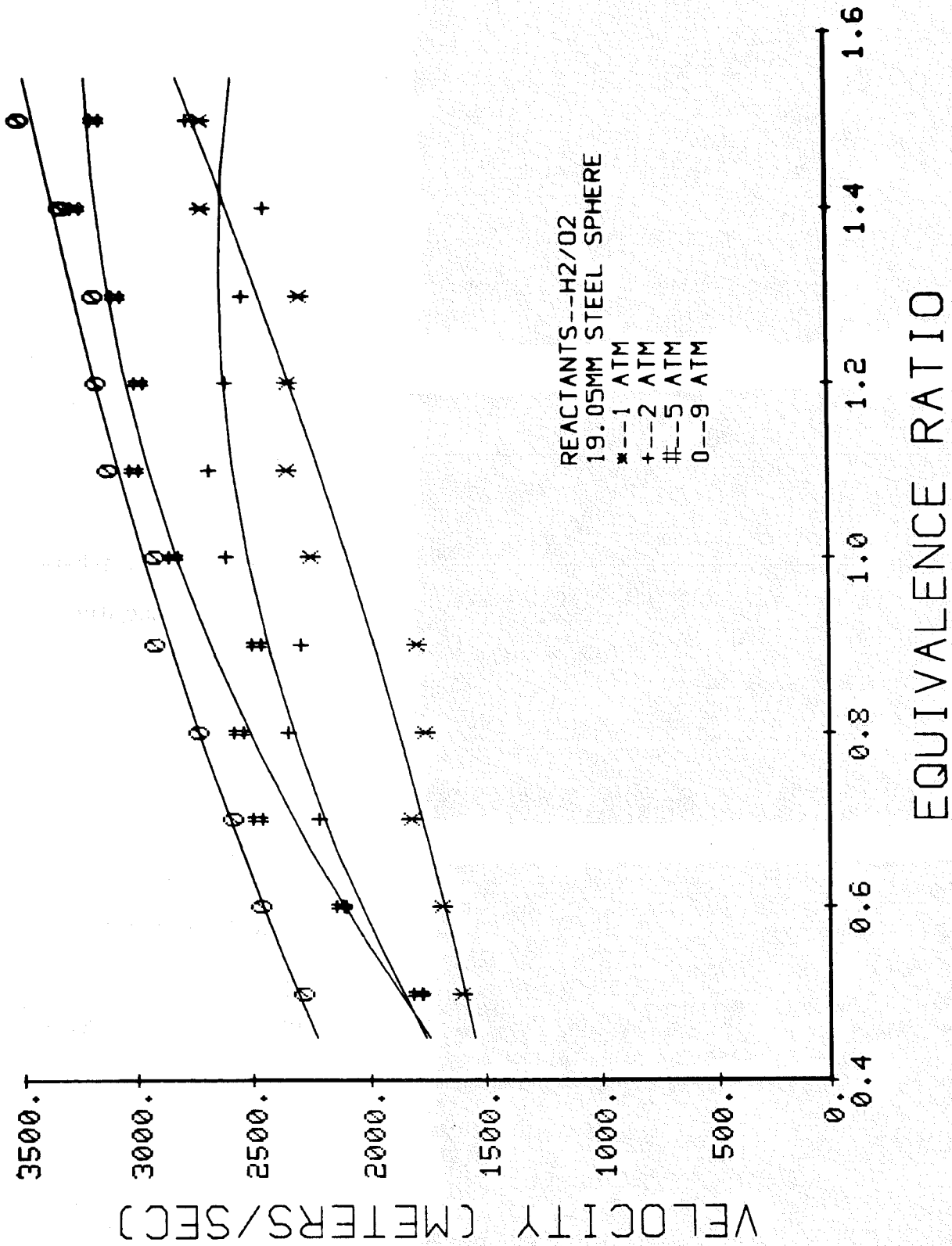


Figure 6. Detonation velocity versus equivalence ratio for various initial pressures.

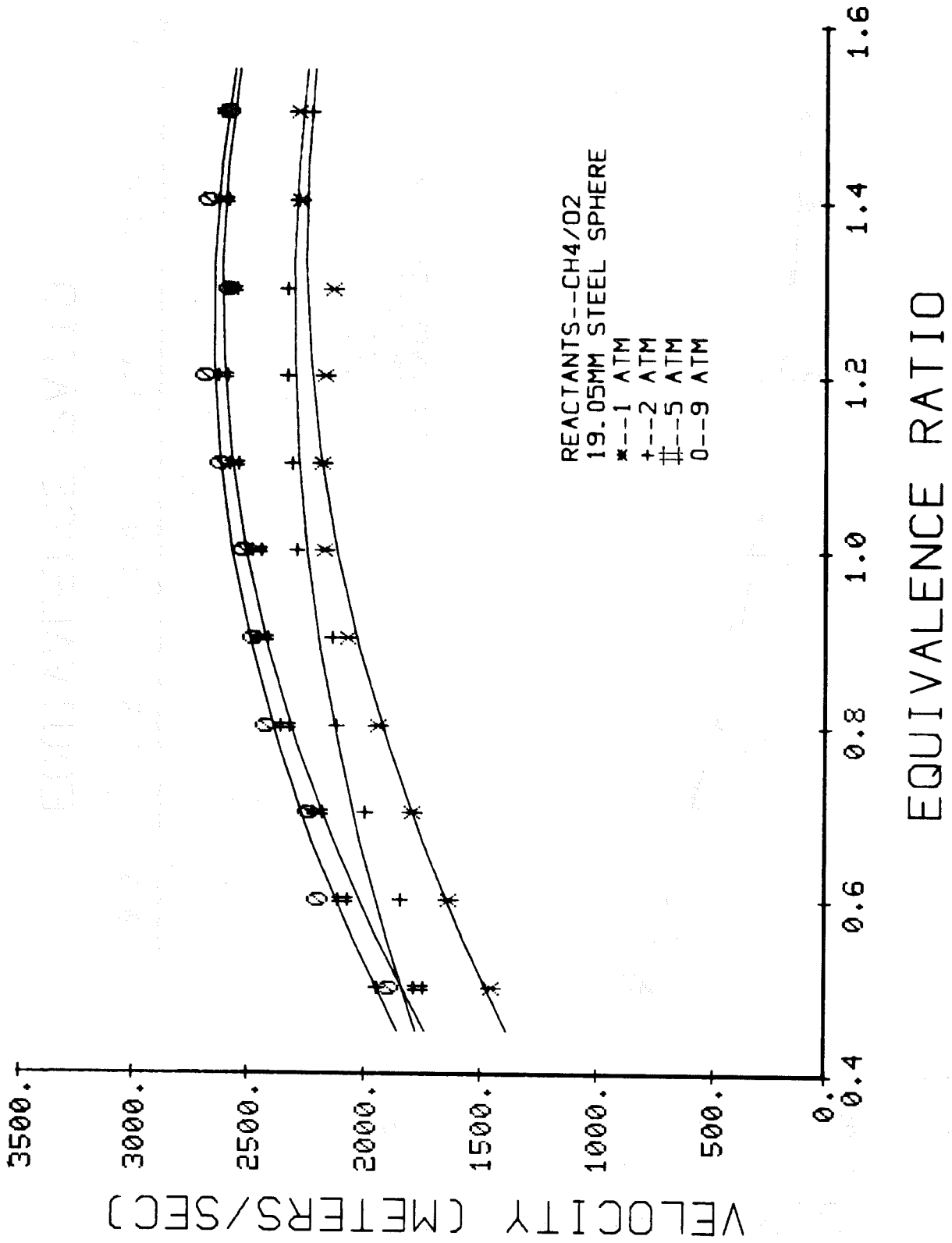


Figure 7. Detonation velocity versus equivalence ratio for various initial pressures.

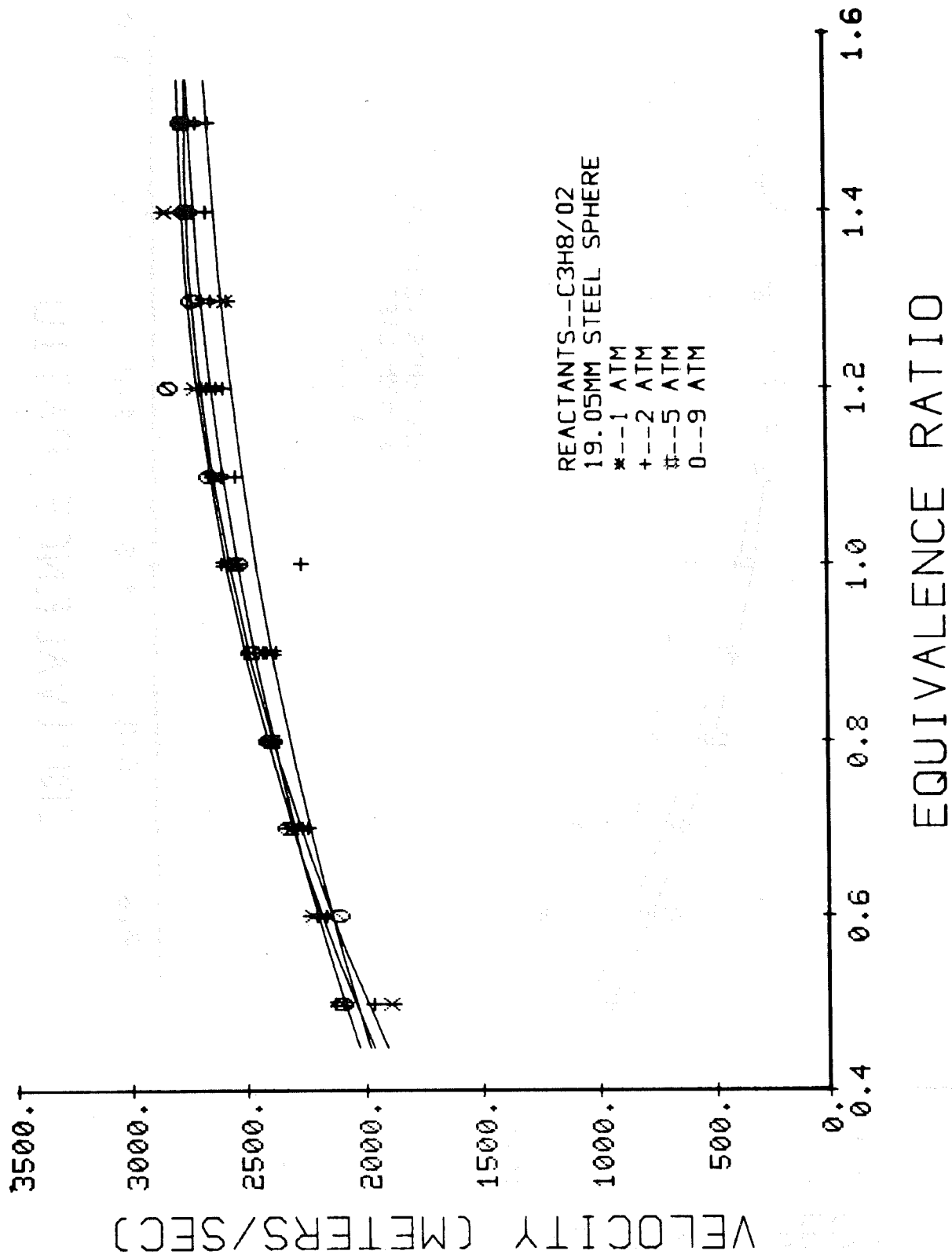


Figure 8. Detonation velocity versus equivalence ratio for various initial pressures.

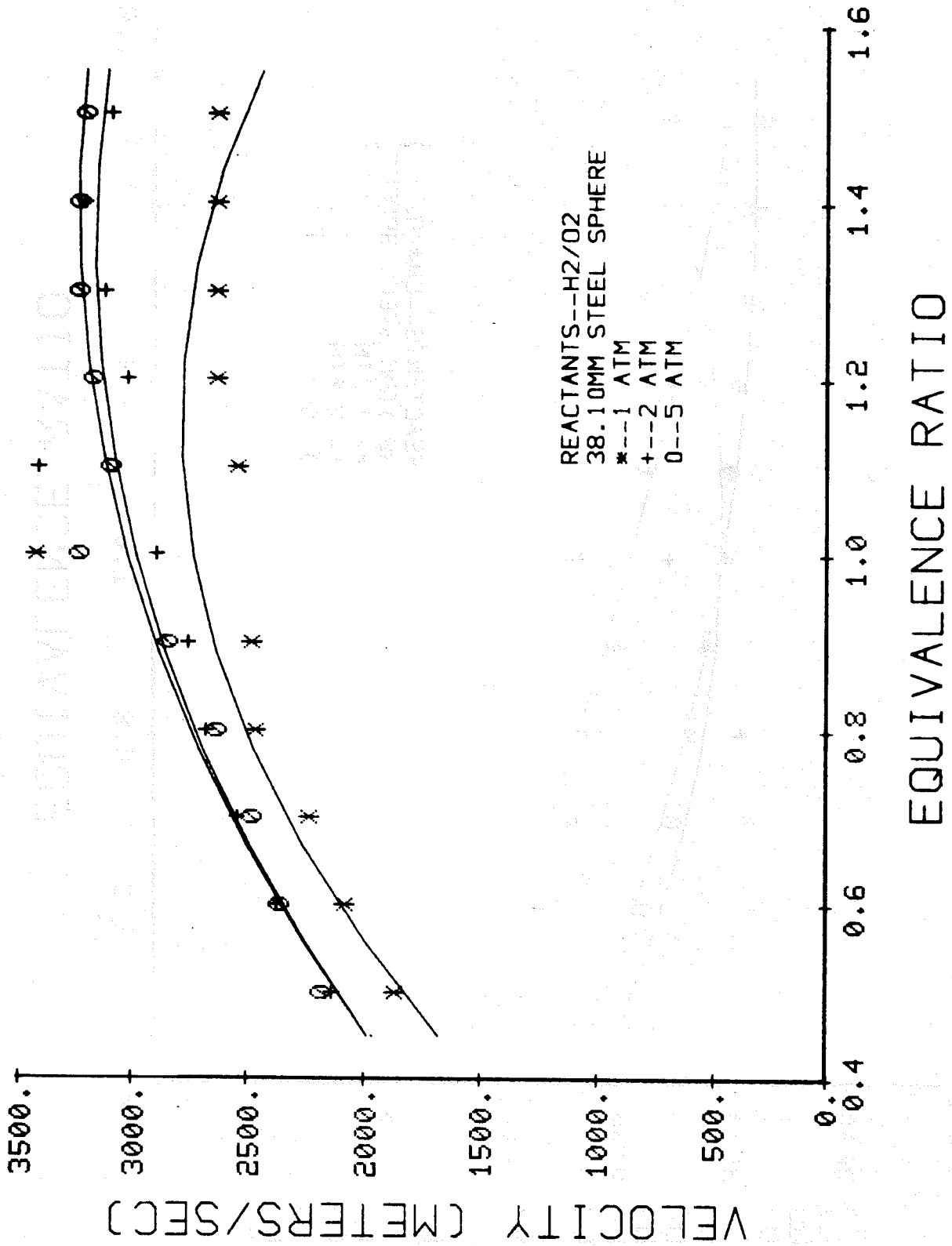


Figure 9. Detonation velocity versus equivalence ratio for various initial pressures.

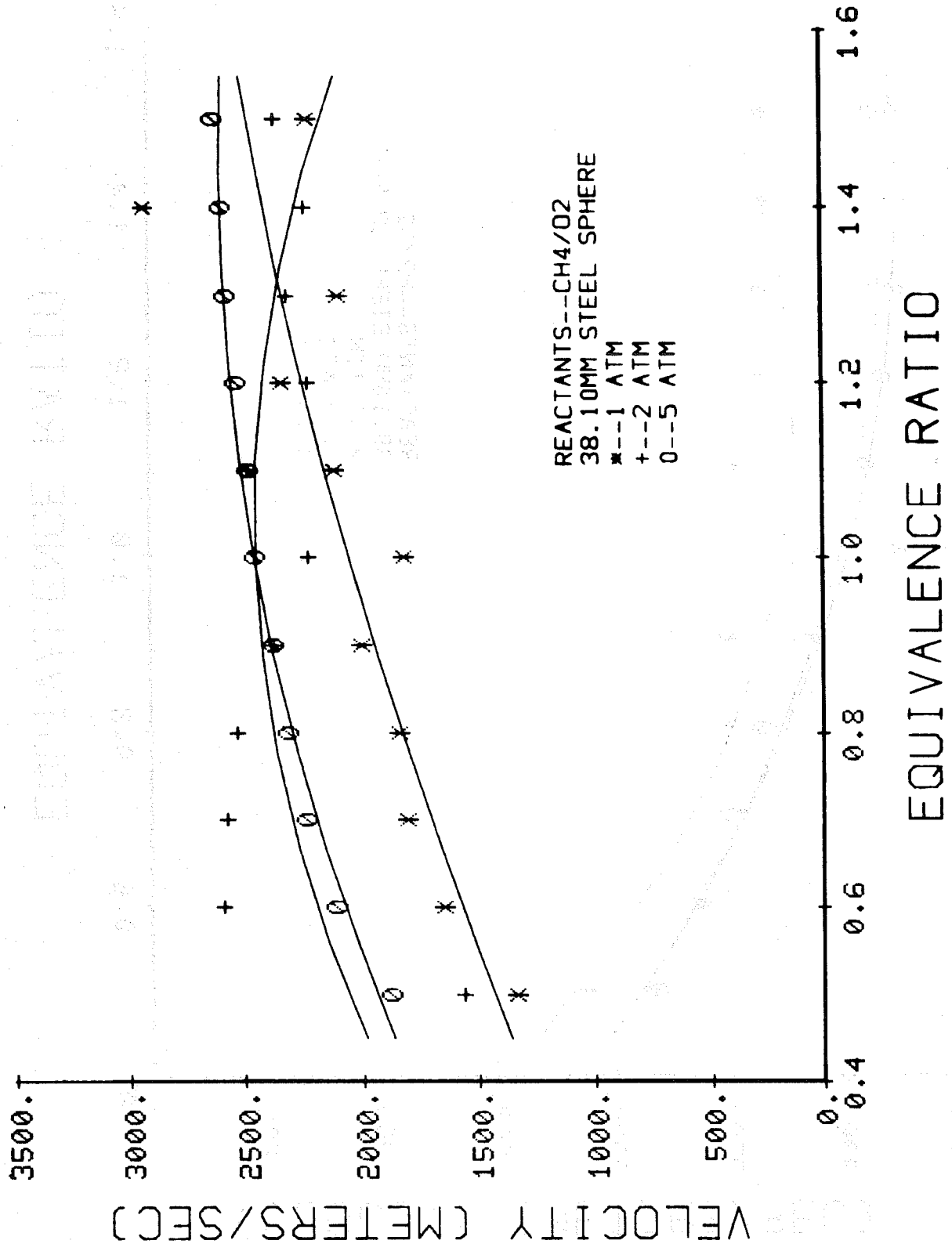


Figure 10. Detonation velocity versus equivalence ratio for various initial pressures.

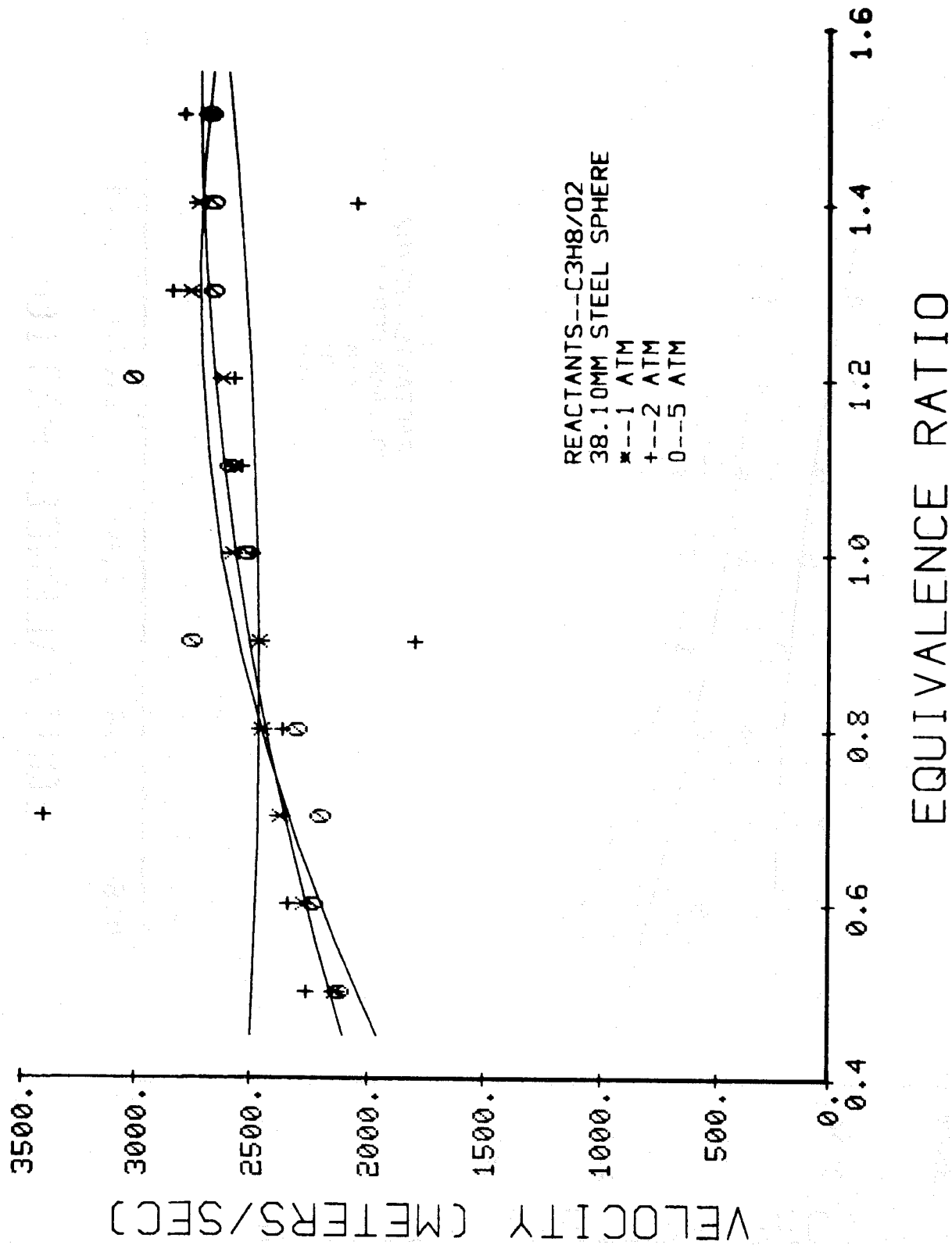


Figure 11. Detonation velocity versus equivalence ratio for various initial pressures.

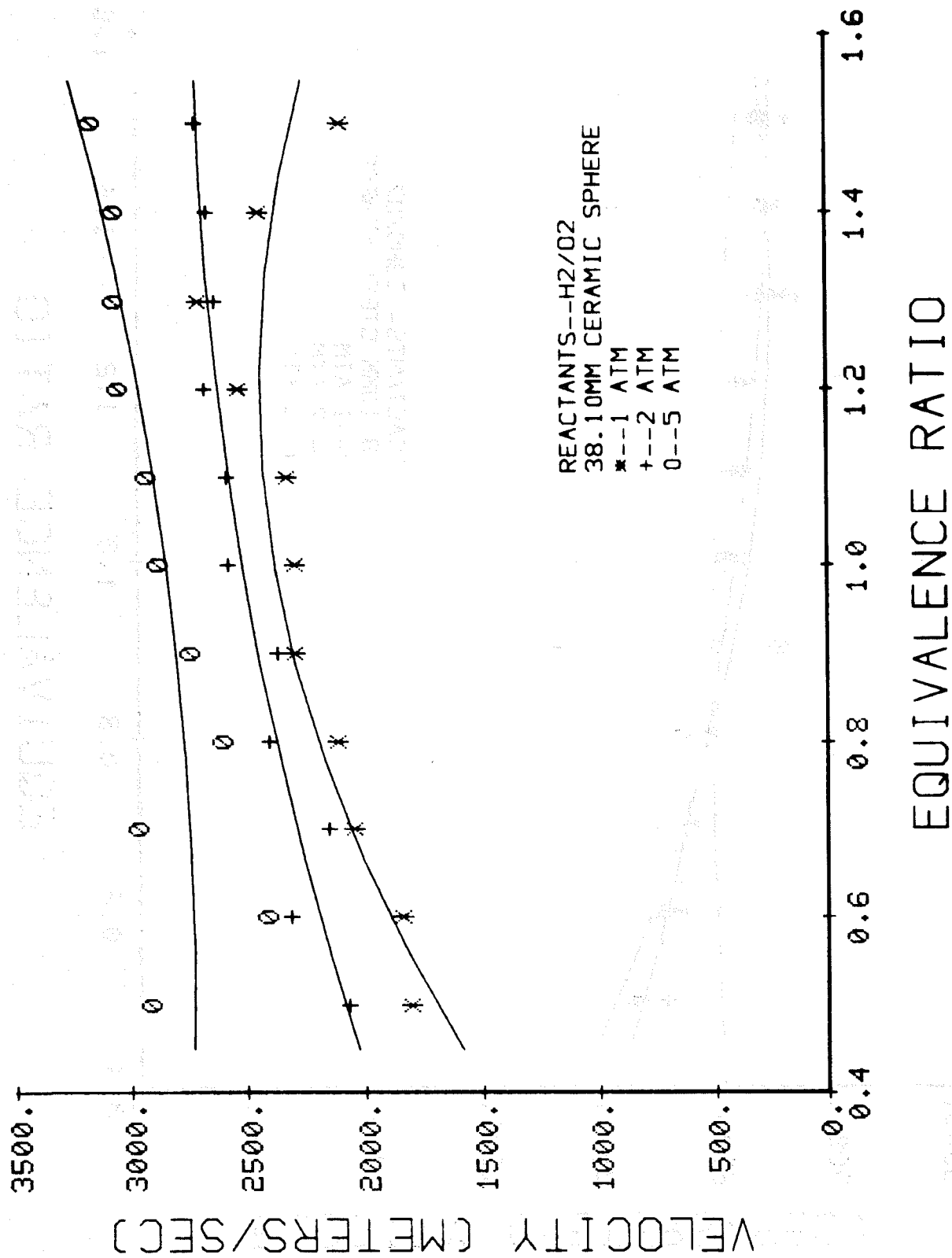


Figure 12. Detonation velocity versus equivalence ratio for various initial pressures.

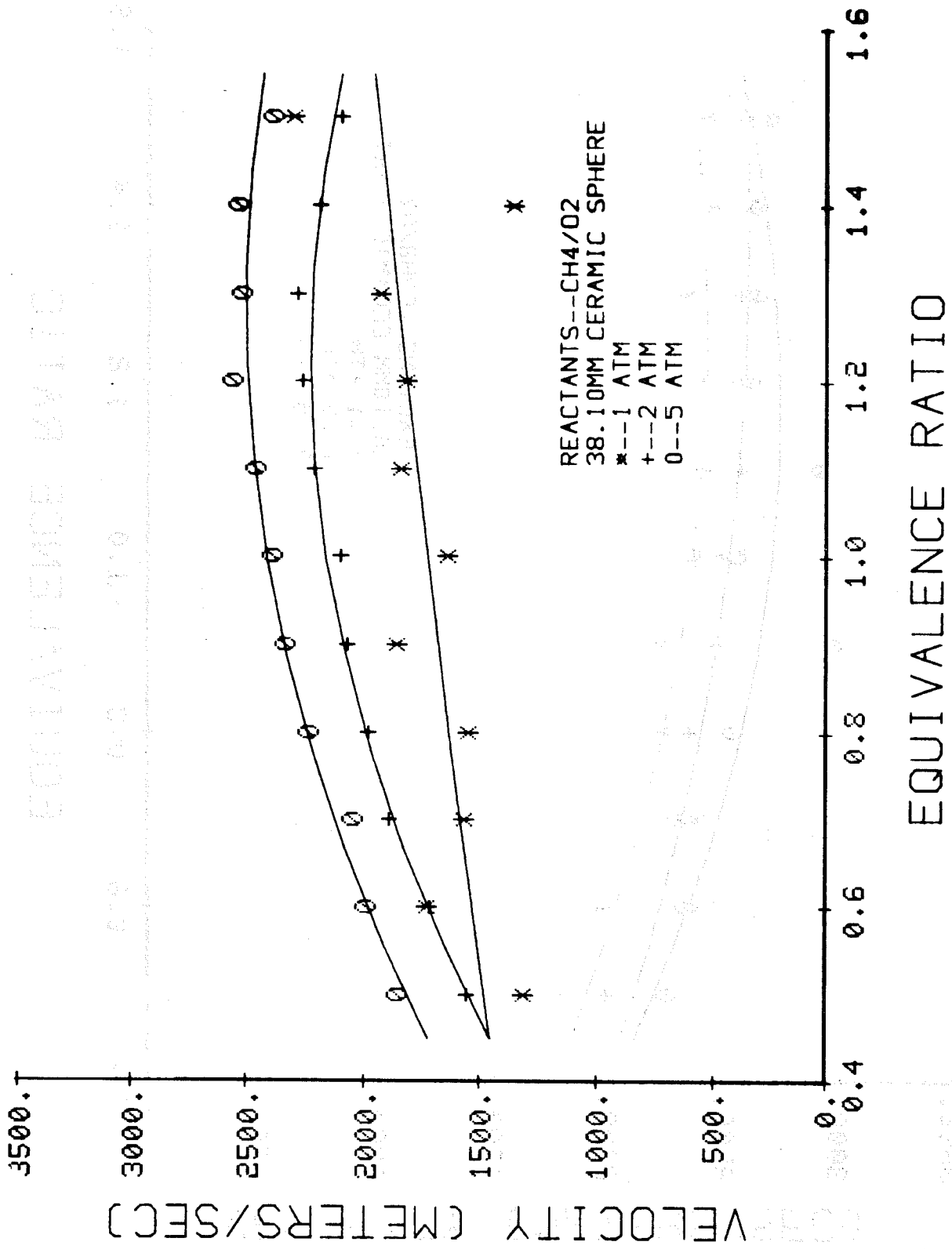


Figure 13. Detonation velocity versus equivalence ratio for various initial pressures.

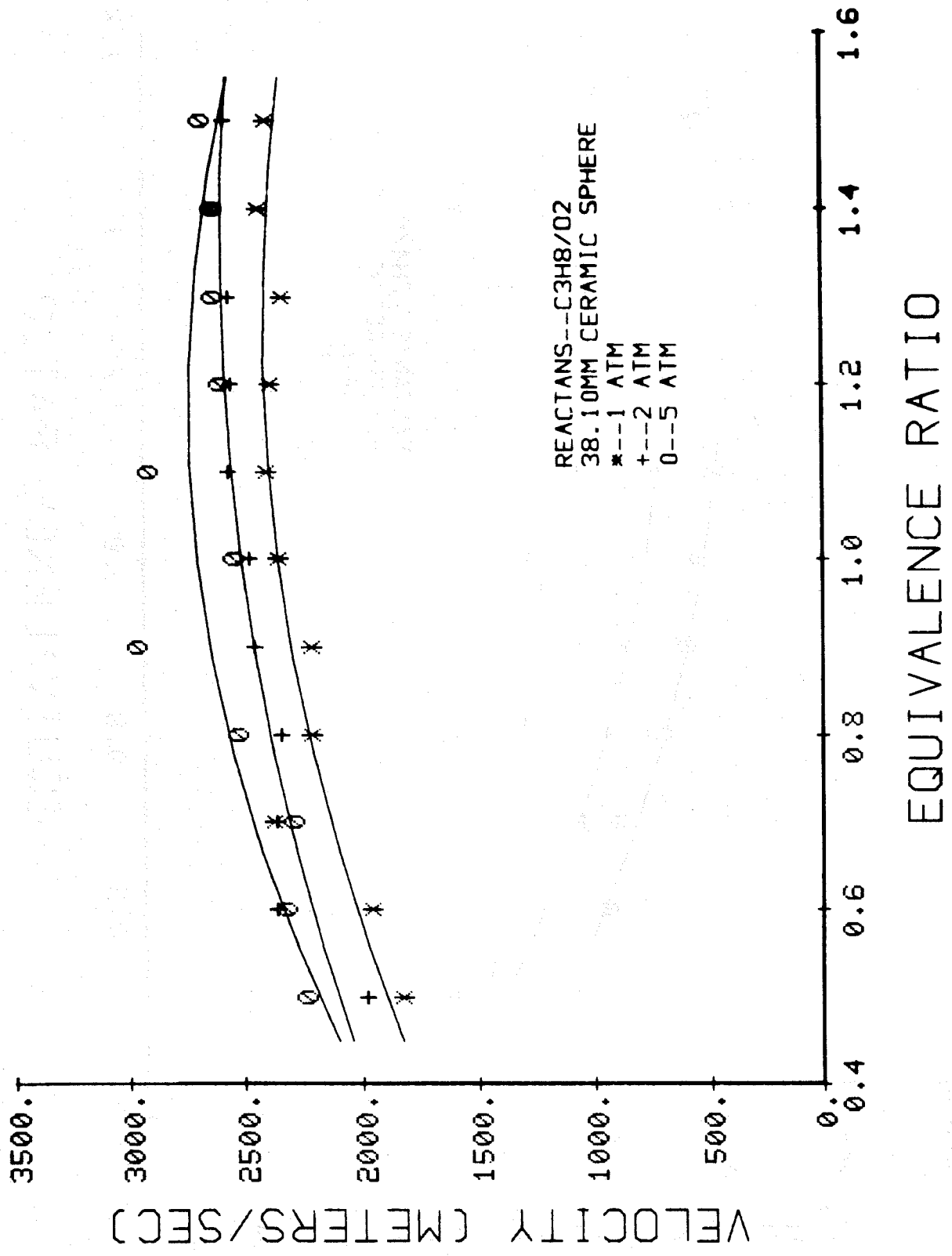


Figure 14. Detonation velocity versus equivalence ratio for various initial pressures.

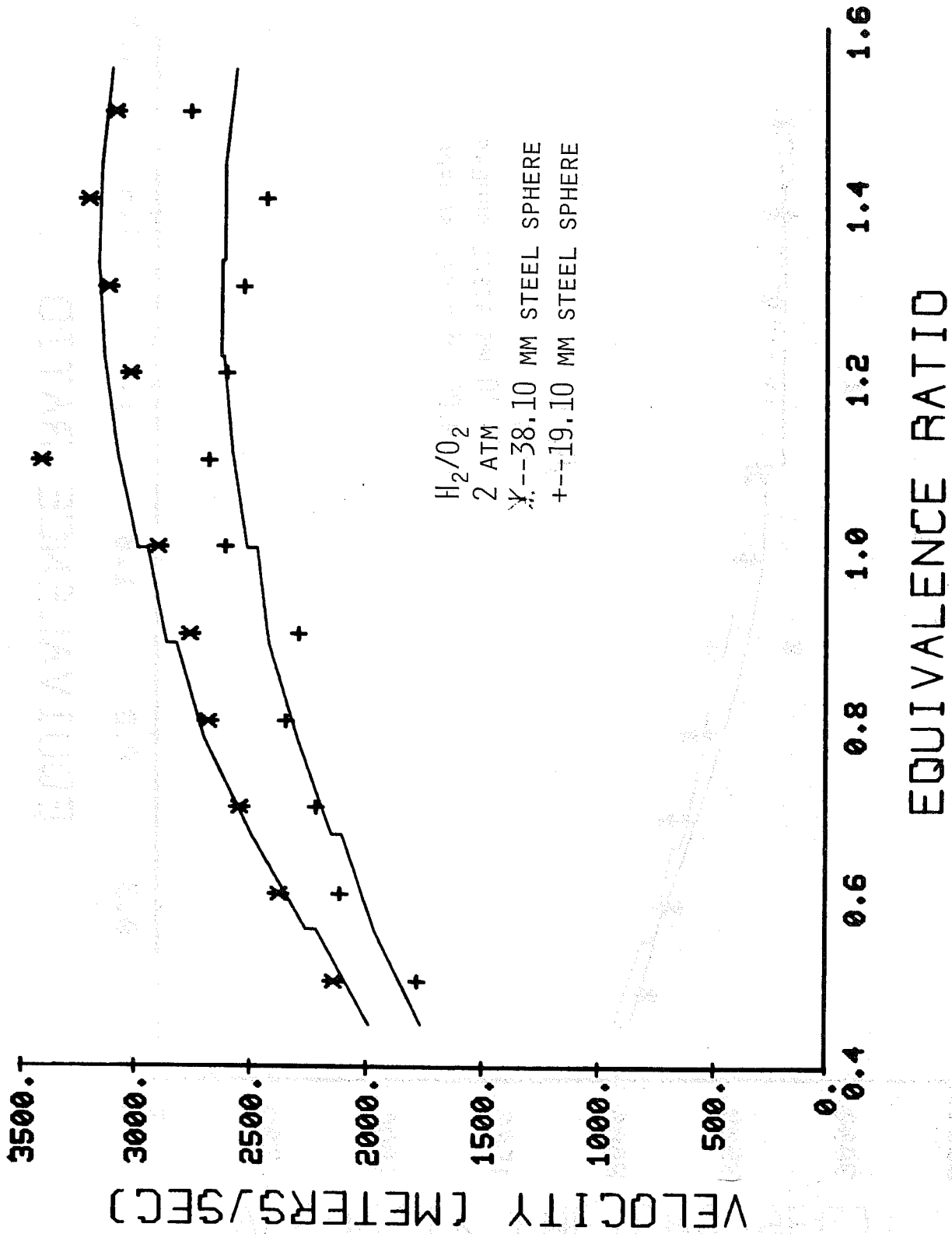


Figure 15. Detonation velocity versus equivalence ratio for different sphere diameters.

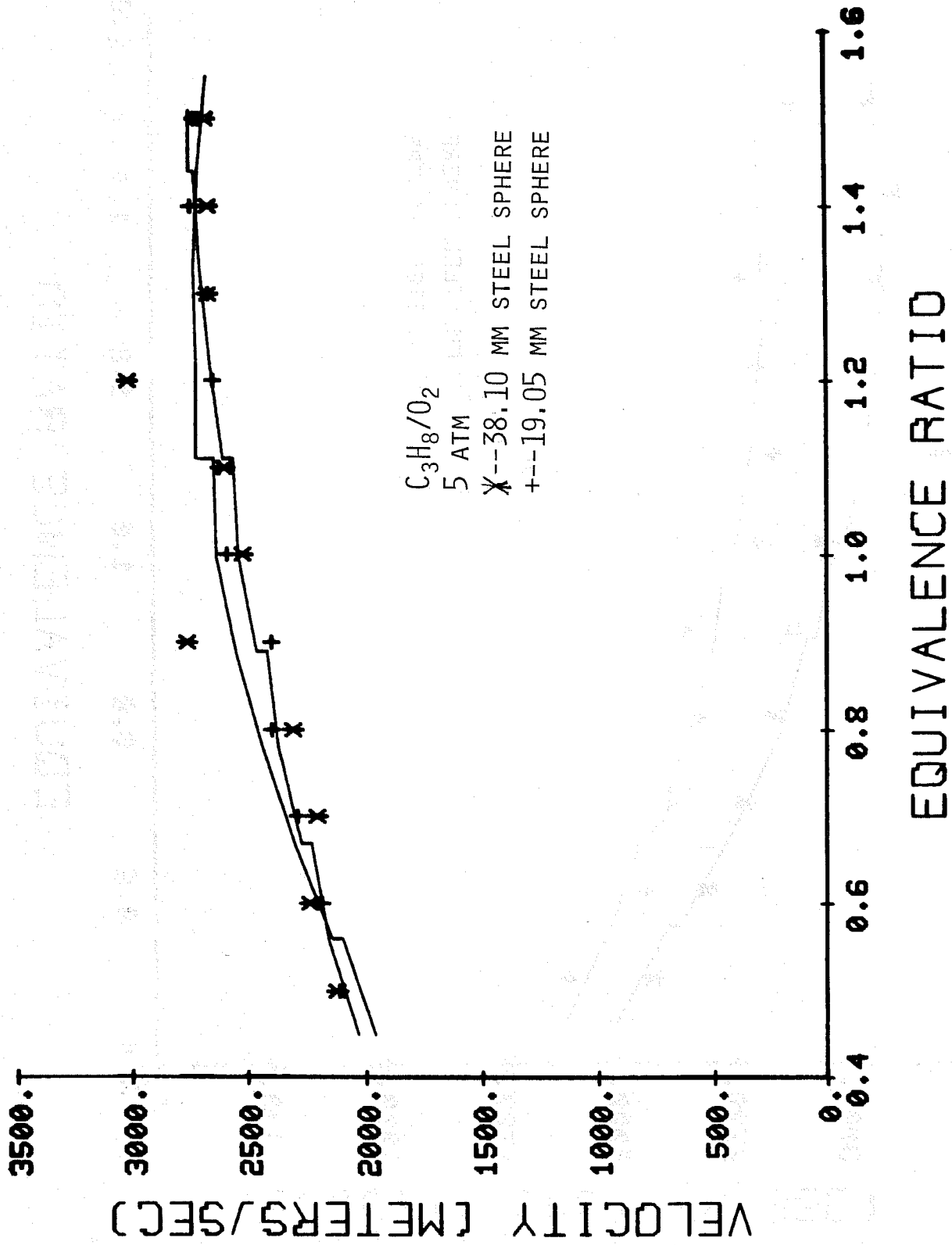


Figure 16. Detonation velocity versus equivalence ratio for different sphere diameters.

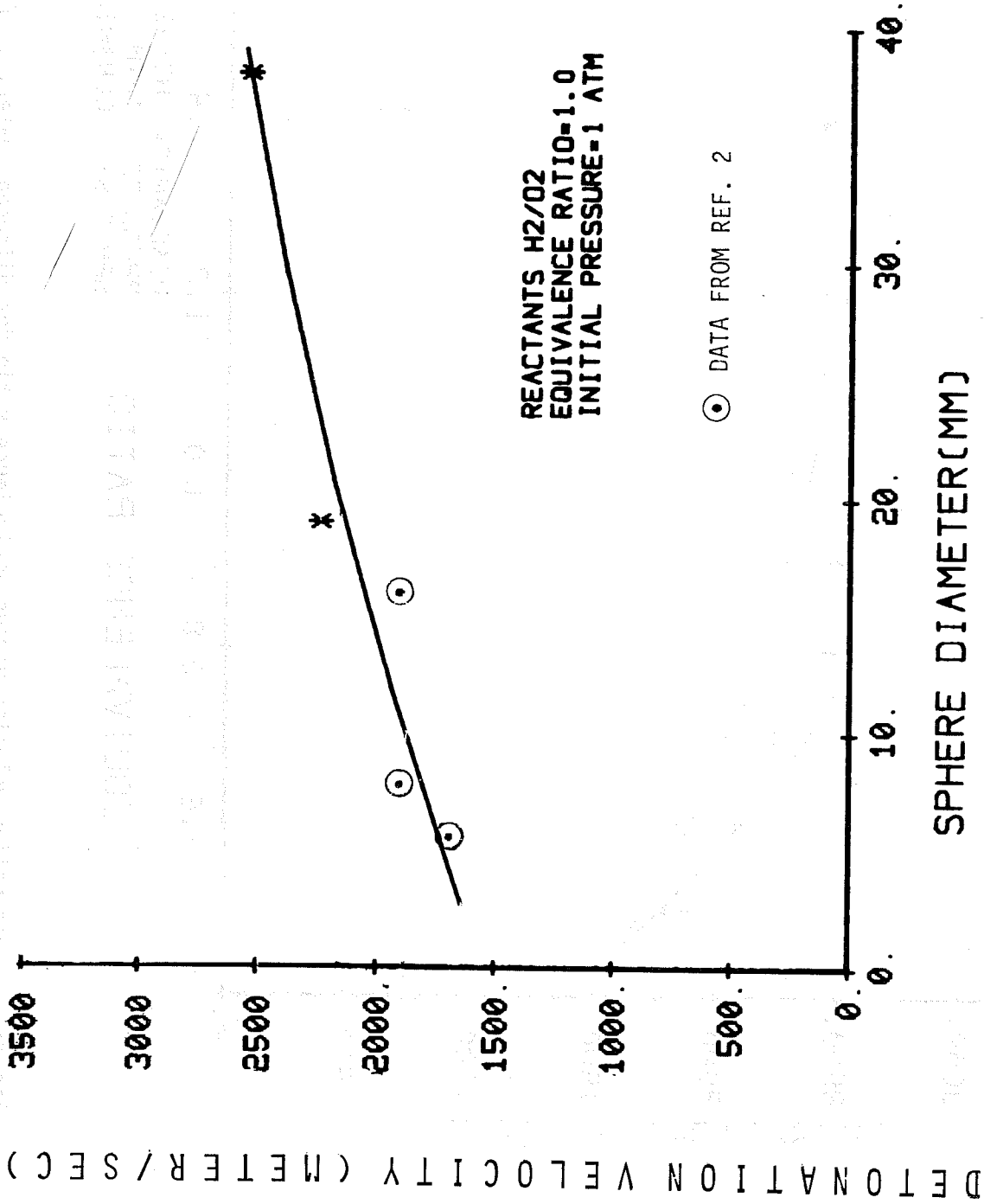


Figure 17. Detonation velocity versus sphere diameter.

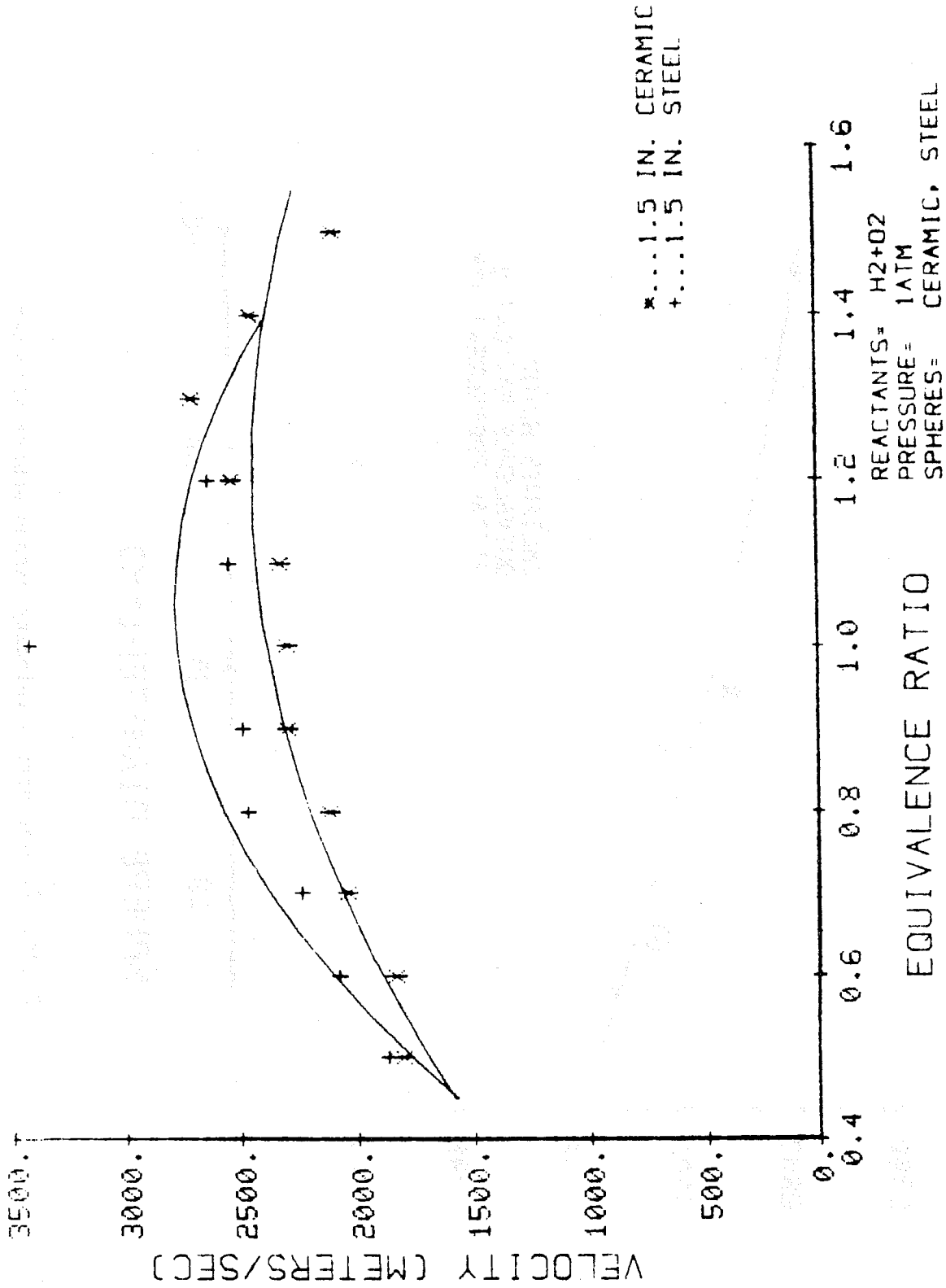


Figure 18. Detonation velocity versus equivalence ratio for different material of spheres.

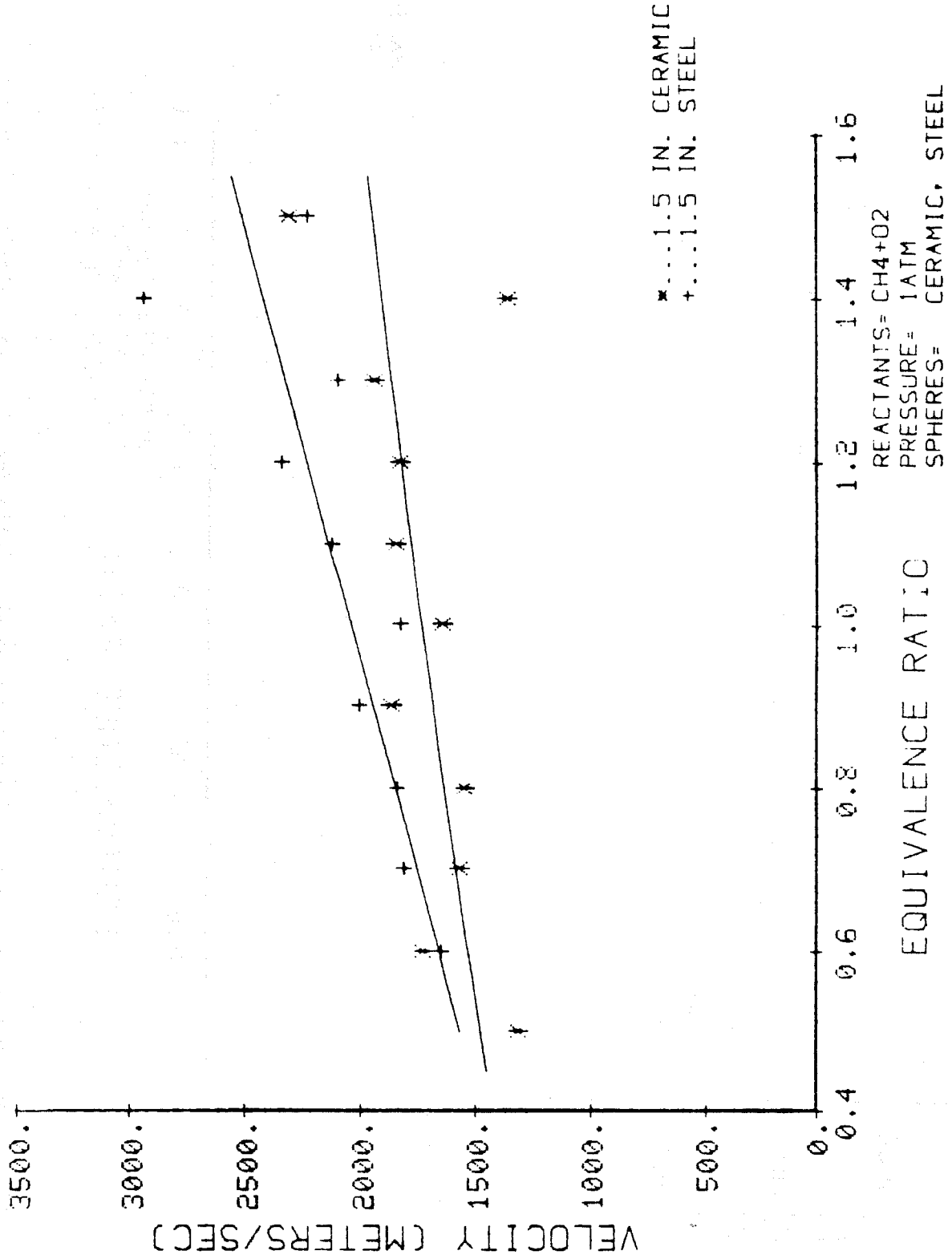


Figure 19. Detonation velocity versus equivalence ratio for different material of spheres.

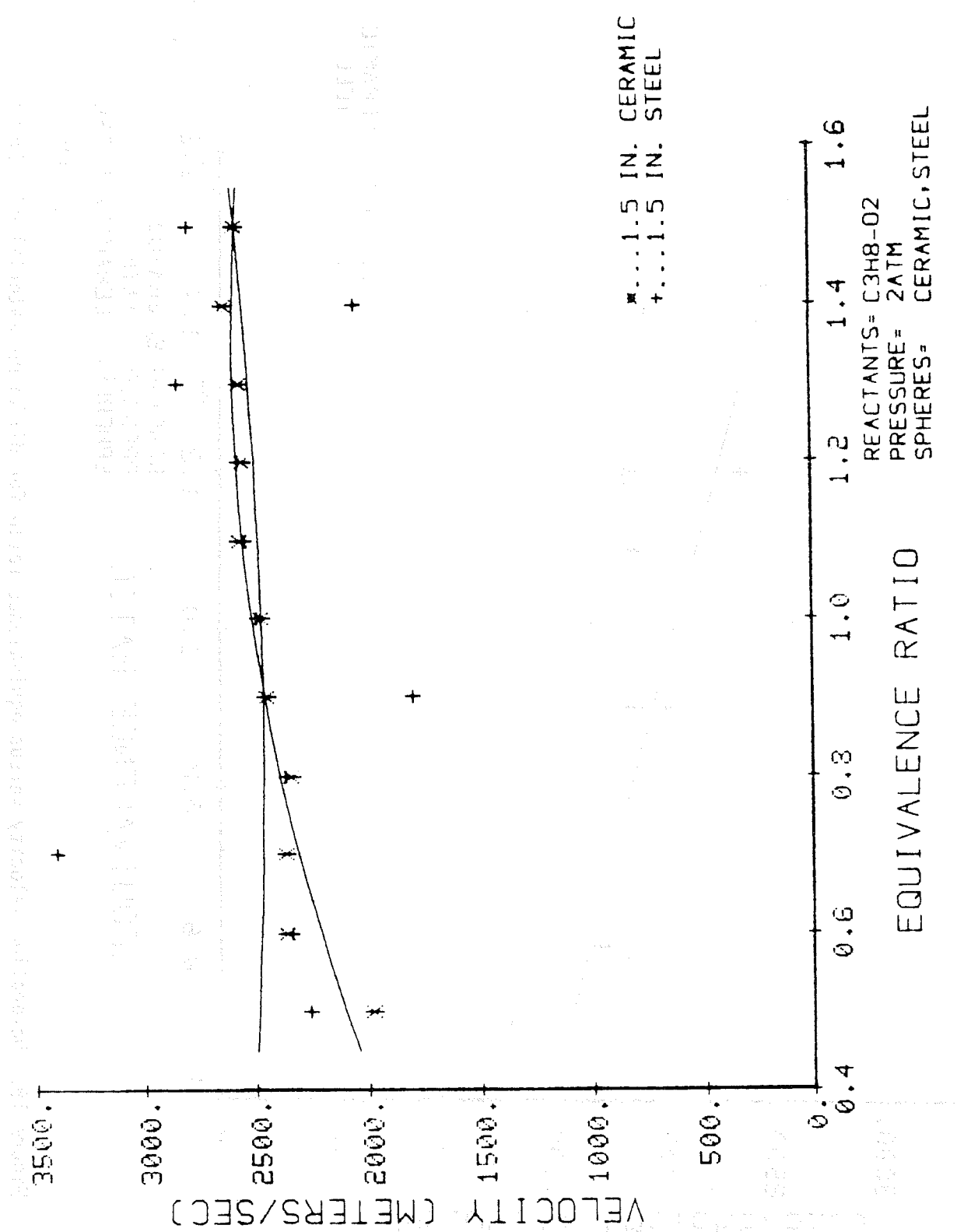
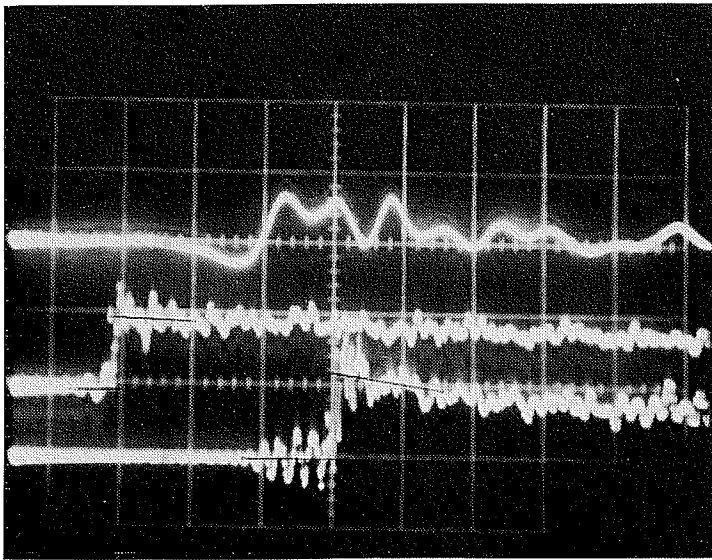


Figure 20. Detonation velocity versus equivalence ratio for different material of spheres.



$H_2/O_2$ ,  $\phi = 0.7$

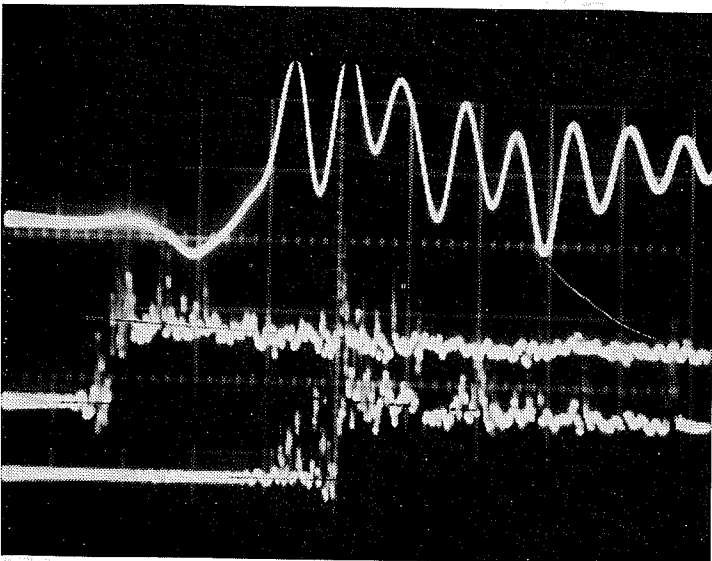
38.10mm steel spheres

$p_1 = 2$  atm

sweep = 100 microsec./div.

0.2 volts/div.

1.01 psi/mv



$CH_4/O_2$ ,  $\phi = 1.0$

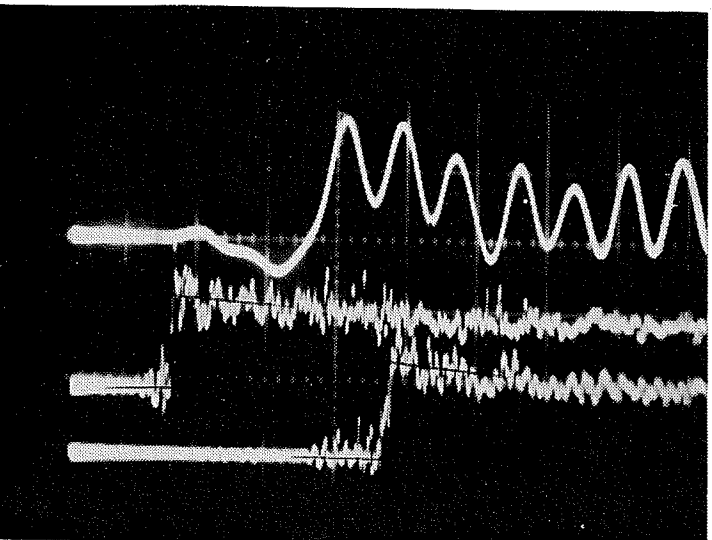
38.10mm steel spheres

$p_1 = 5$  atm

sweep = 100 microsec./div.

1.0 volts/div.

1.01 psi/mv



$C_3H_8/O_2$ ,  $\phi = 1.3$

38.10mm steel spheres

$p_1 = 2$  atm

sweep = 100 microsec./div.

0.5 volts/div.

1.01 psi/mv

Figure 21. Oscilloscope traces of detonation pressures.

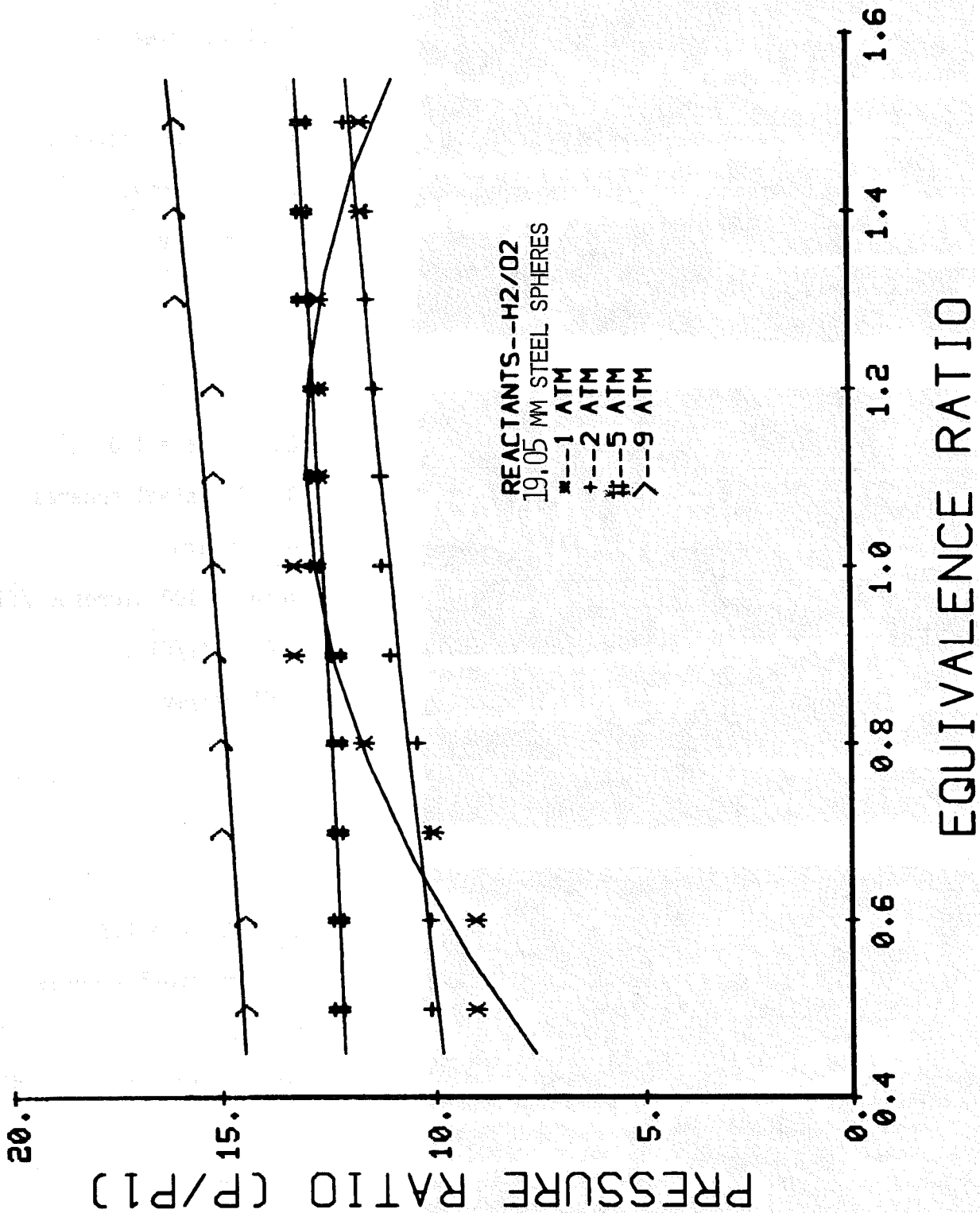


Figure 22. Pressure ratio versus equivalence ratio for various initial pressures.

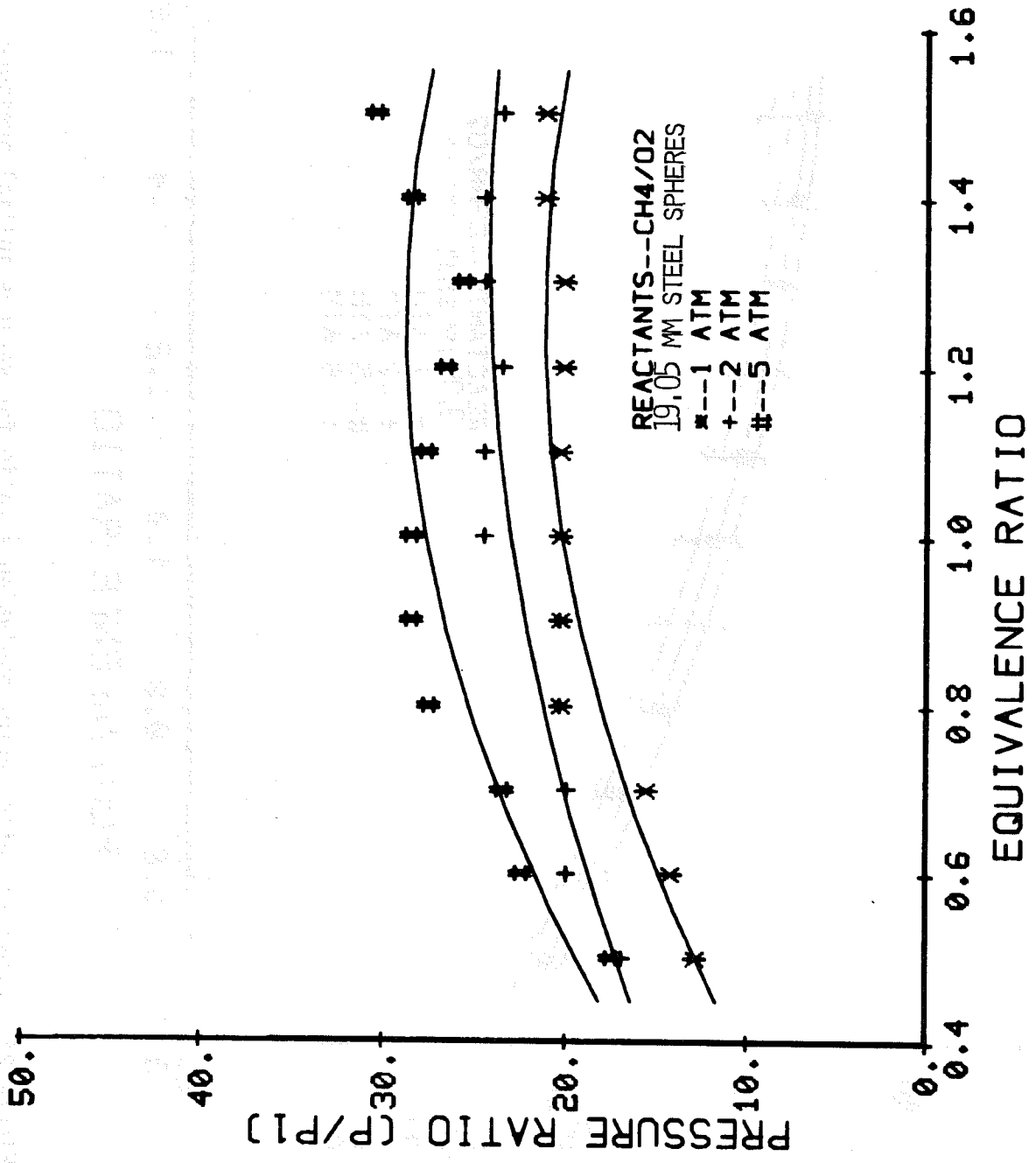


Figure 23. Pressure ratio versus equivalence ratio for various initial pressures.

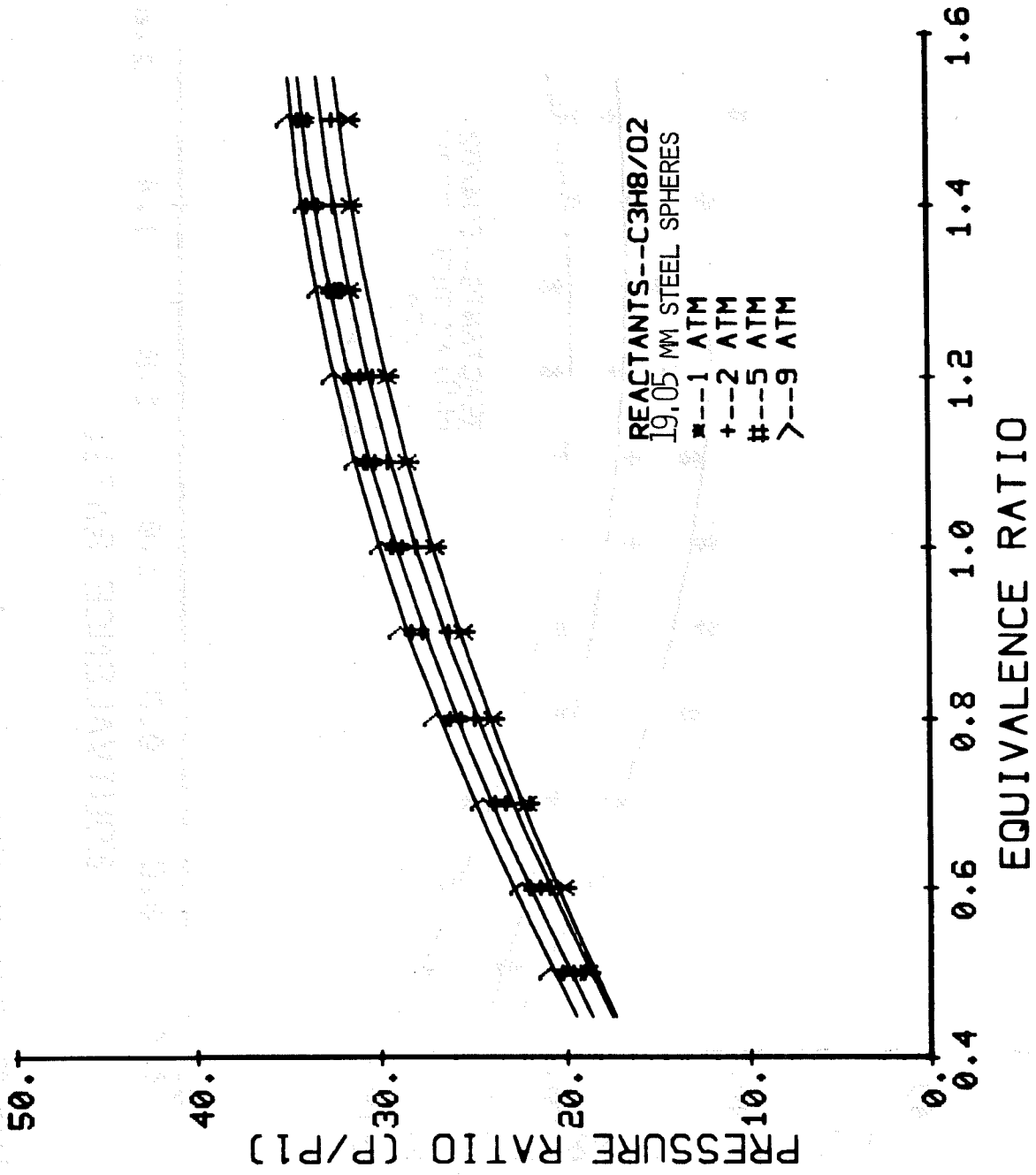


Figure 24. Pressure ratio versus equivalence ratio for various initial pressures.

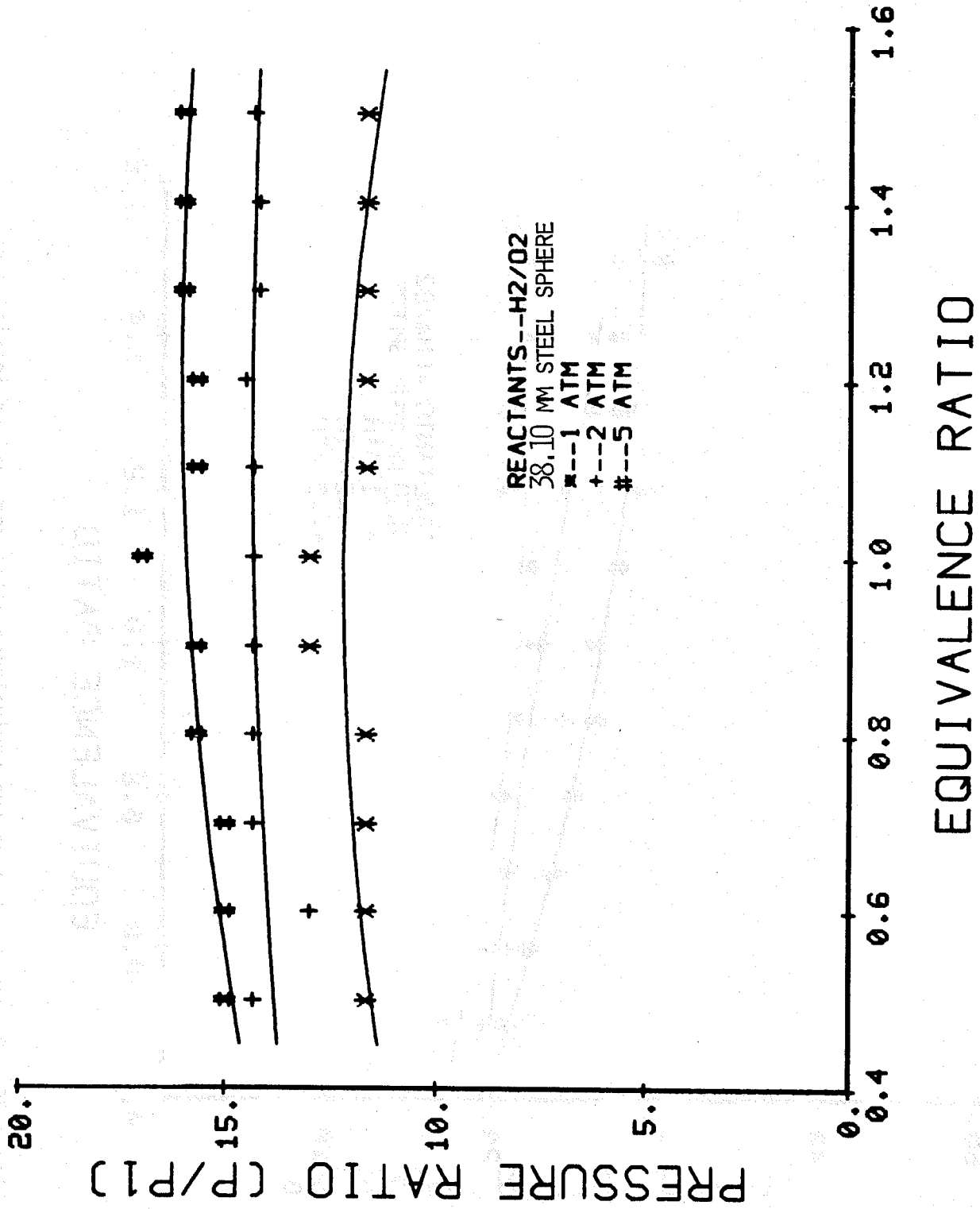


Figure 25. Pressure ratio versus equivalence ratio for various initial pressures.

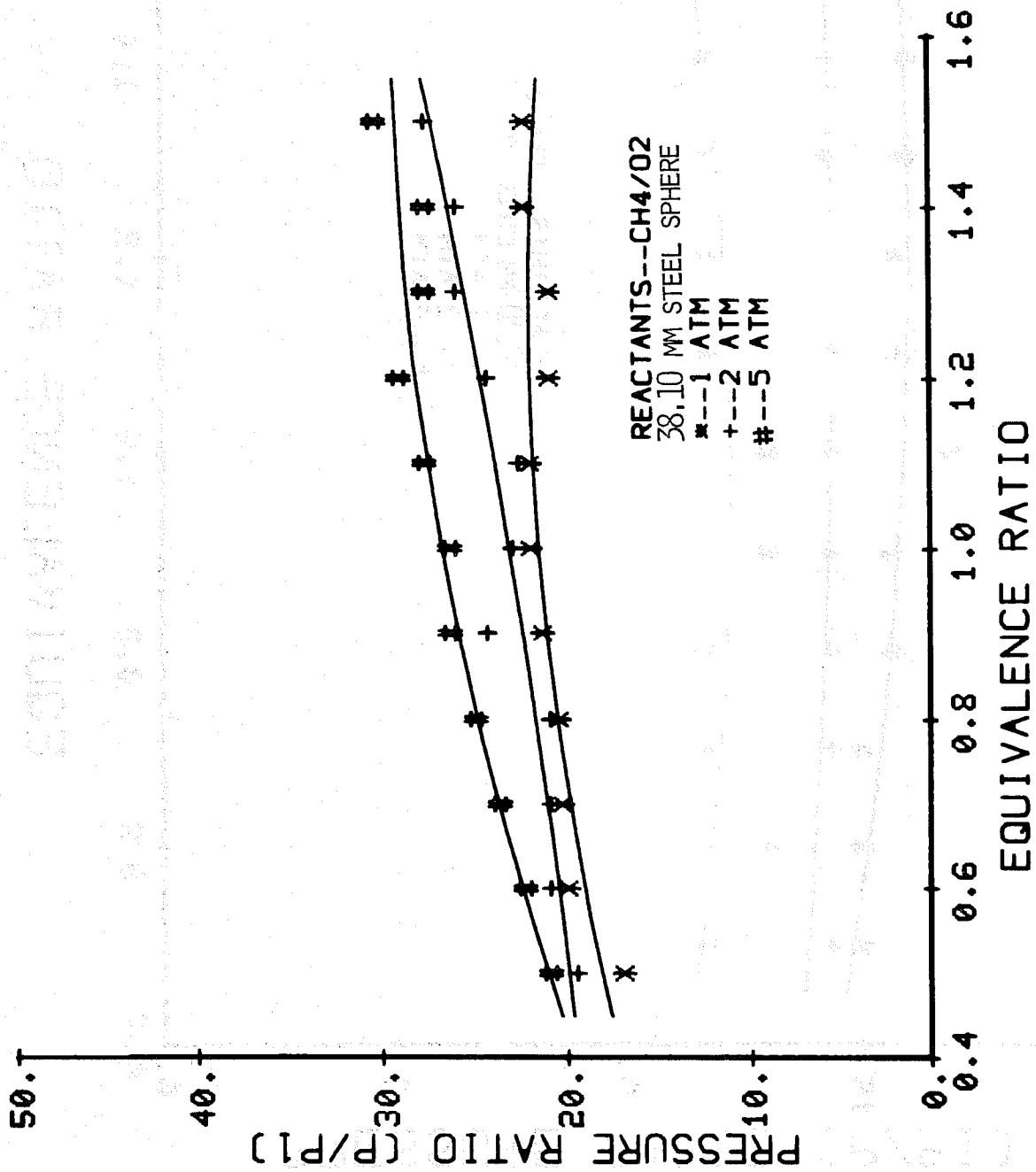


Figure 26. Pressure ratio versus equivalence ratio for various initial pressures.

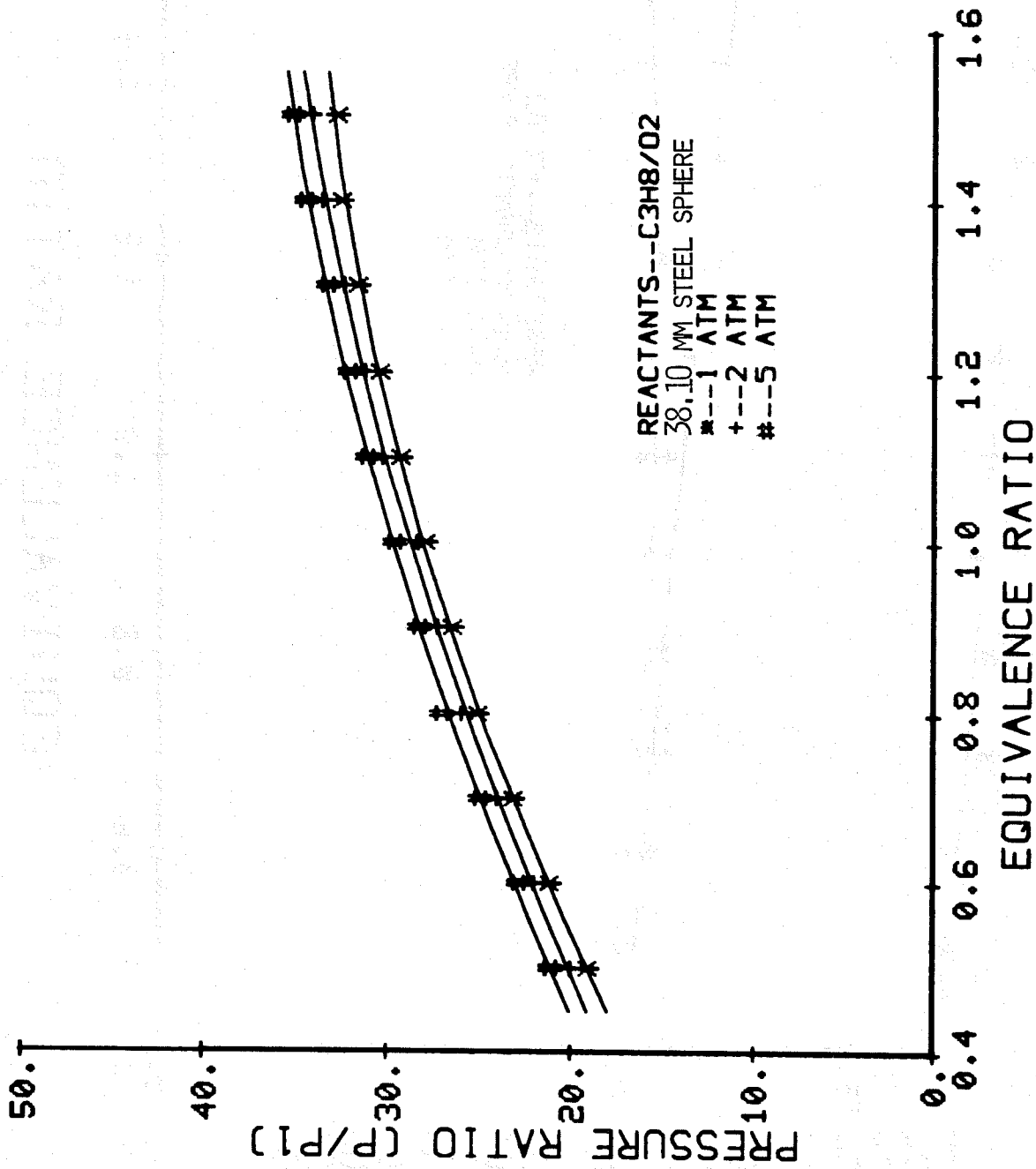


Figure 27. Pressure ratio versus equivalence ratio for various initial pressures.

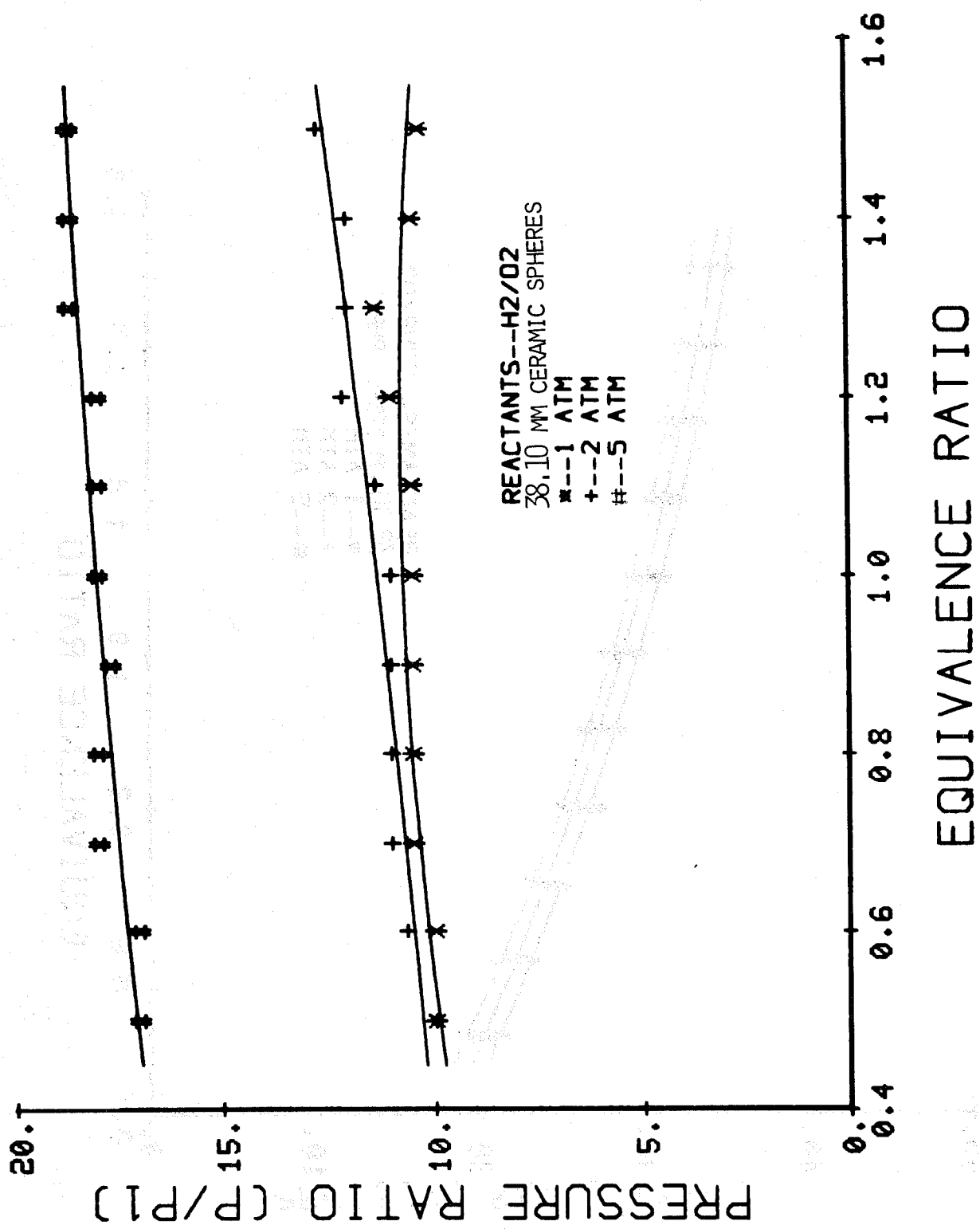


Figure 28. Pressure ratio versus equivalence ratio for various initial pressures.

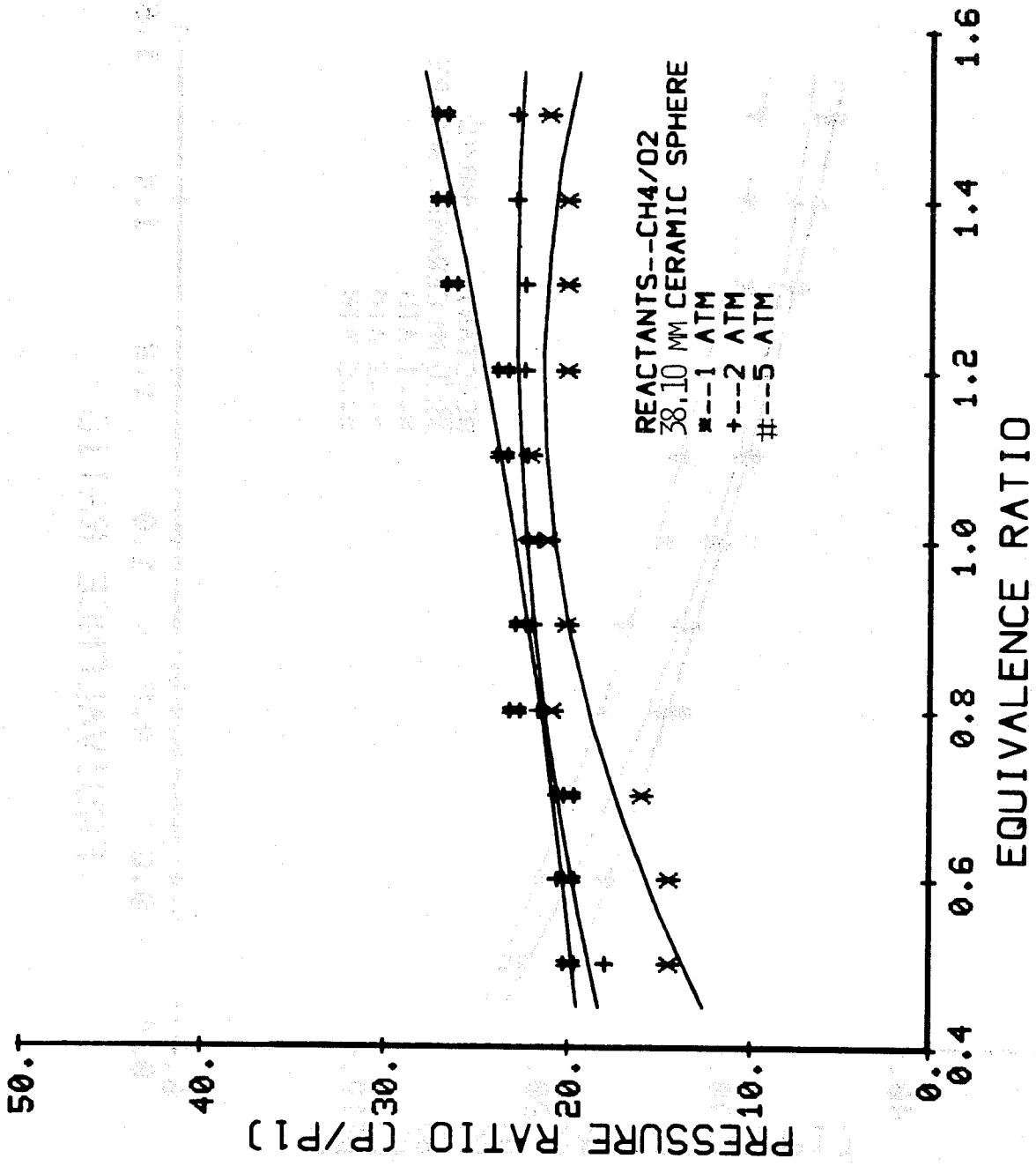


Figure 29. Pressure ratio versus equivalence ratio for various initial pressures.

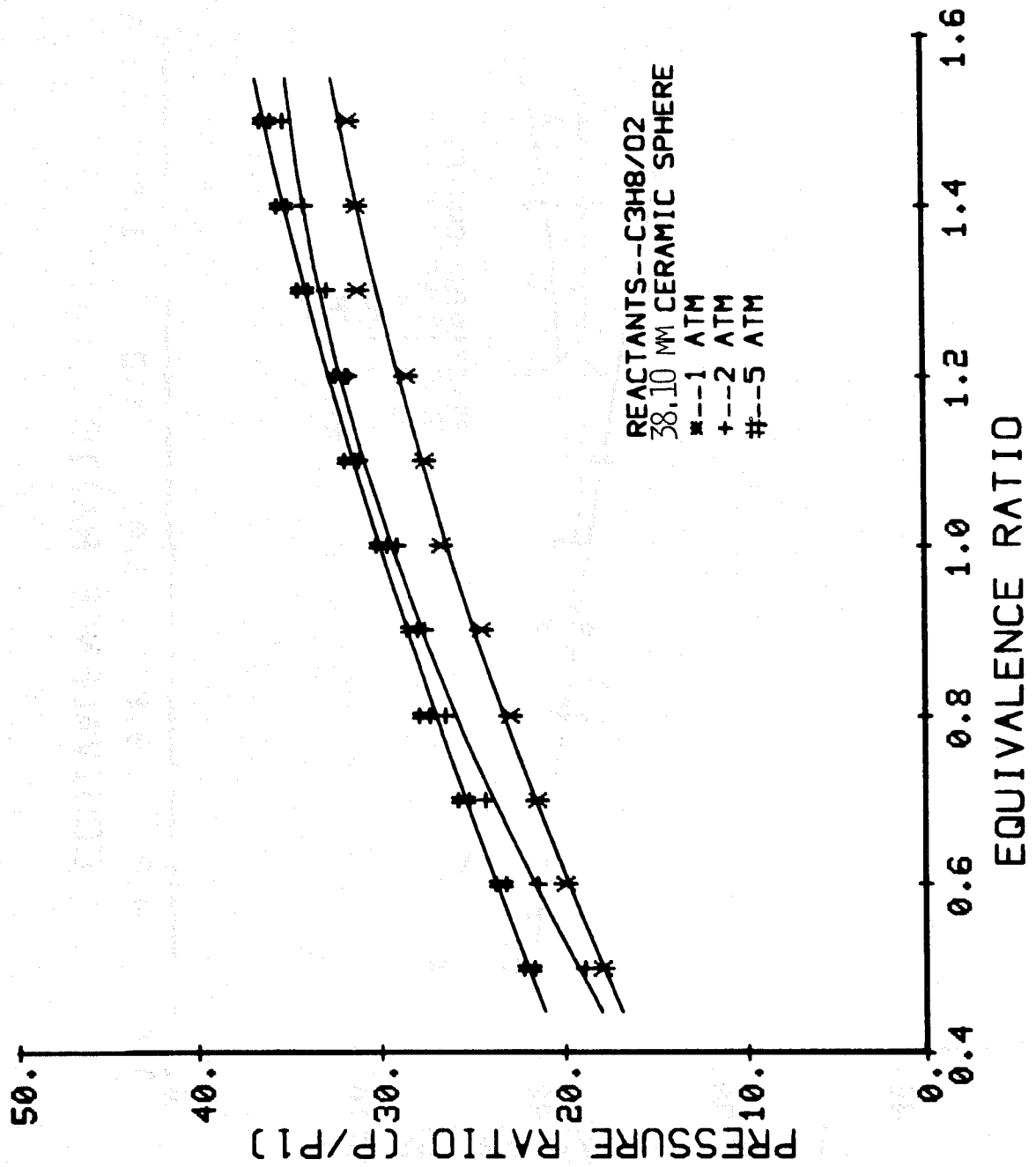


Figure 30. Pressure ratio versus equivalence ratio for various initial pressures.

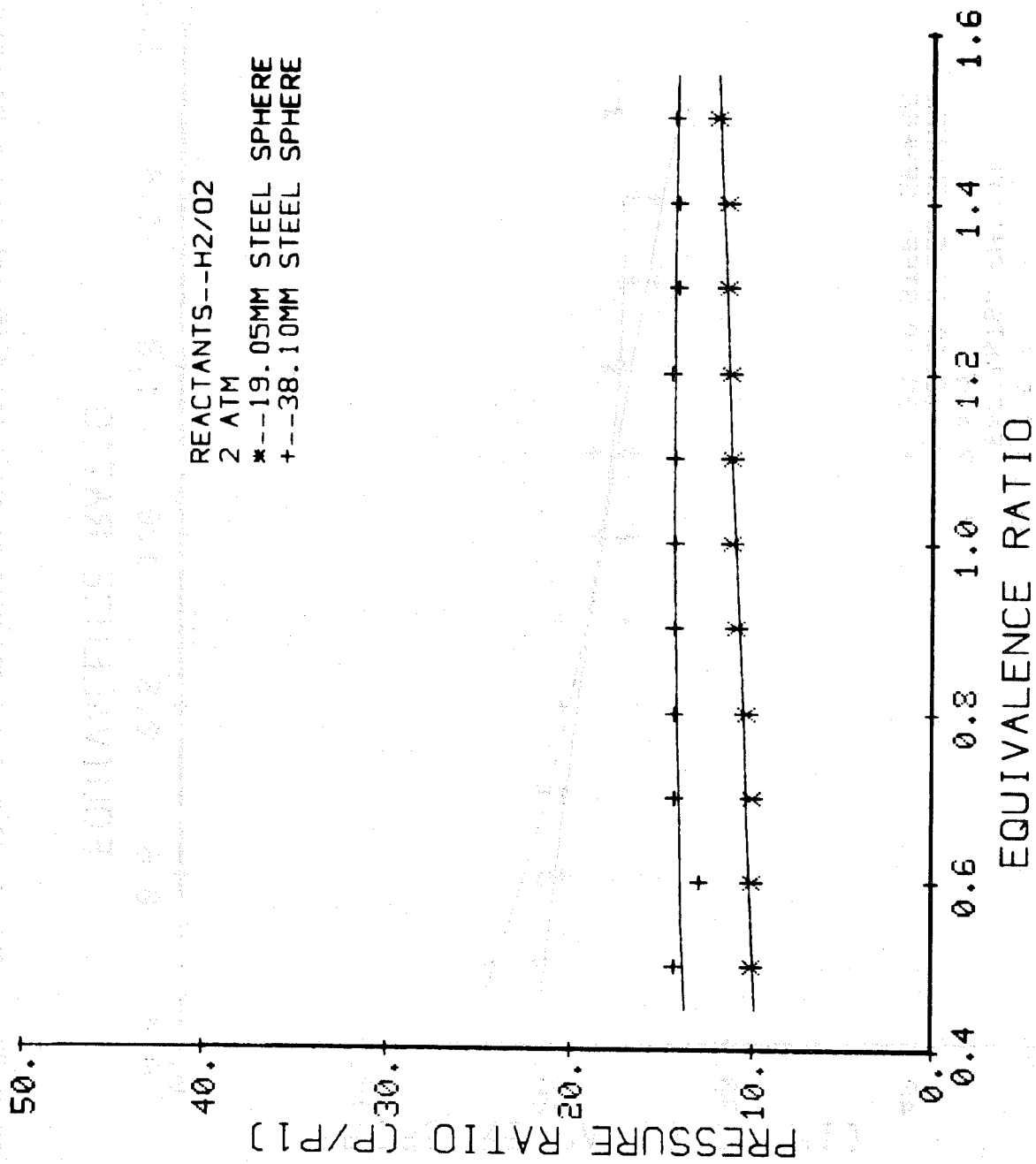


Figure 31. Pressure ratio versus equivalence ratio for different sphere diameters.

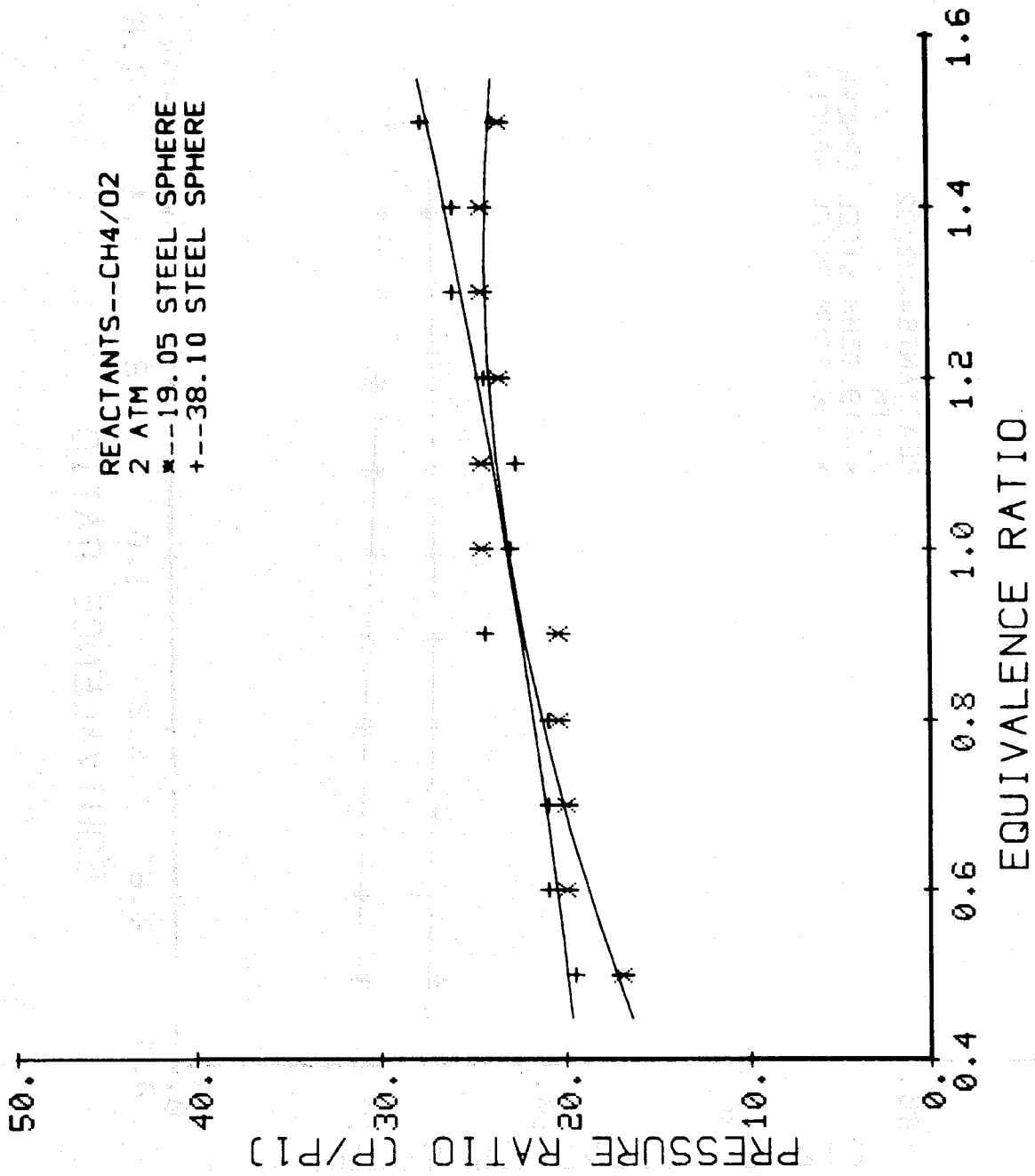


Figure 32. Pressure ratio versus equivalence ratio for different sphere diameters.

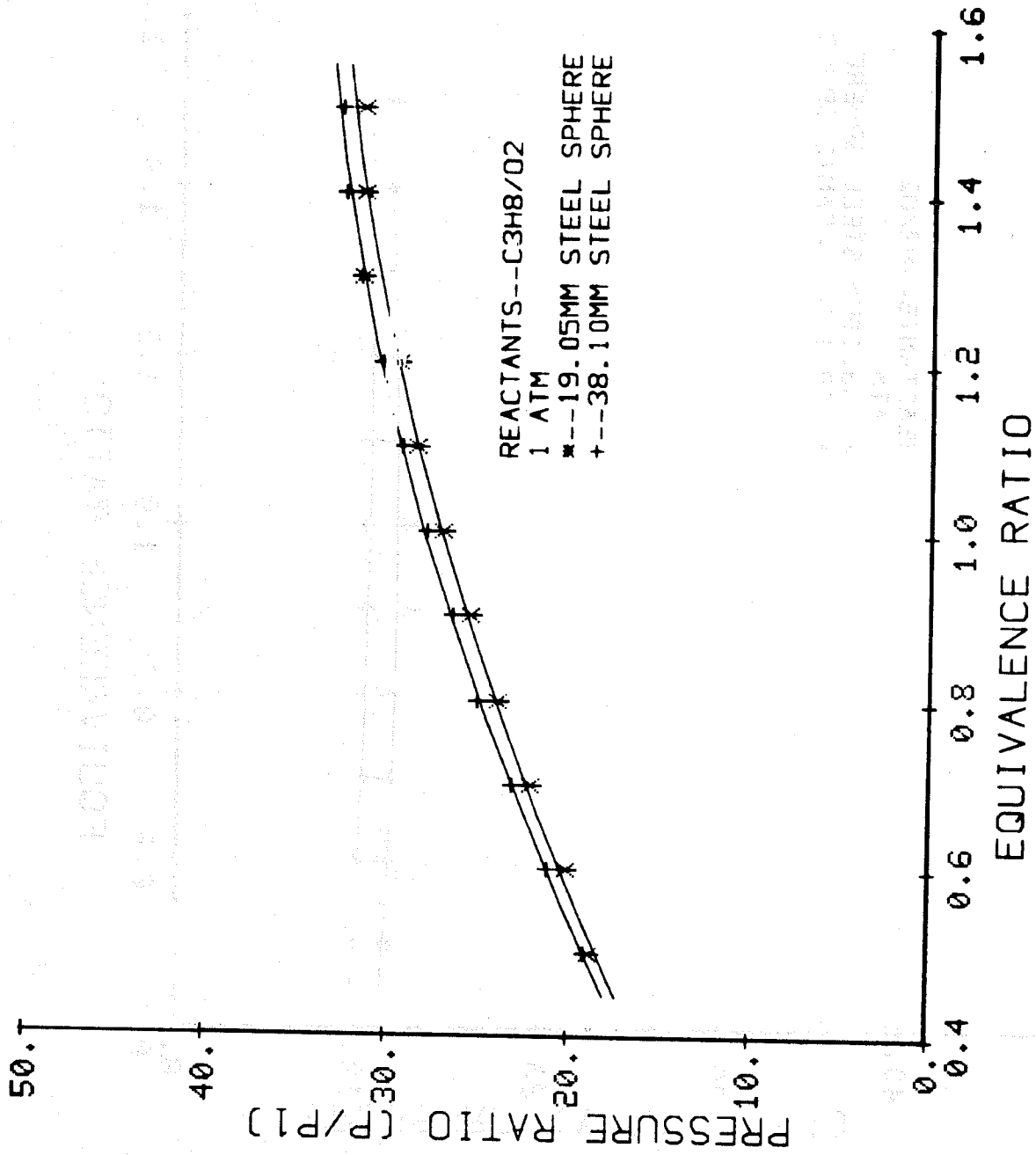


Figure 33. Pressure ratio versus equivalence ratio for different sphere diameters.

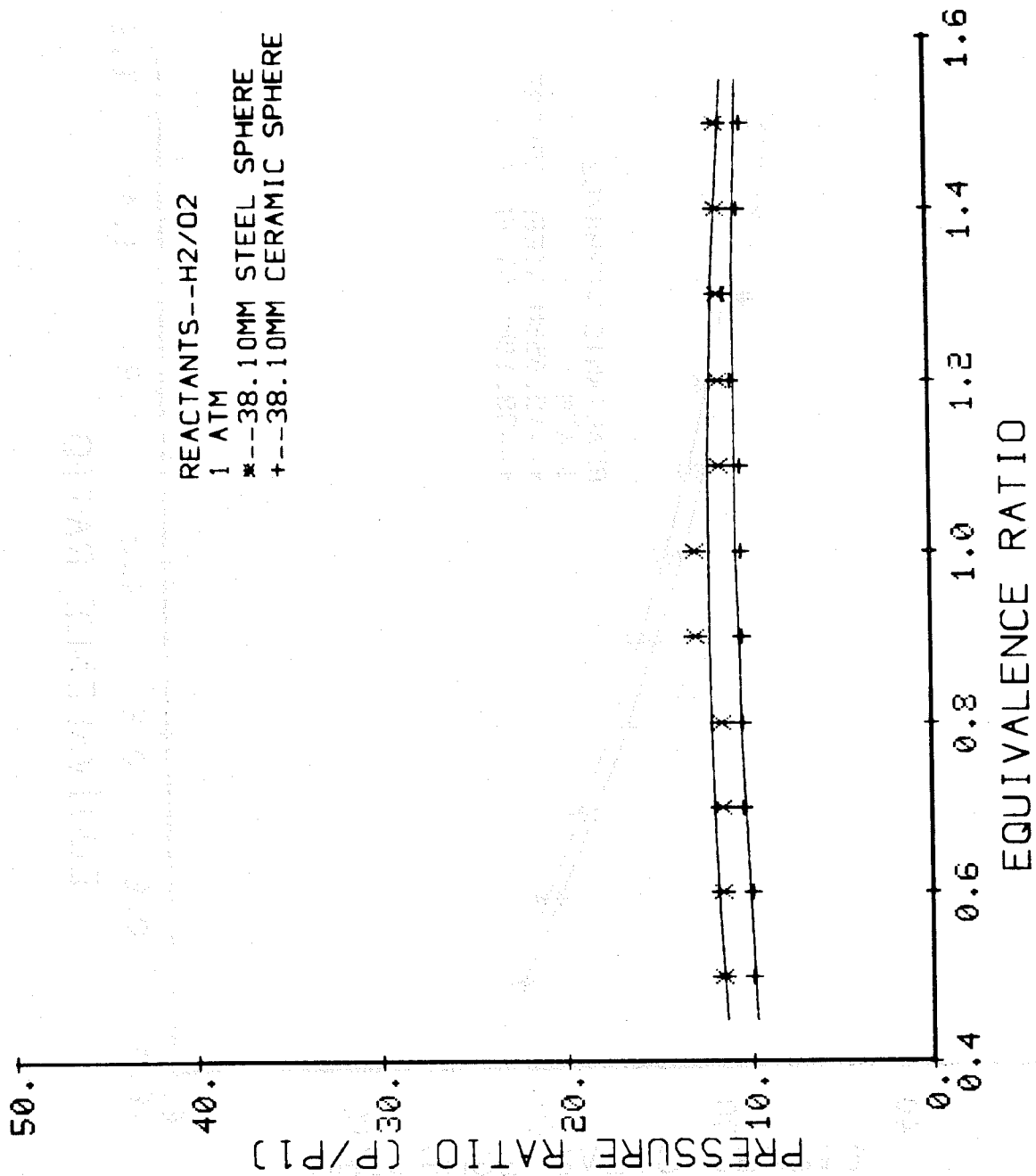


Figure 34. Pressure ratio versus equivalence ratio for different sphere materials.

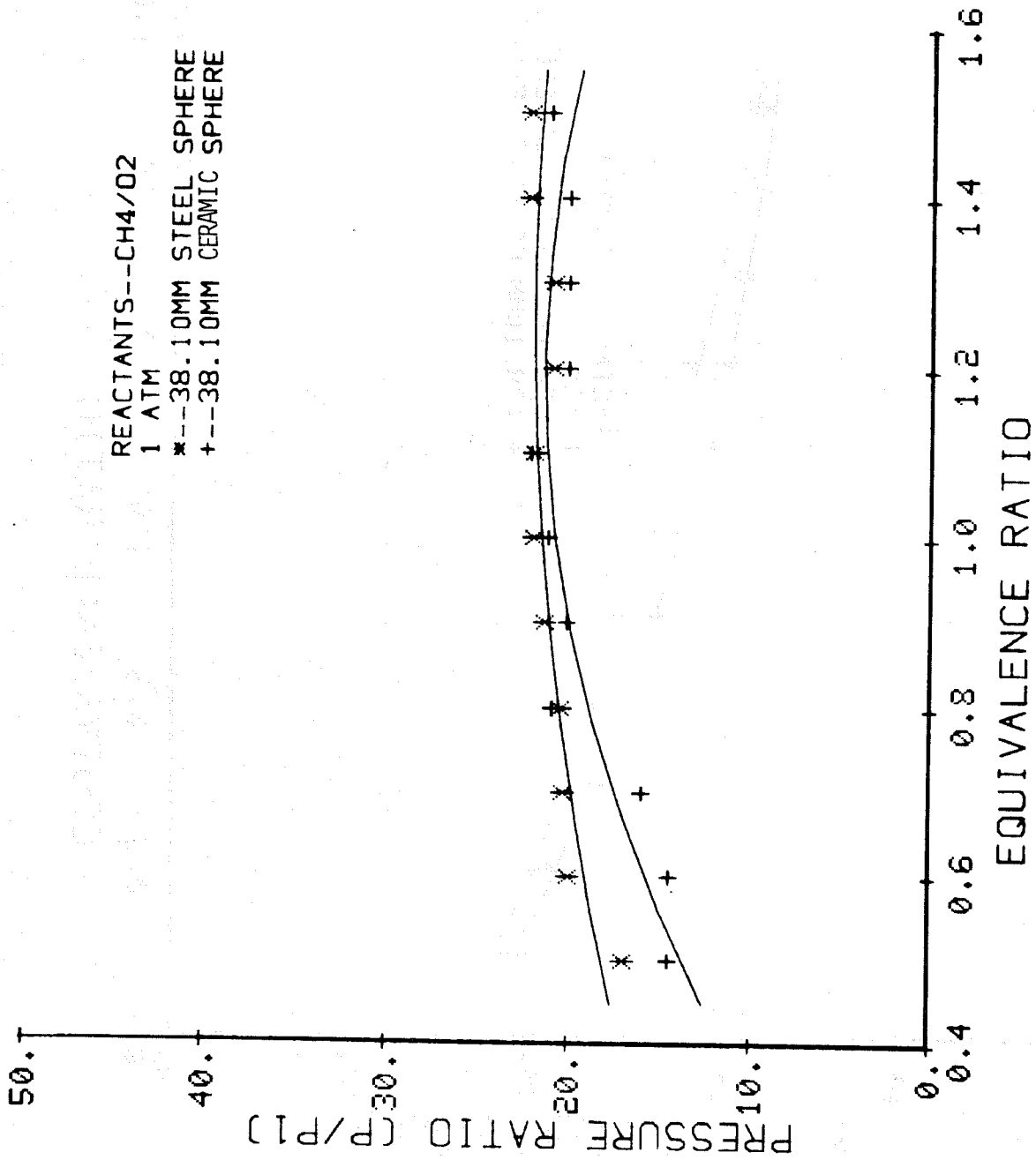


Figure 35. Pressure ratio versus equivalence ratio for different sphere materials.

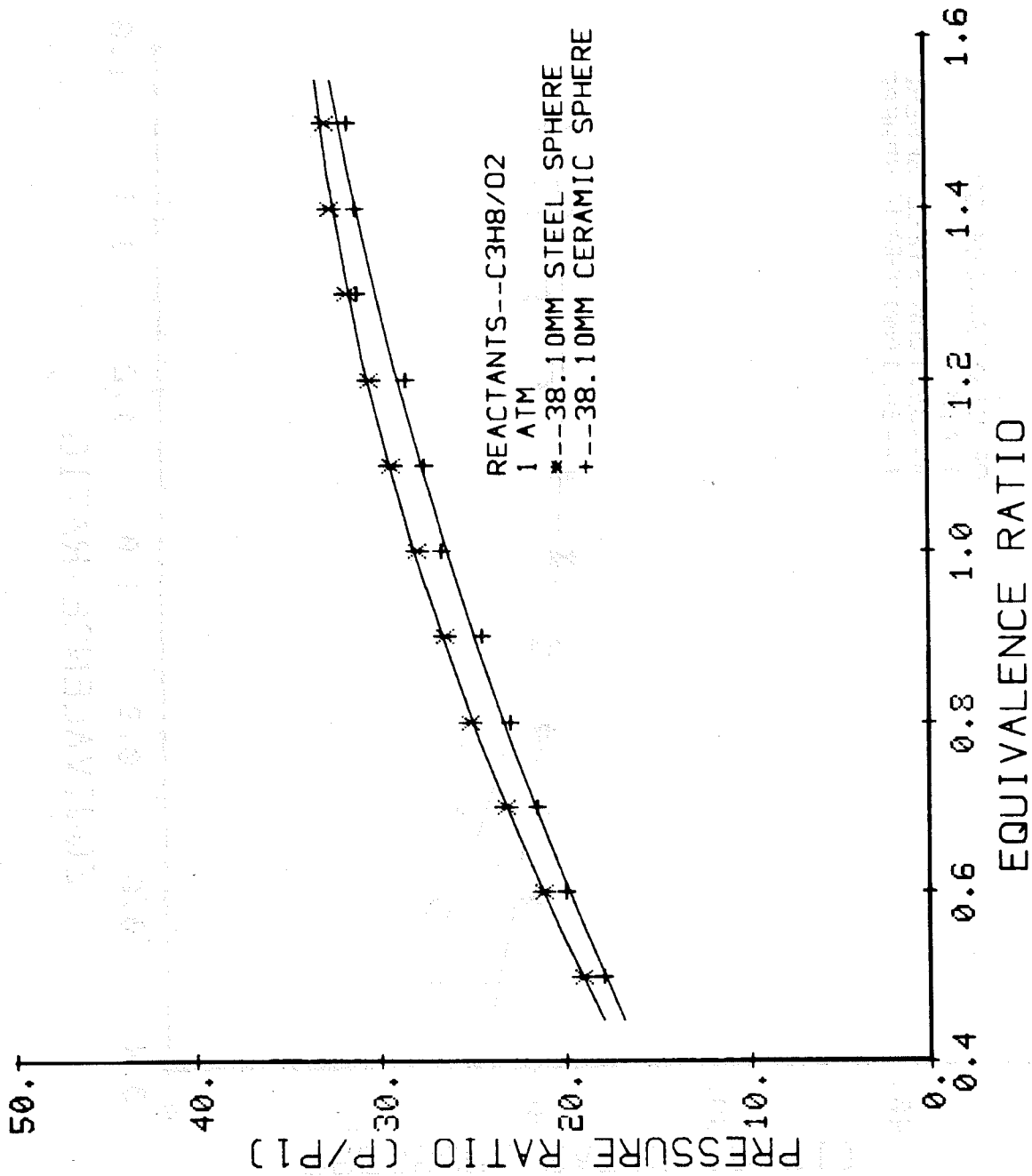
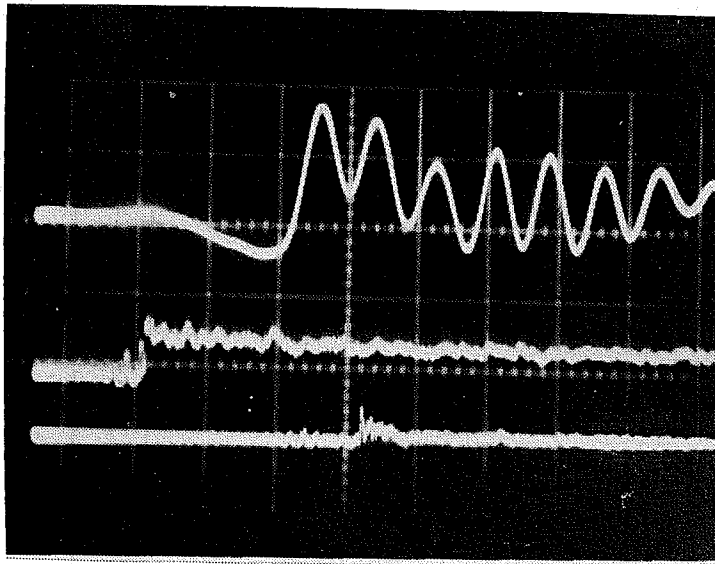


Figure 36. Pressure ratio versus equivalence ratio for different sphere materials.



$C_3H_8/O_2, = 1.0$

38.10mm steel sphere

$p_1 = 2 \text{ atm}$

sweep = 100 microsec./div.

1.0 volt/div.

50  $\mu$ strain/div.

1.01 psi/mv

Figure 37. Typical oscilloscope trace of dynamic strain.

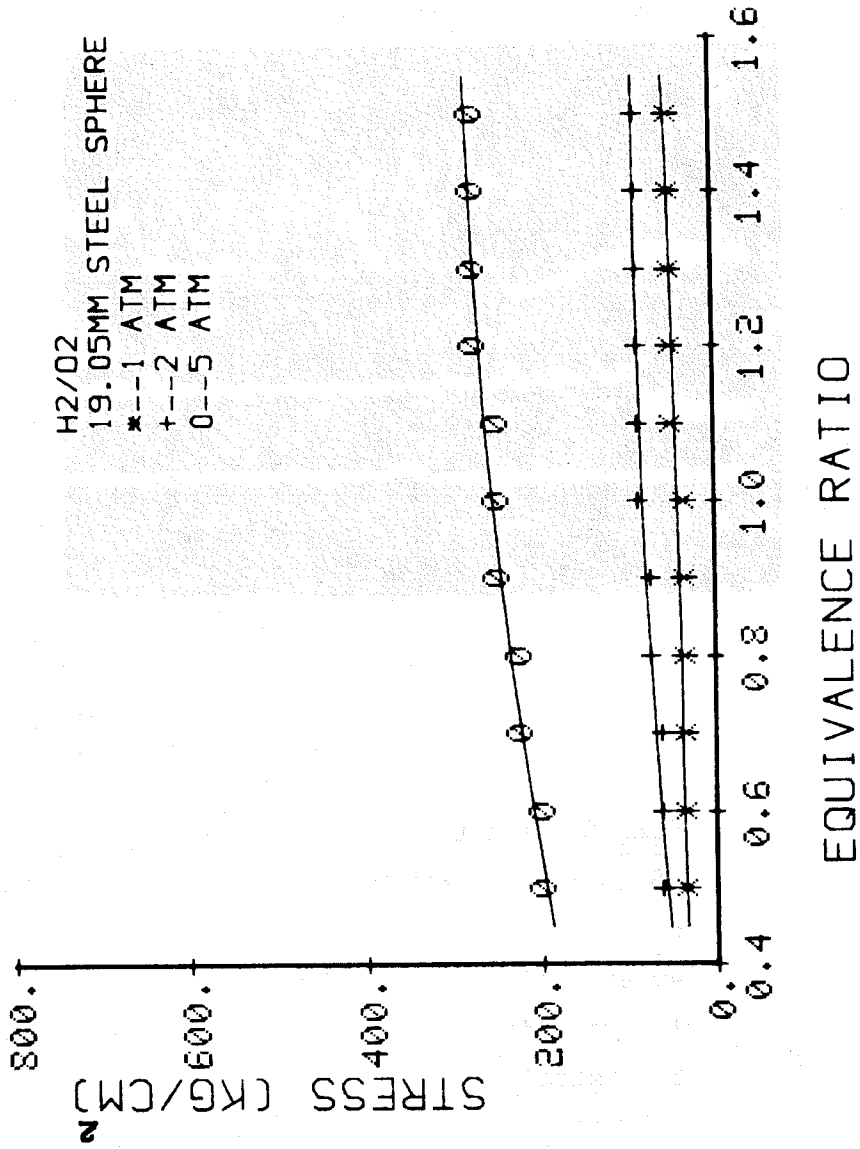


Figure 38. Dynamic stress versus equivalence ratio for various initial pressures.

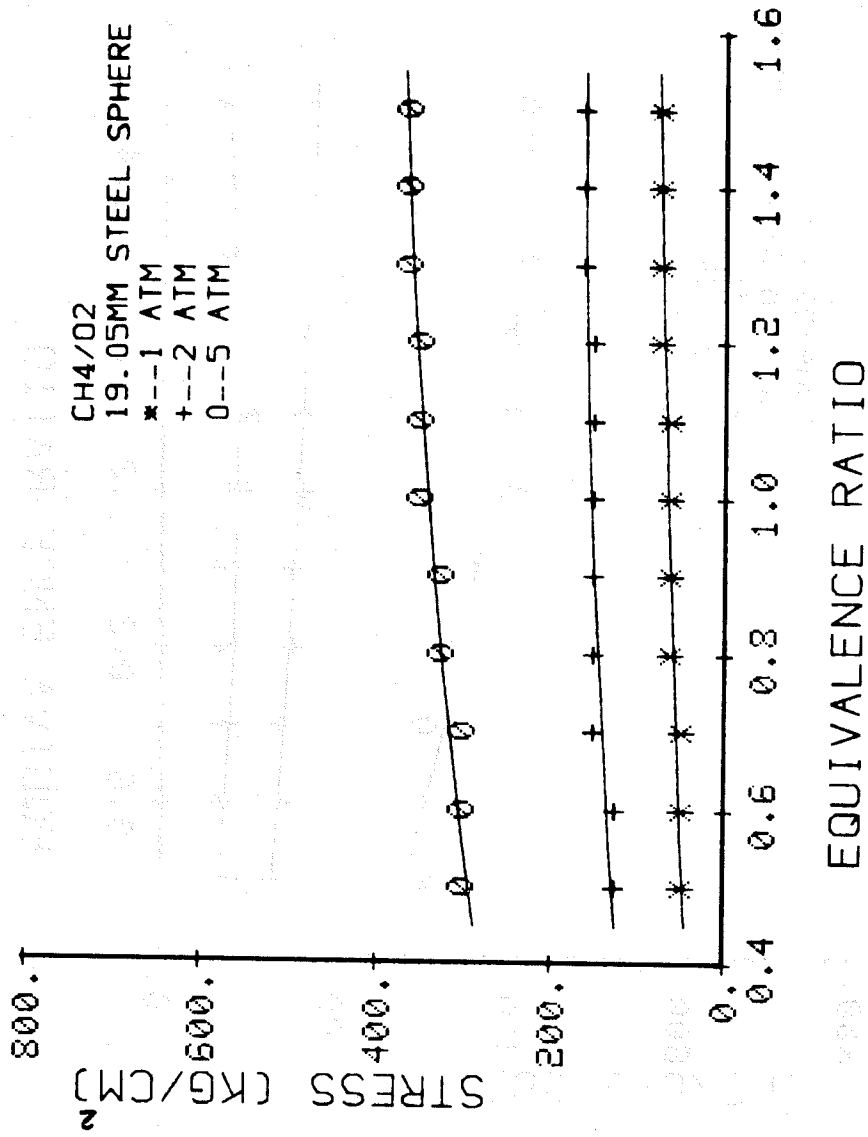


Figure 39. Dynamic stress versus equivalence ratio for various initial pressures.

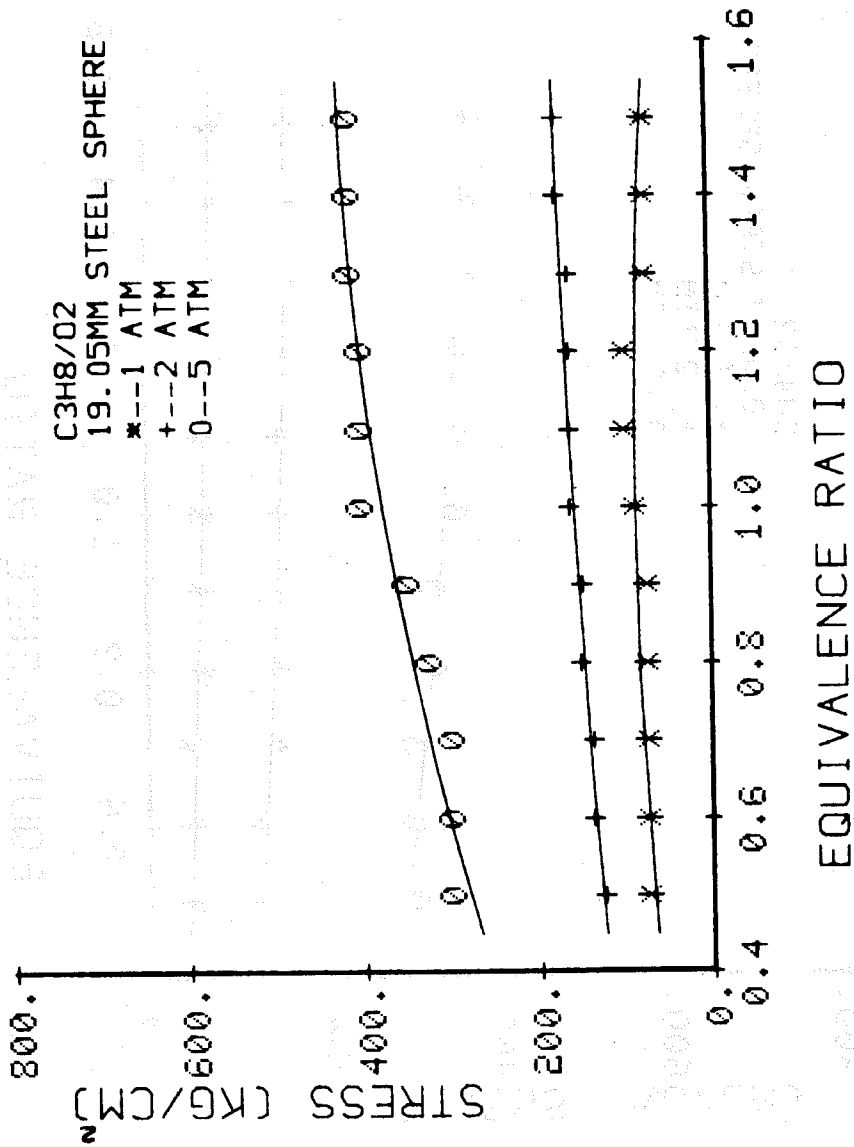


Figure 40. Dynamic stress versus equivalence ratio for various initial pressures.

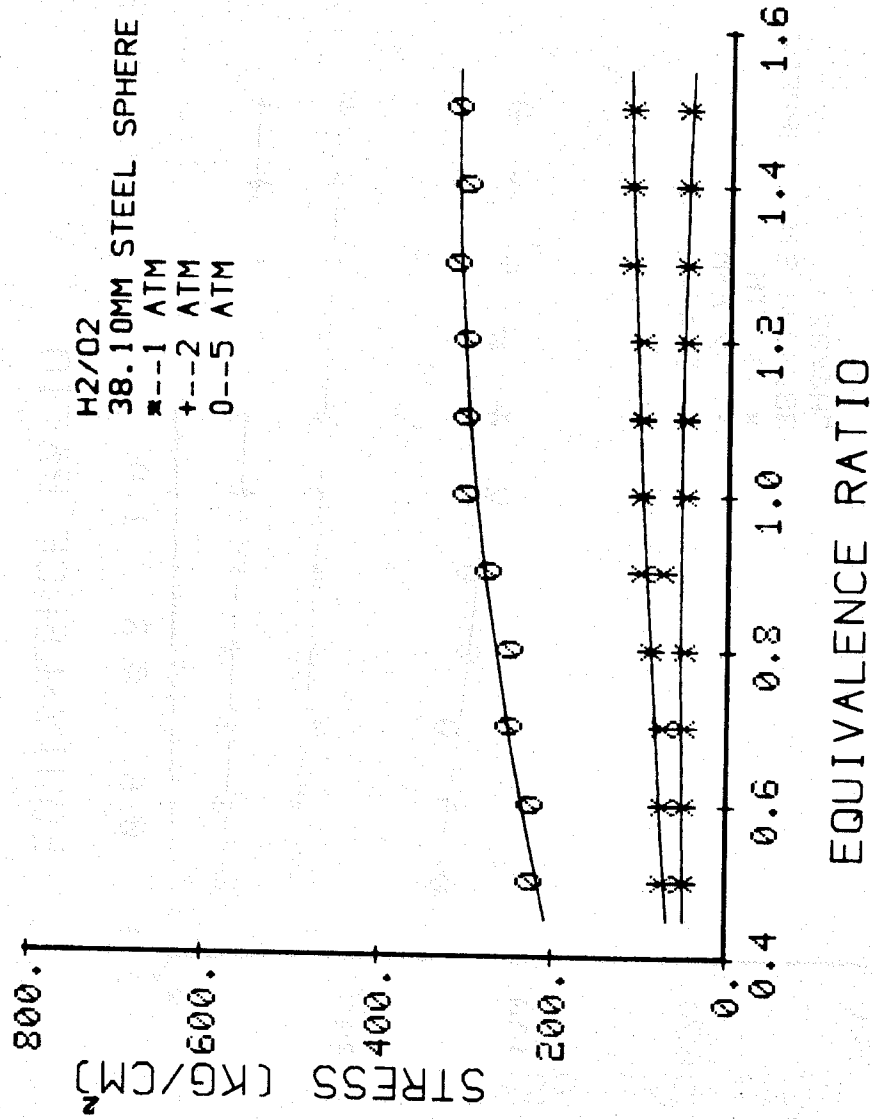


Figure 41. Dynamic stress versus equivalence ratio for various initial pressures.

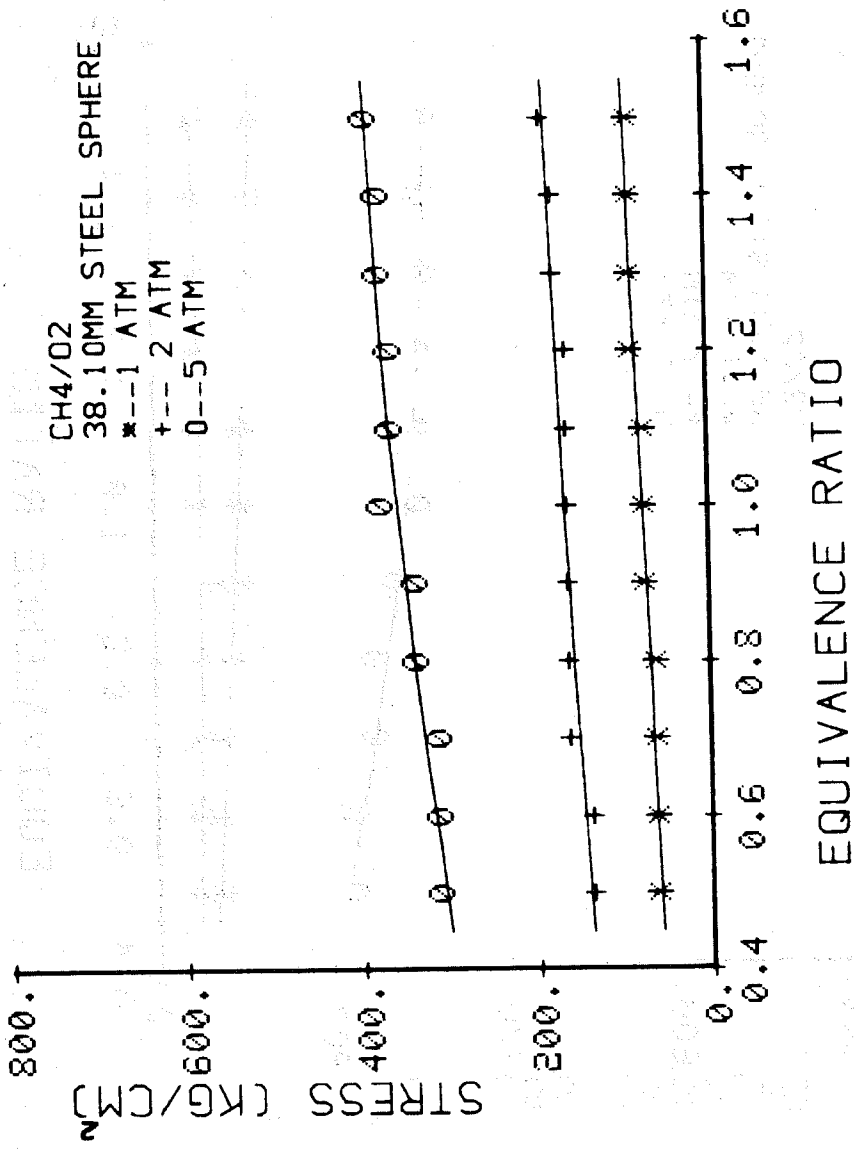


Figure 42. Dynamic stress versus equivalence ratio for various initial pressures.

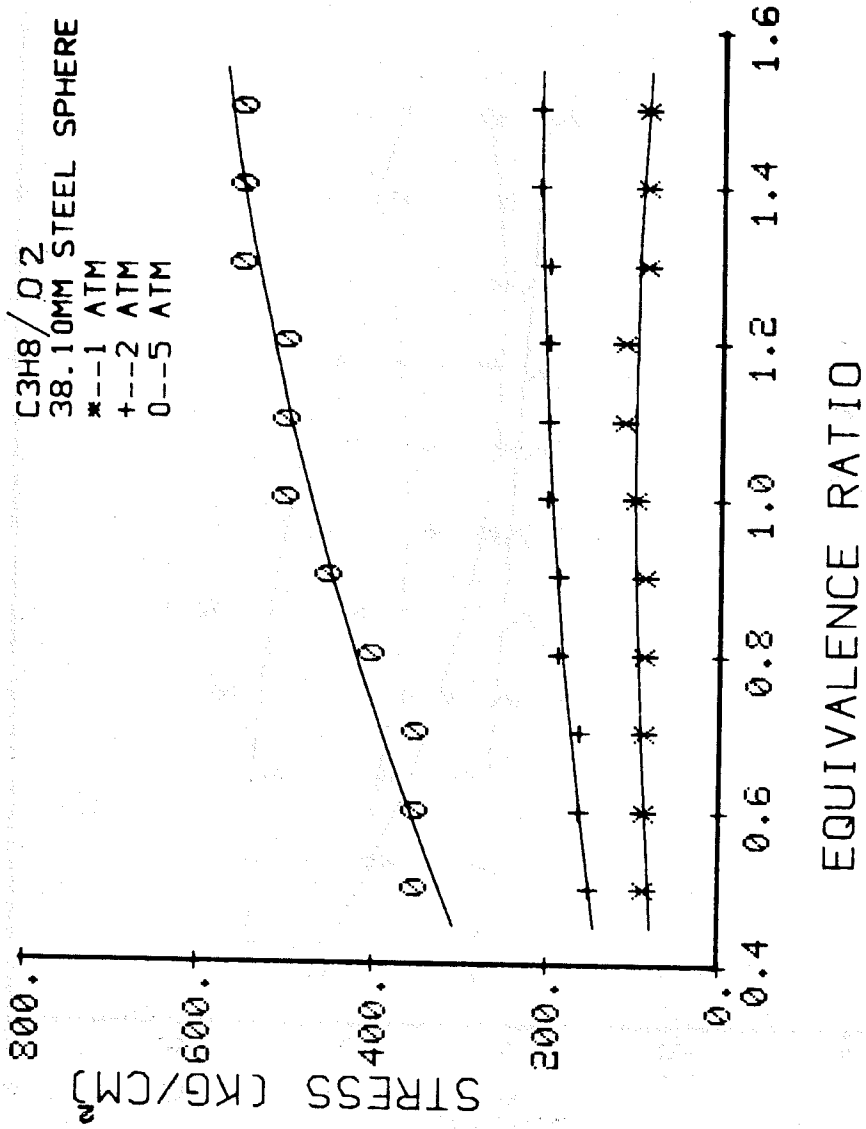


Figure 43. Dynamic stress versus equivalence ratio for various initial pressures.

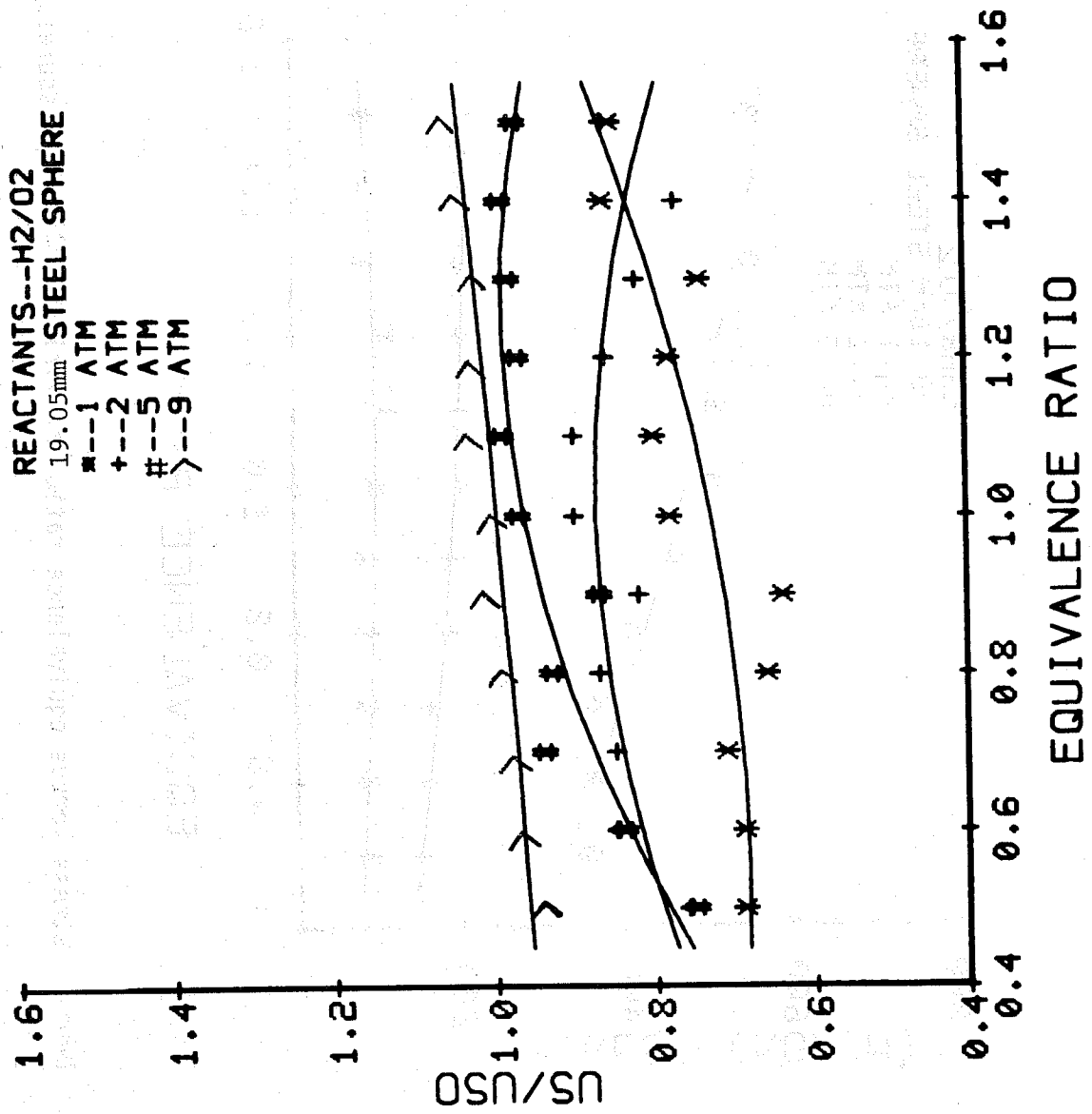


Figure 44. Normalized velocities versus equivalence ratio for various initial pressures.

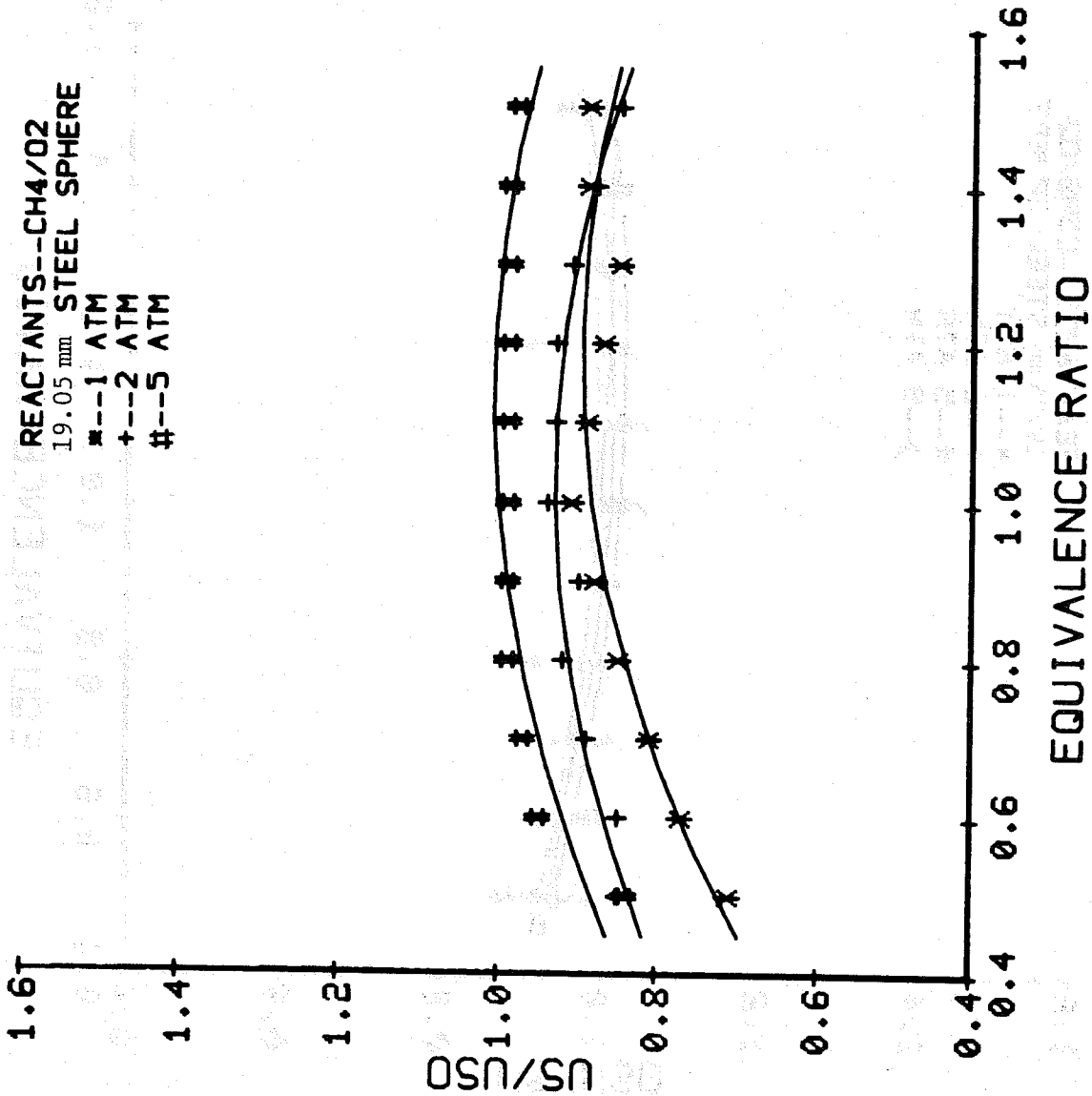


Figure 45. Normalized velocities versus equivalence ratio for various initial pressures.

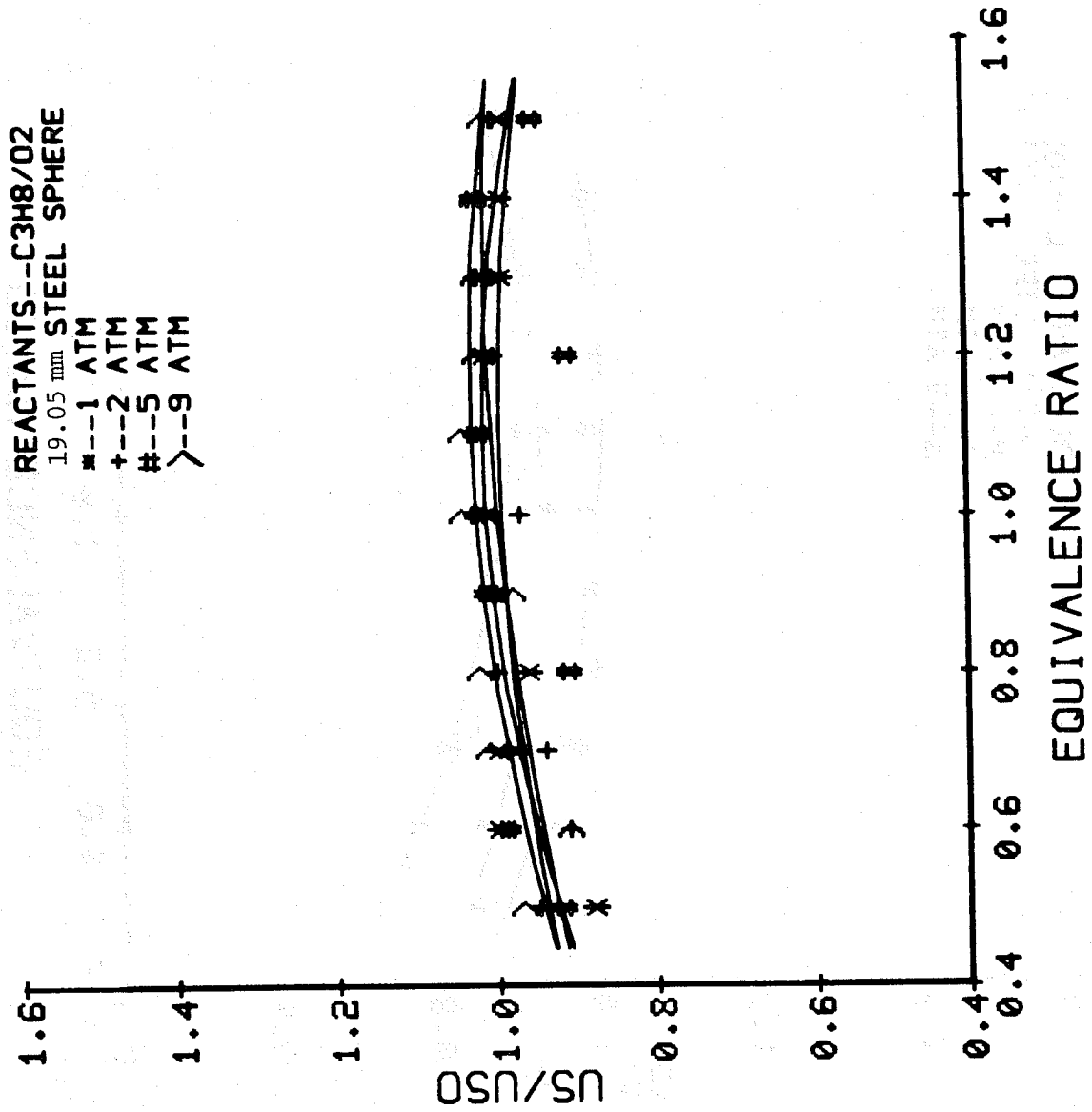


Figure 46. Normalized velocities versus equivalence ratio for various initial pressures.

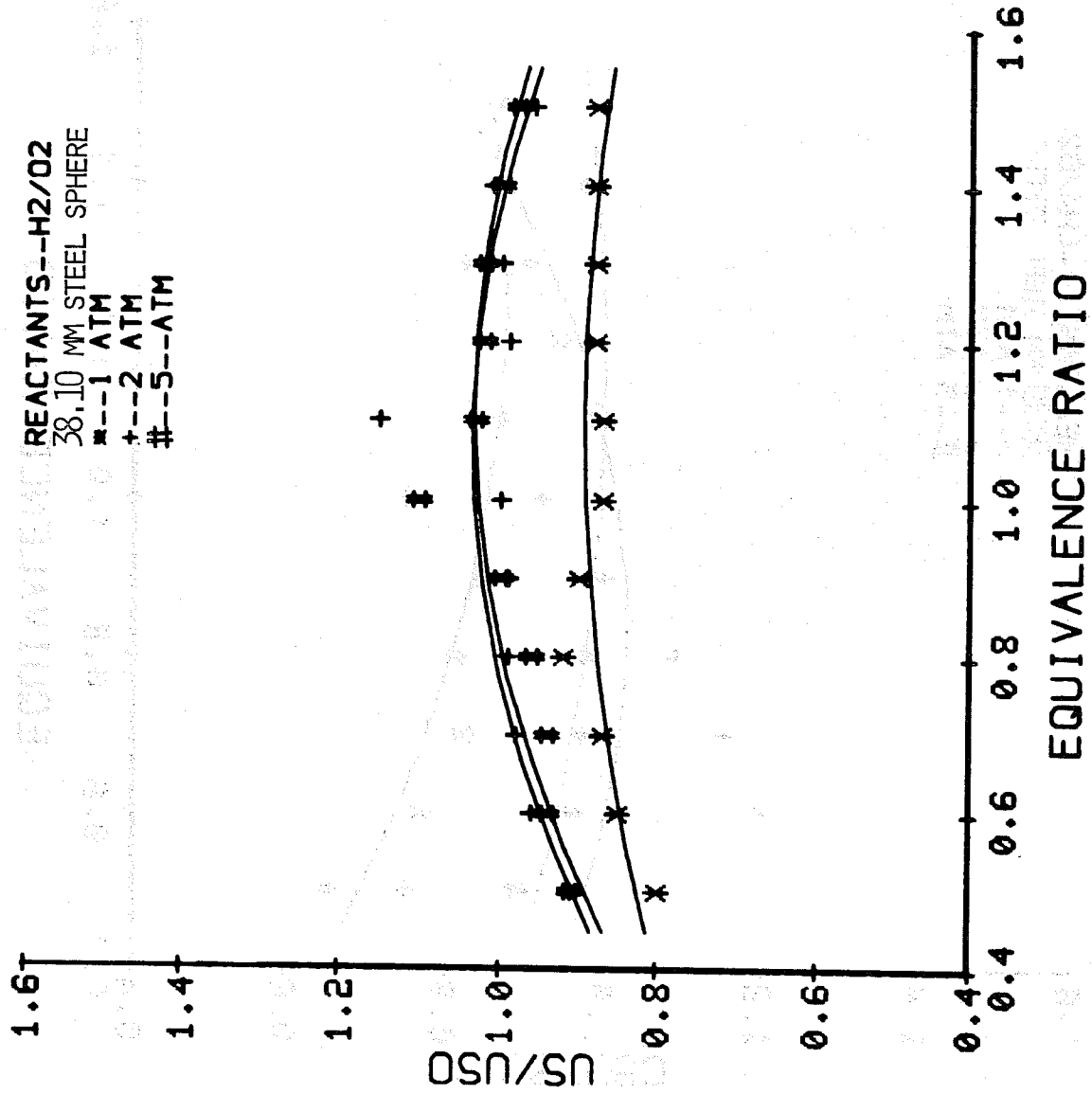


Figure 47. Normalized velocities versus equivalence ratio for various initial pressures.

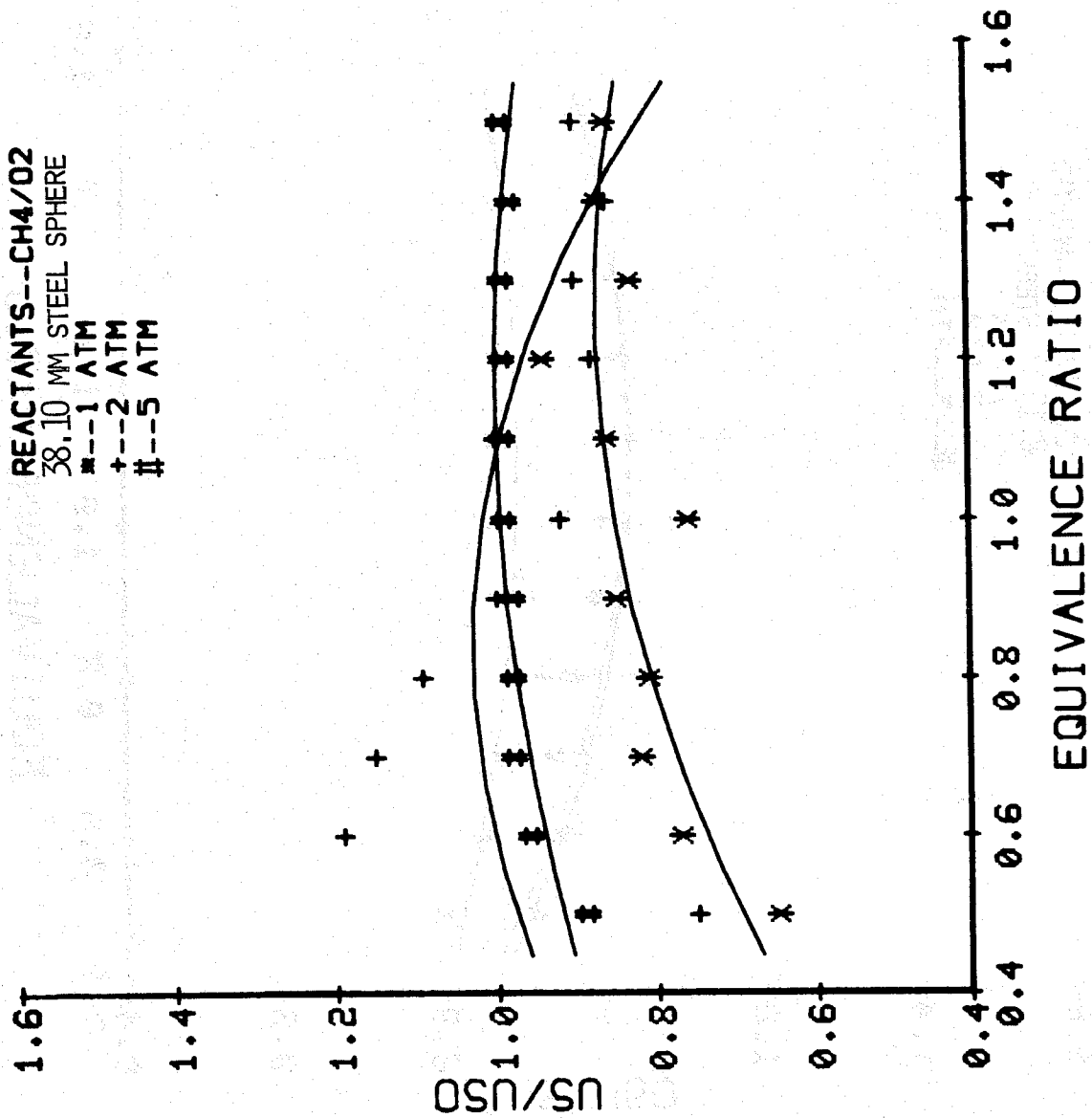


Figure 48. Normalized velocities versus equivalence ratio for various initial pressures.

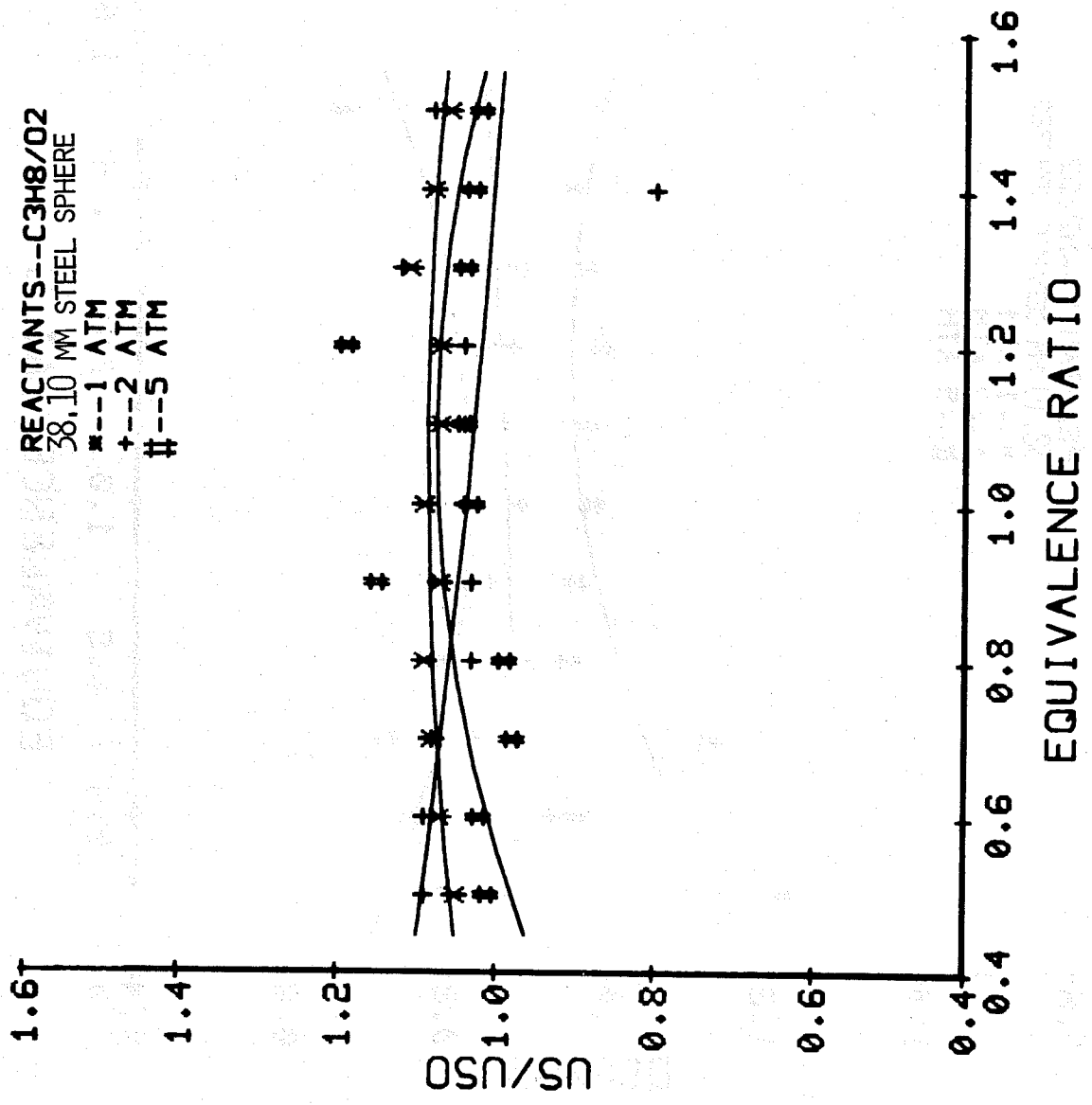


Figure 49. Normalized velocities versus equivalence ratio for various initial pressures.

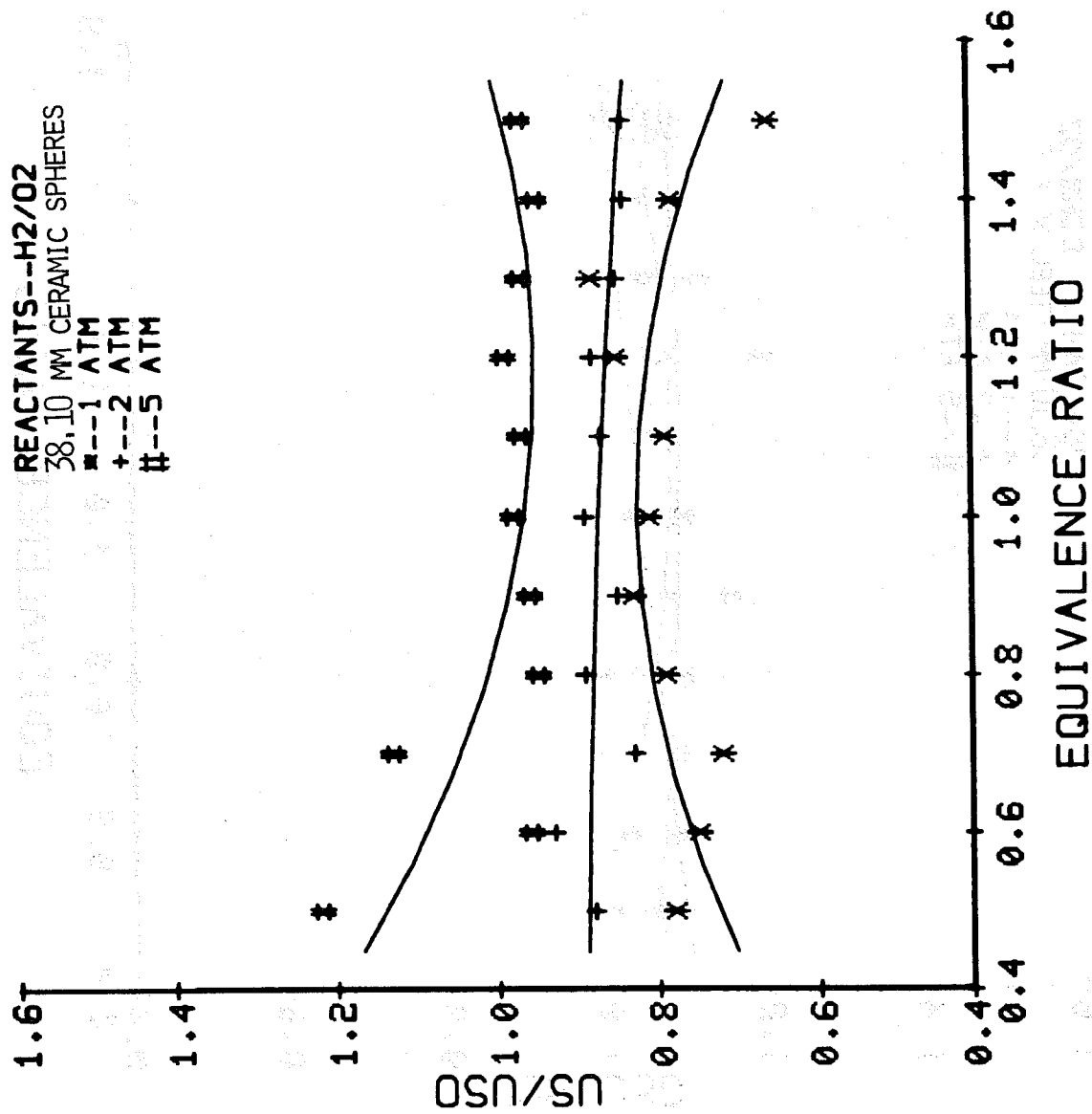


Figure 50. Normalized velocities versus equivalence ratio for various initial pressures.

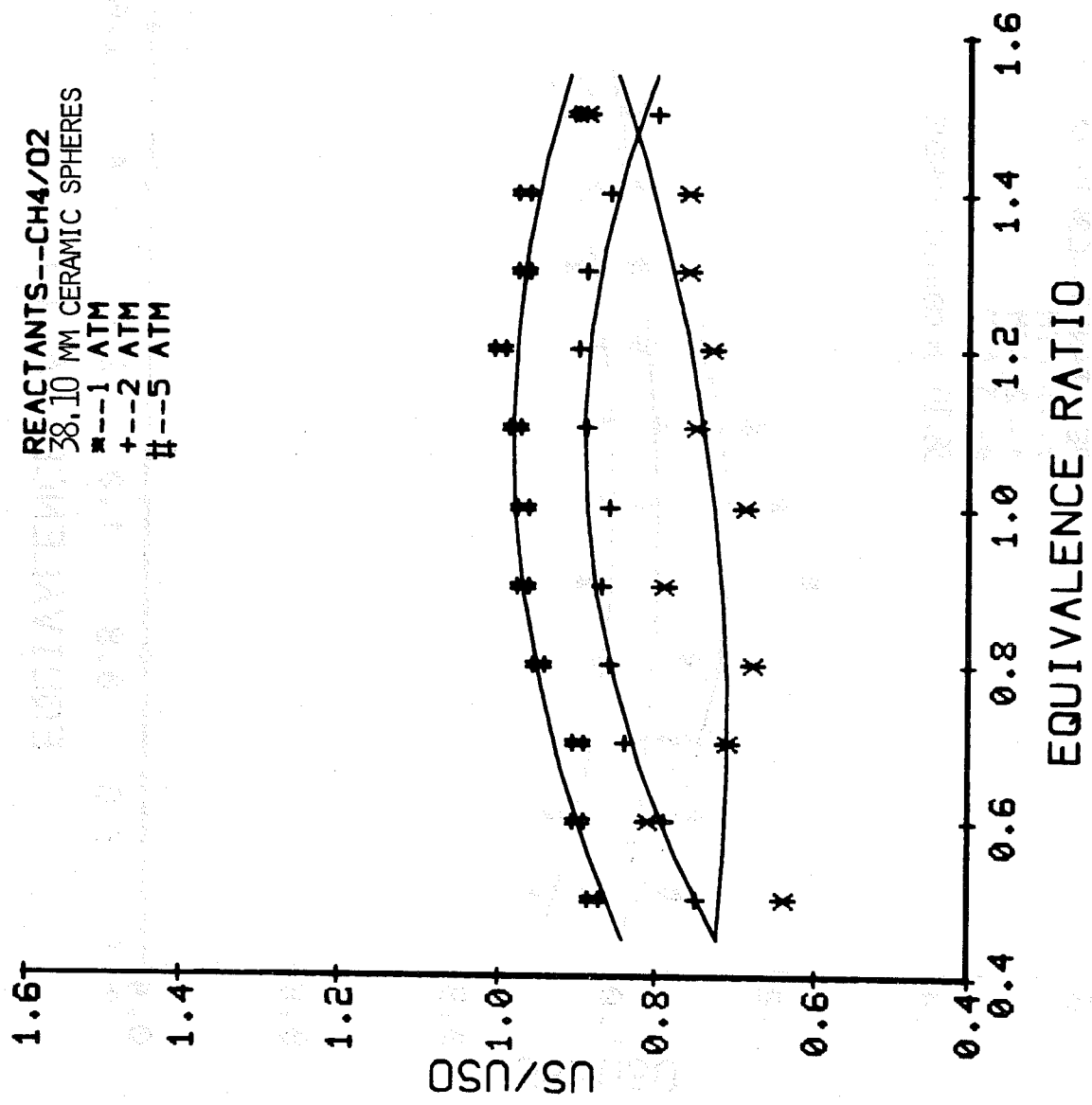


Figure 51. Normalized velocities versus equivalence ratio for various initial pressures.

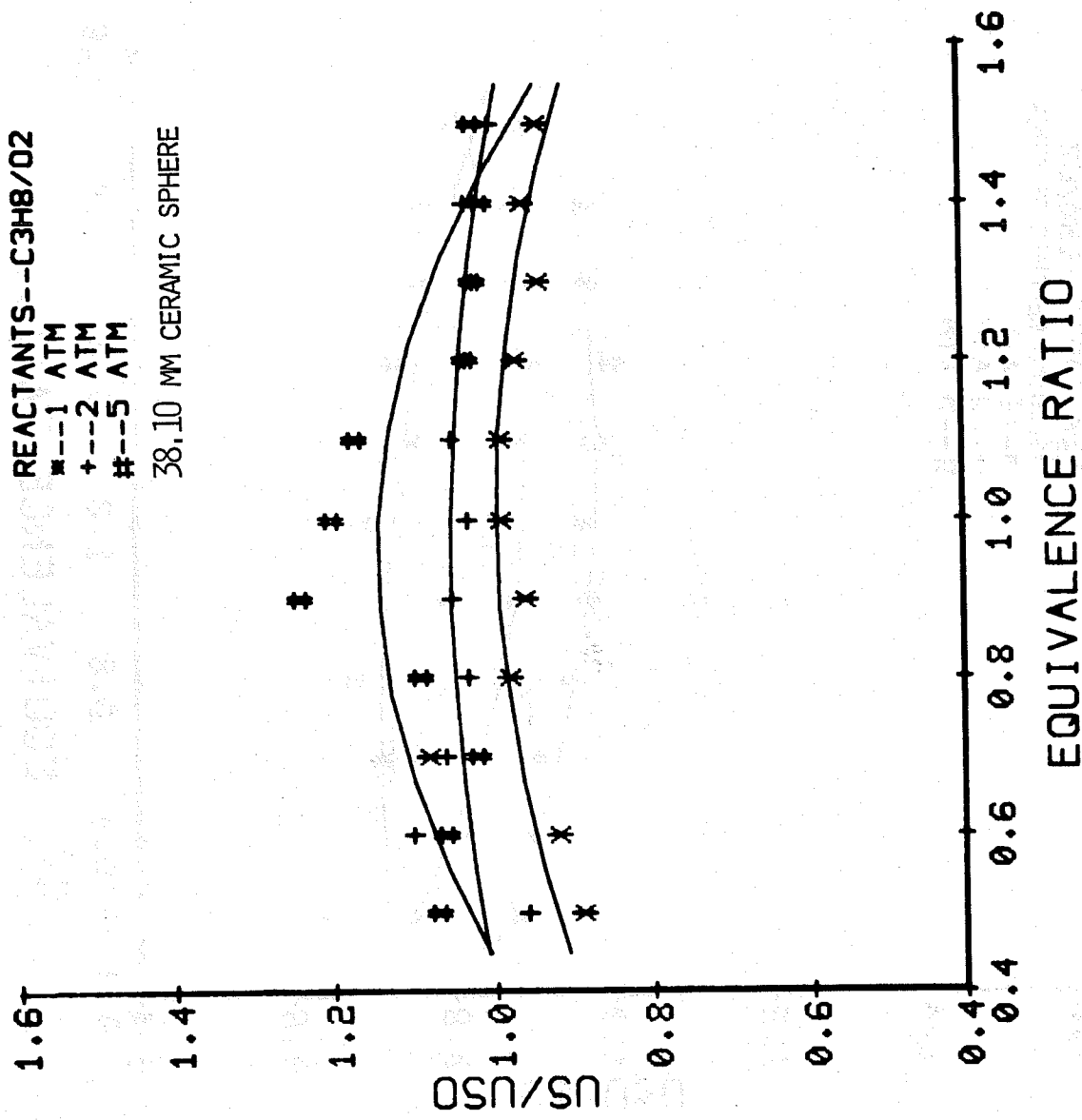


Figure 52. Normalized velocities versus equivalence ratio for various initial pressures.

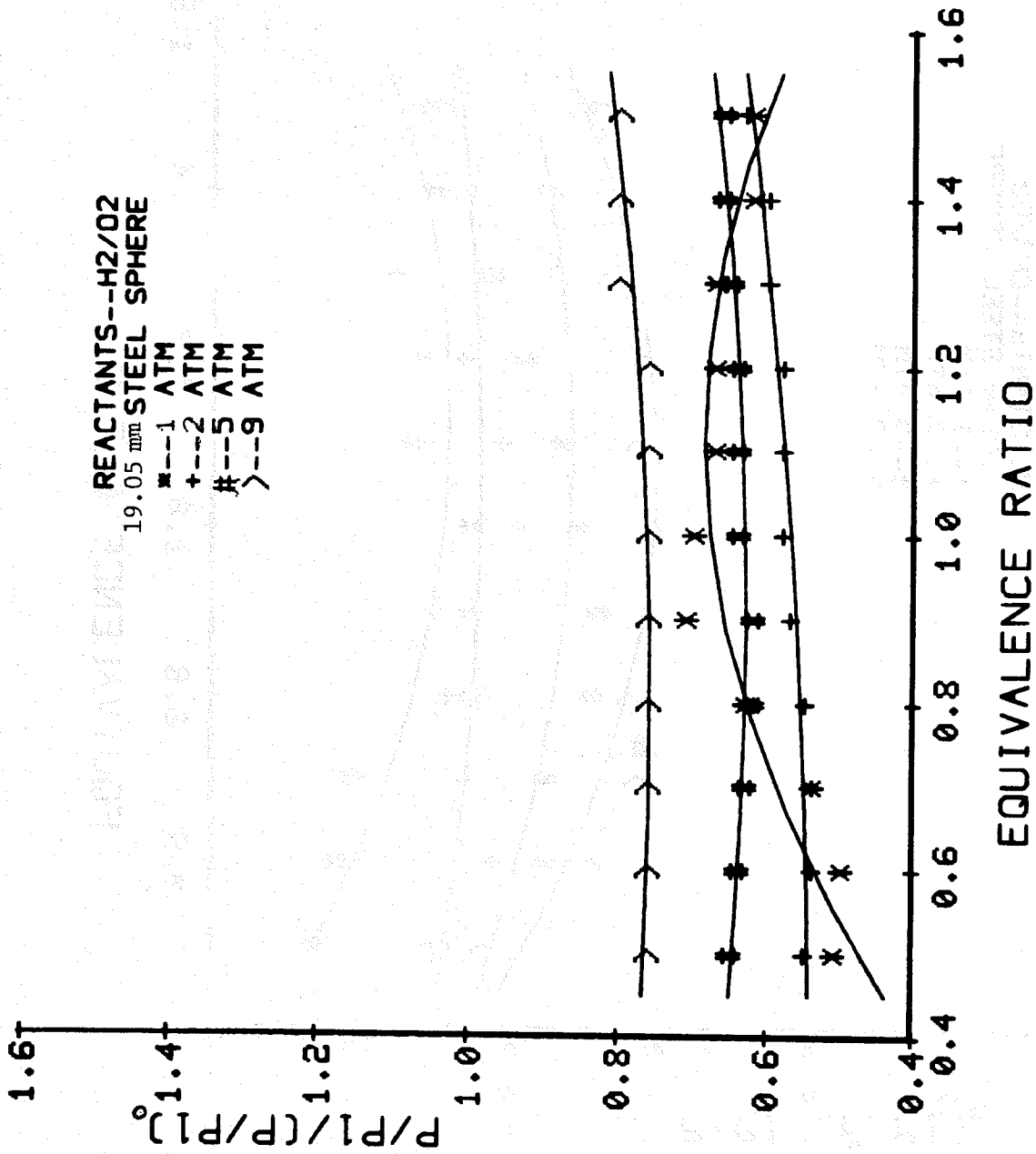


Figure 53. Normalized pressure ratios versus equivalence ratio for various initial pressures.

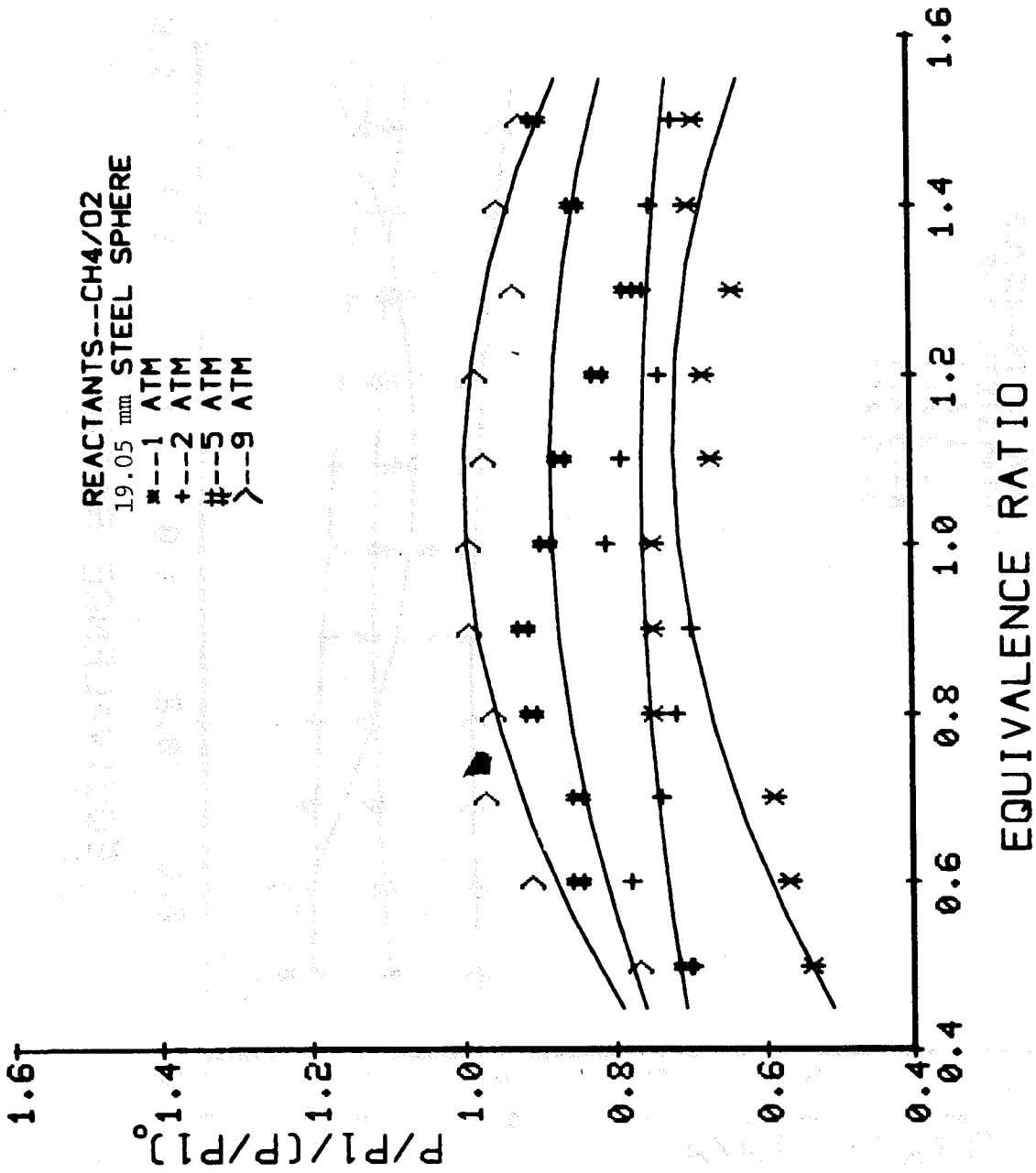


Figure 54. Normalized pressure ratios versus equivalence ratio for various initial pressures.

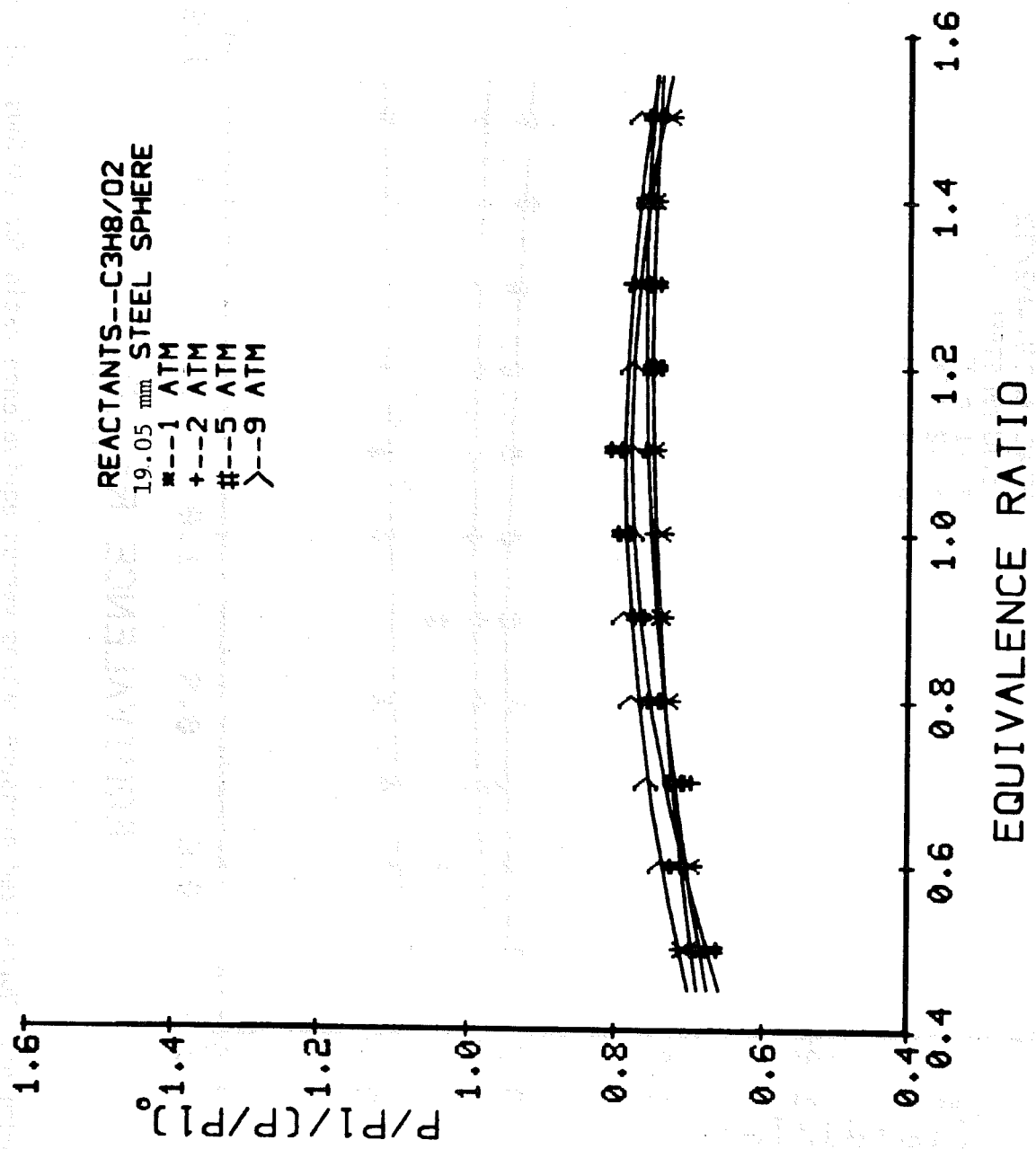


Figure 55. Normalized pressure ratios versus equivalence ratio for various initial pressures.

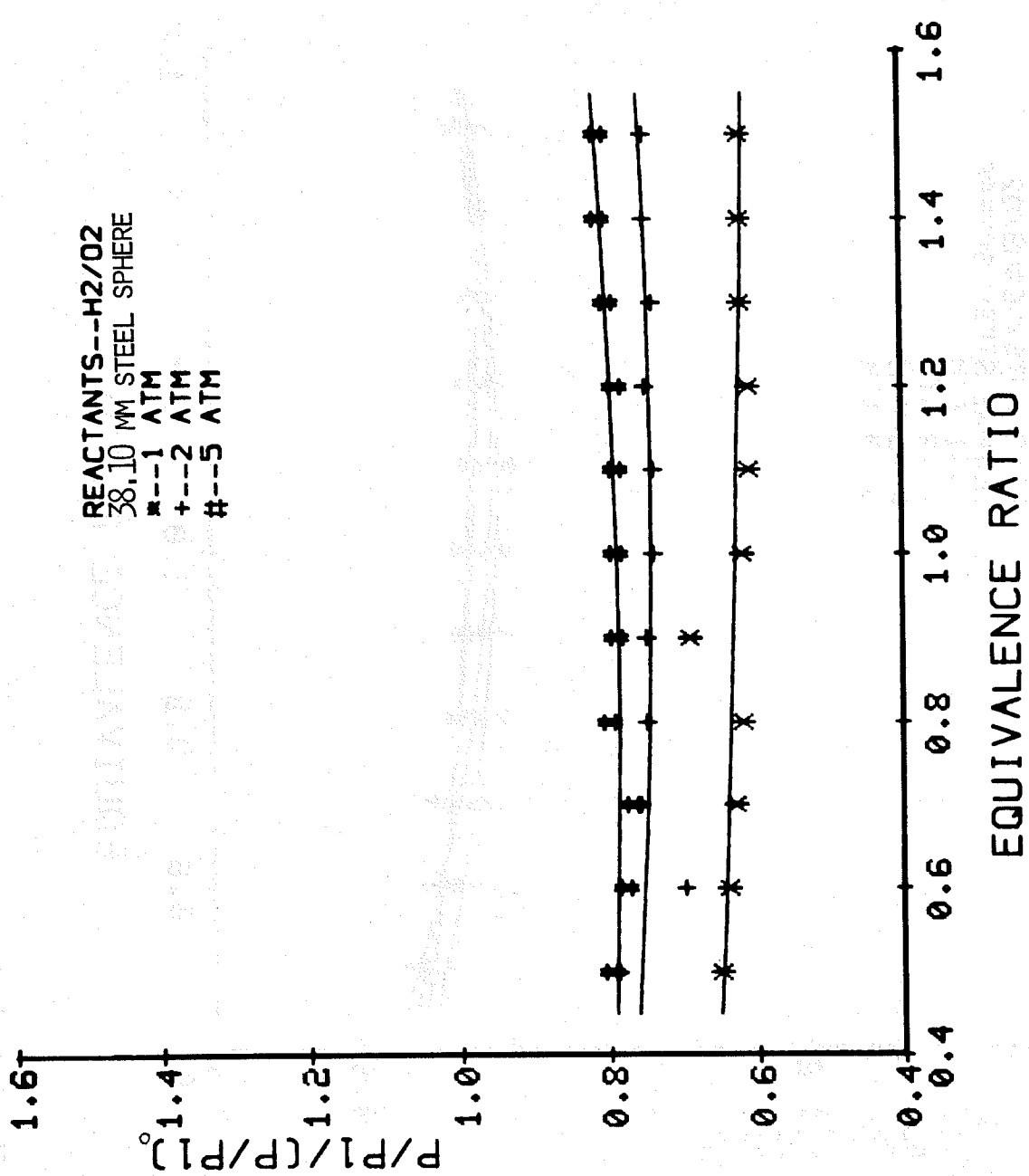


Figure 56. Normalized pressure ratios versus equivalence ratio for various initial pressures.

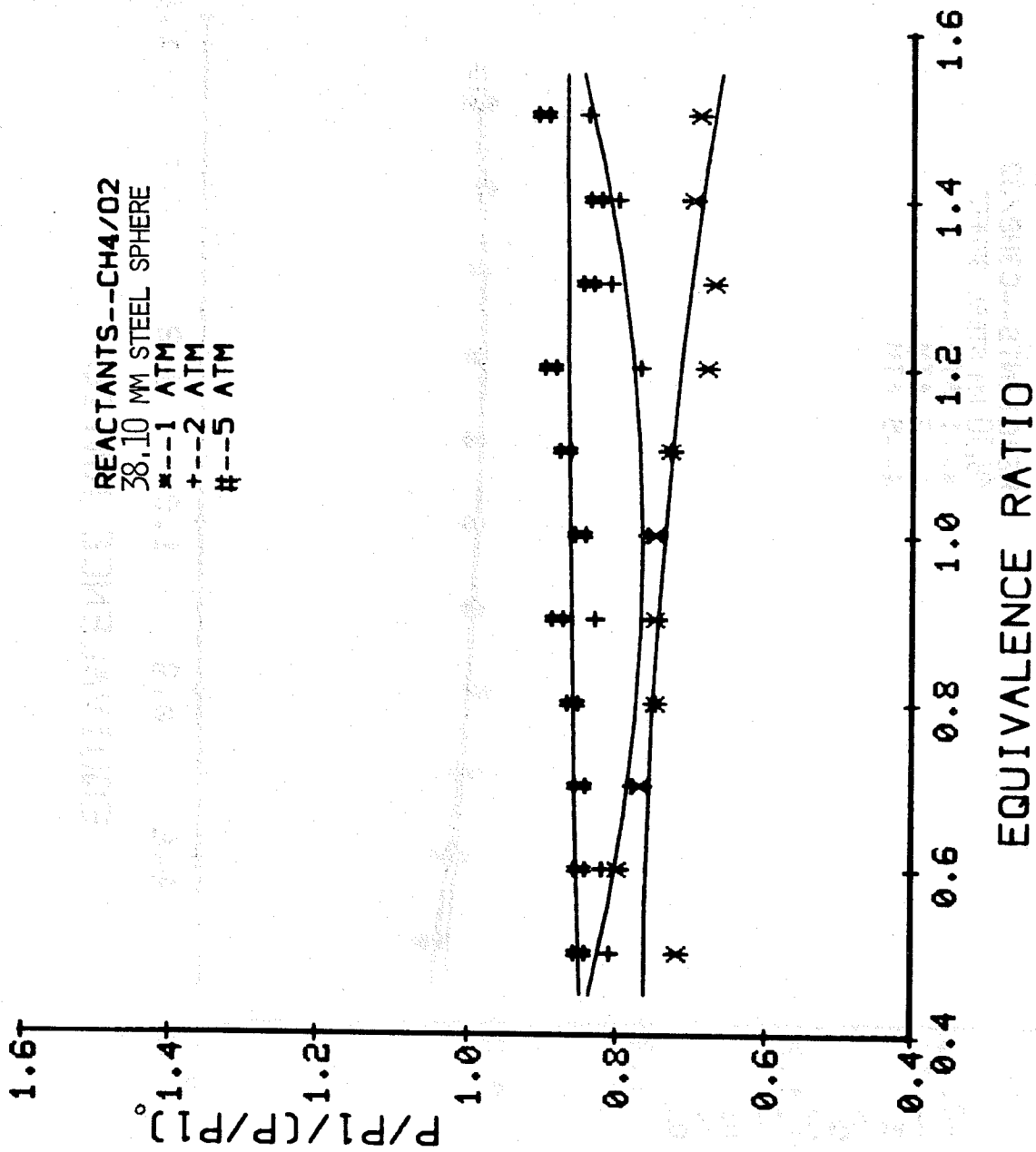


Figure 57. Normalized pressure ratios versus equivalence ratio for various initial pressures.

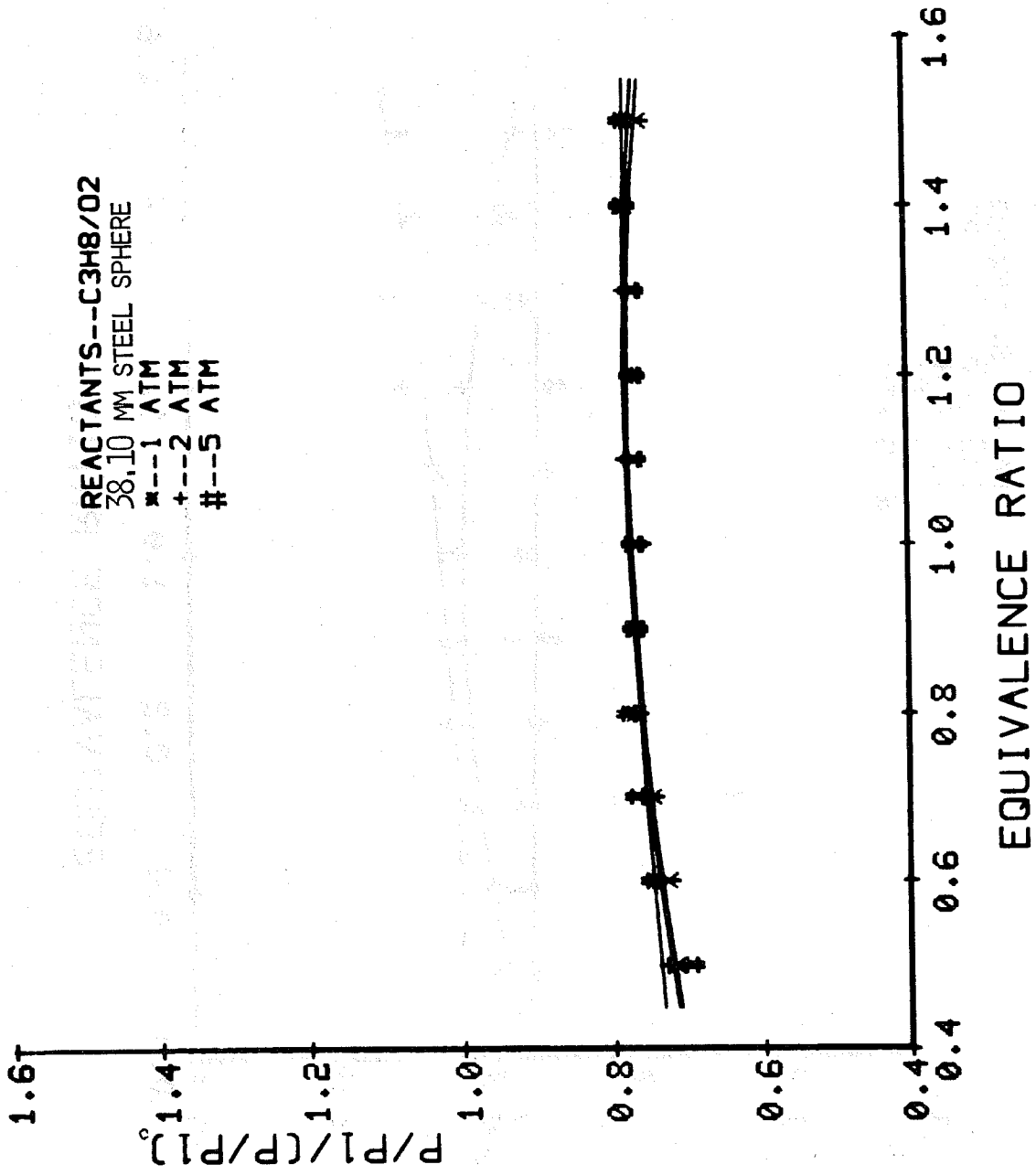


Figure 58. Normalized pressure ratios versus equivalence ratio for various initial pressures.

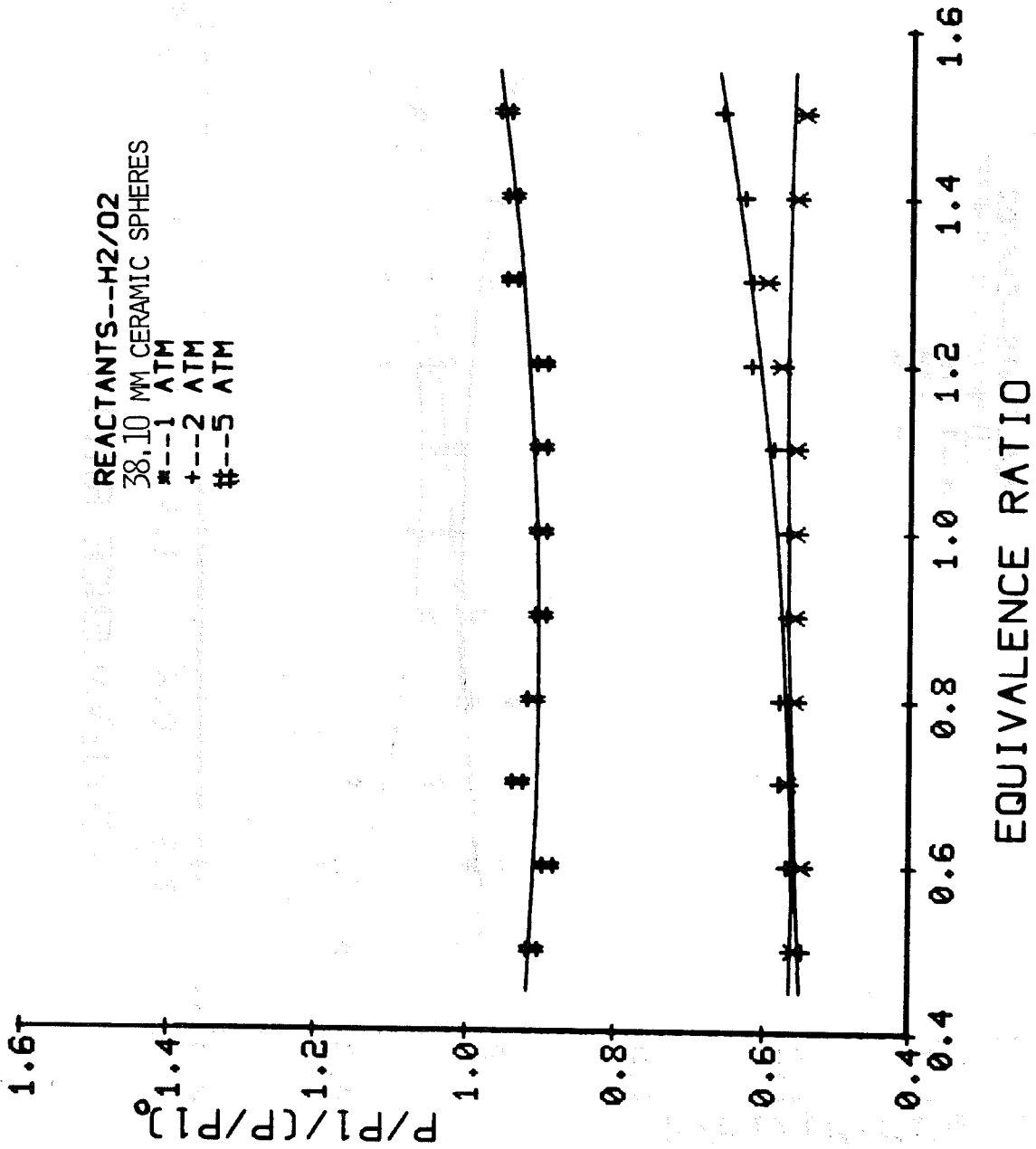


Figure 59. Normalized pressure ratios versus equivalence ratio for various initial pressures.

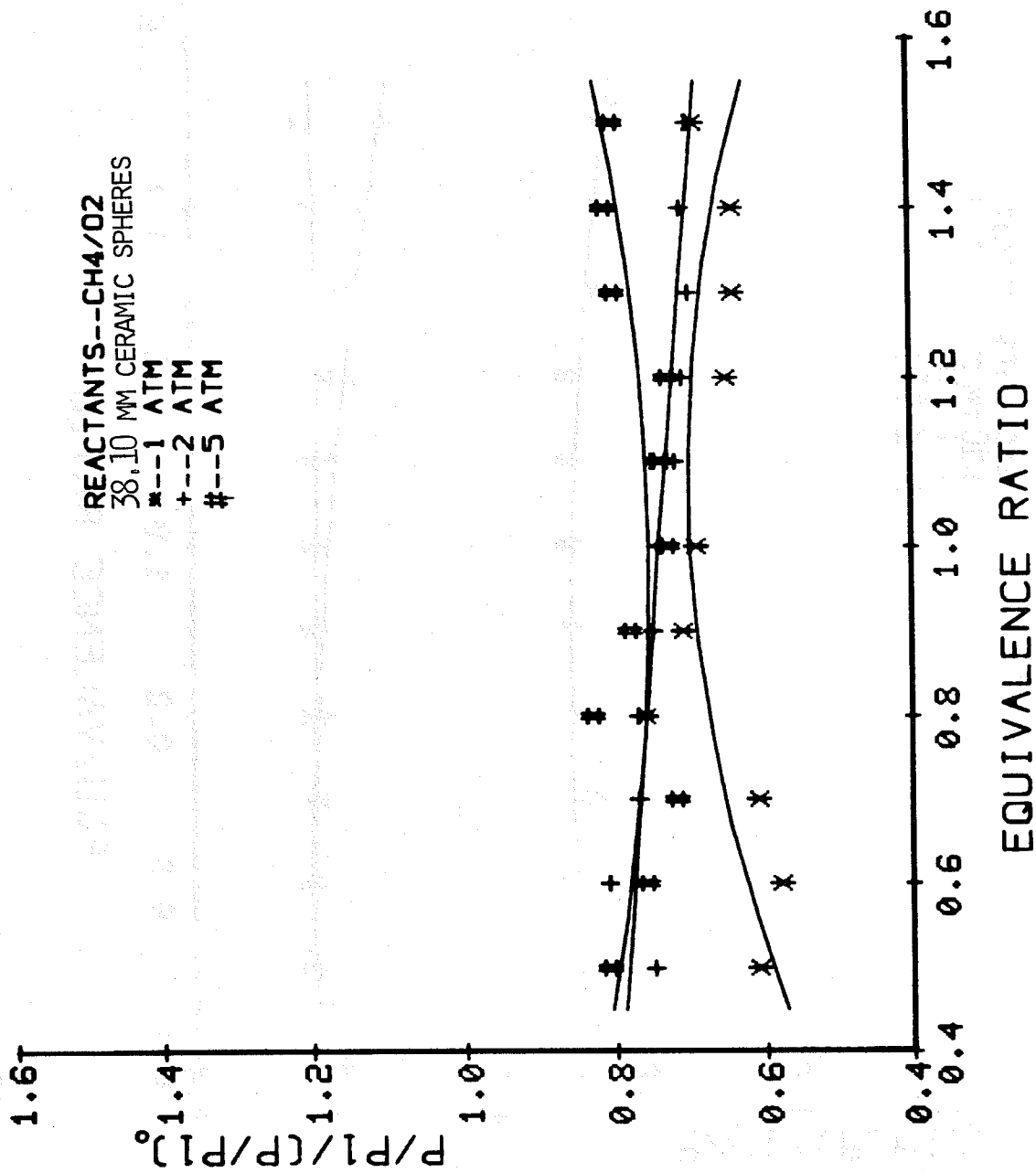


Figure 60. Normalized pressure ratios versus equivalence ratio for various initial pressures.

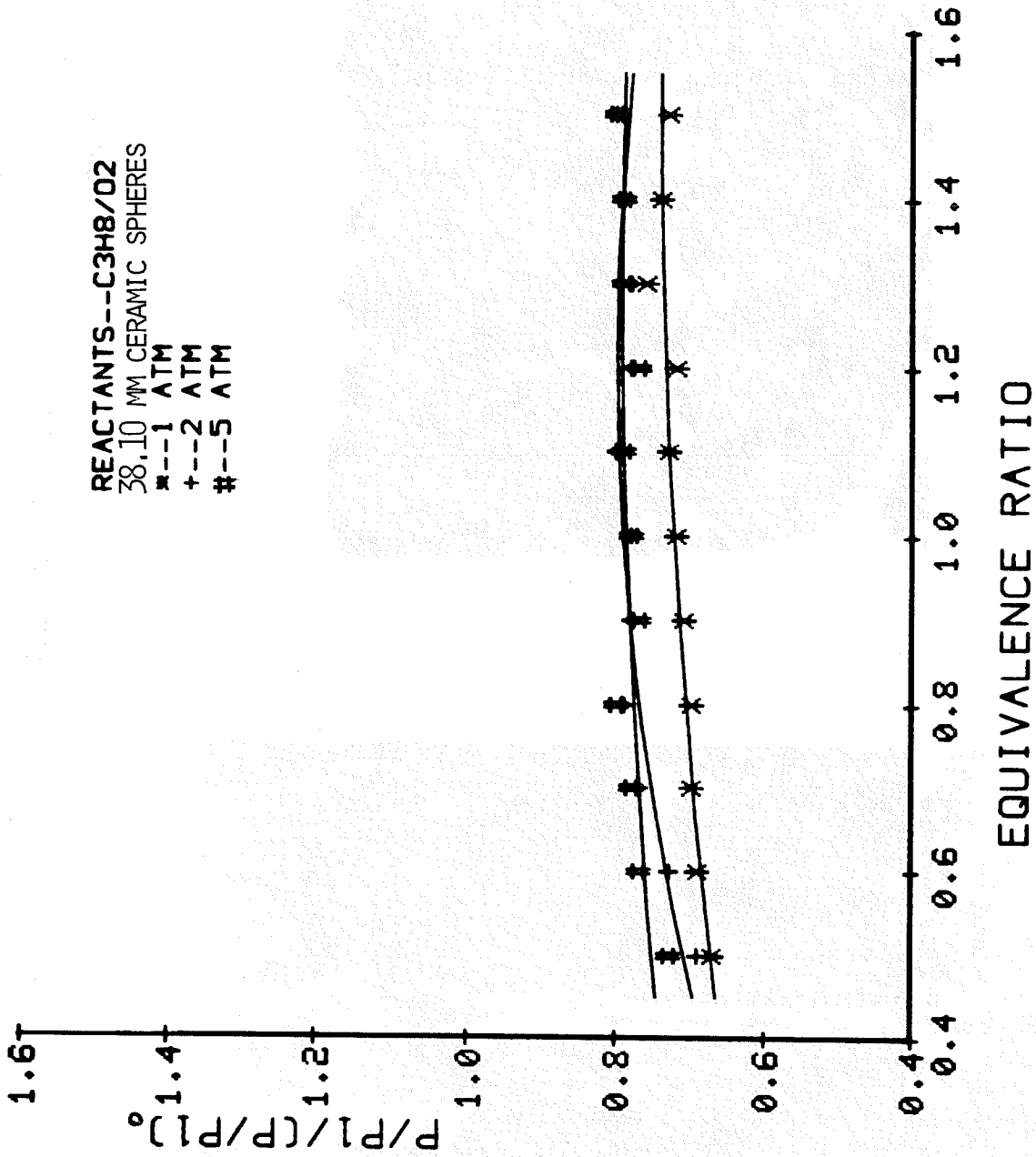
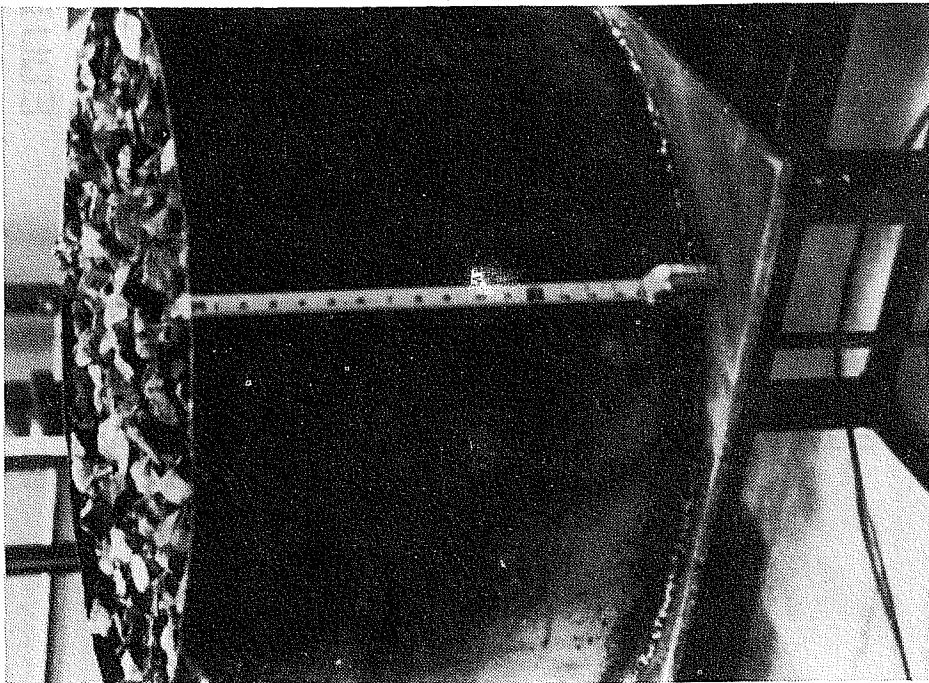
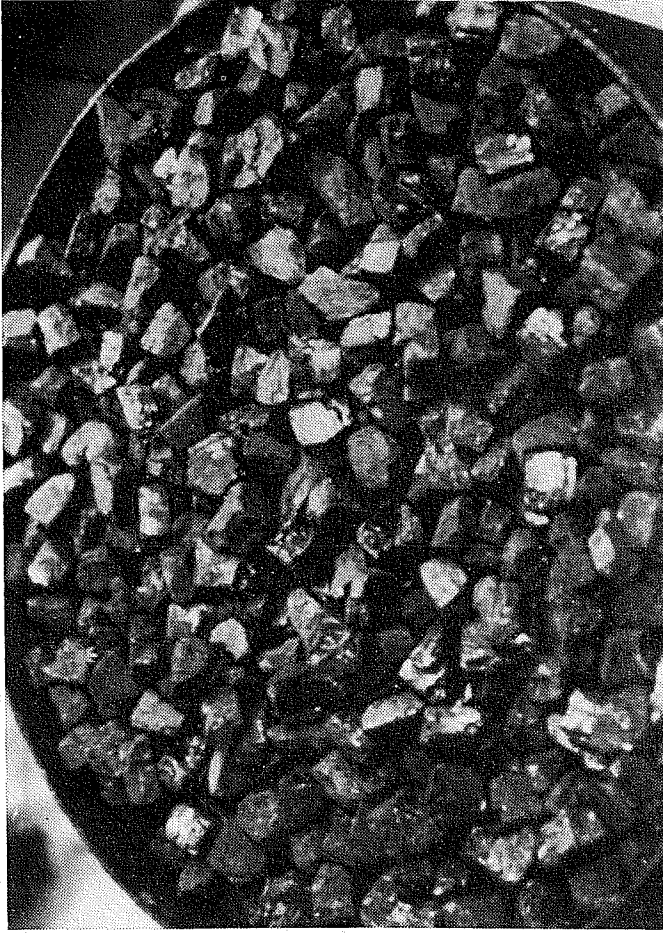


Figure 61. Normalized pressure ratios versus equivalence ratio for various initial pressures.



a. Tank

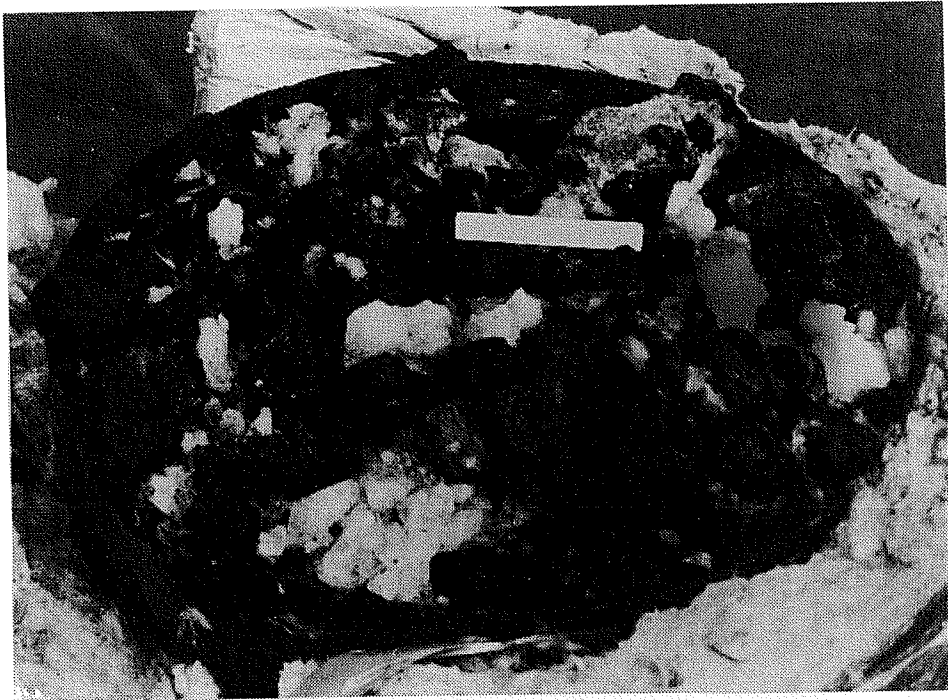


b. Unfrozen

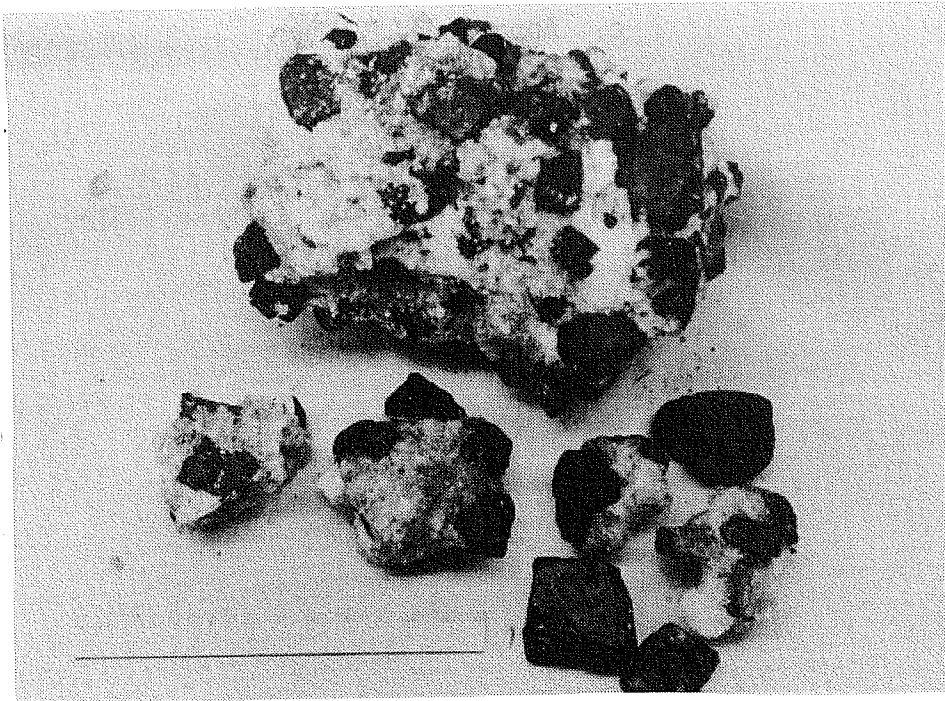
Figure 62. Coal Pile



c. Apparatus

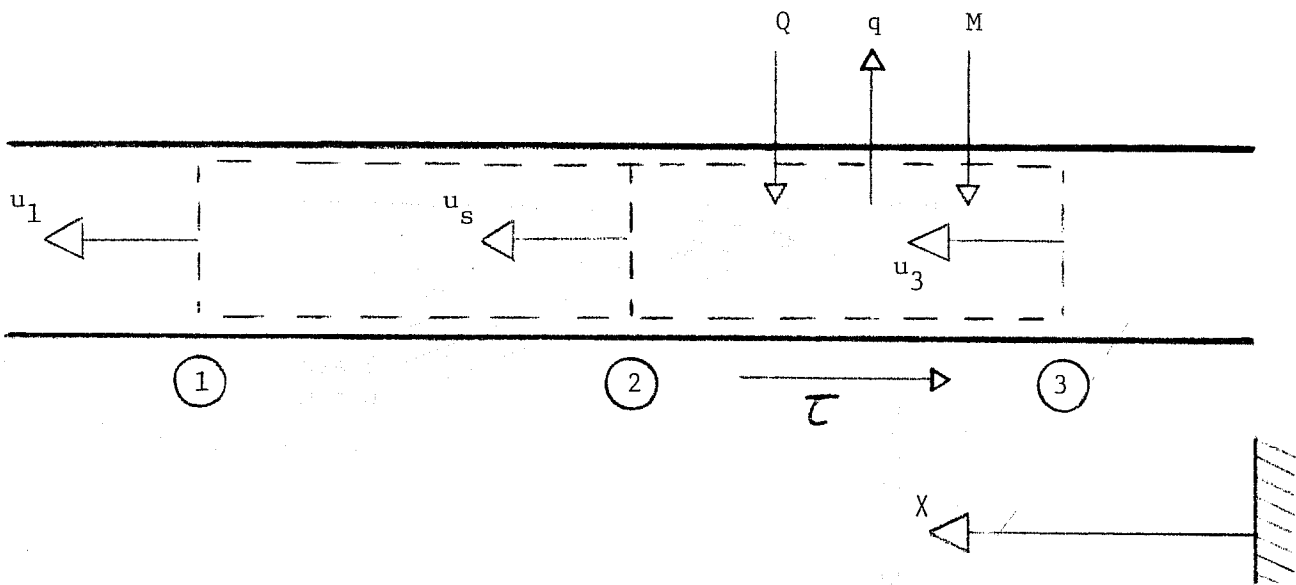


a

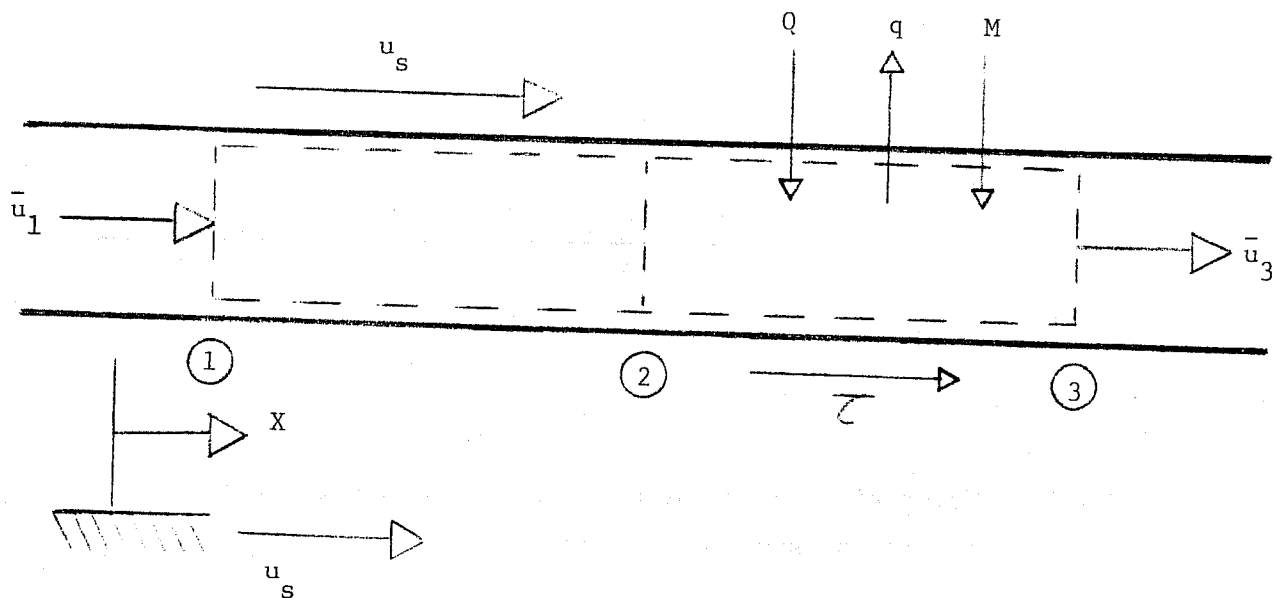


b

Figure 63. Fractured Coal Pile



(a) Wall Fixed Coordinates



(b) Shock Fixed Coordinates

Fig. 64 Control volume and coordinate system for the one-dimensional analysis.

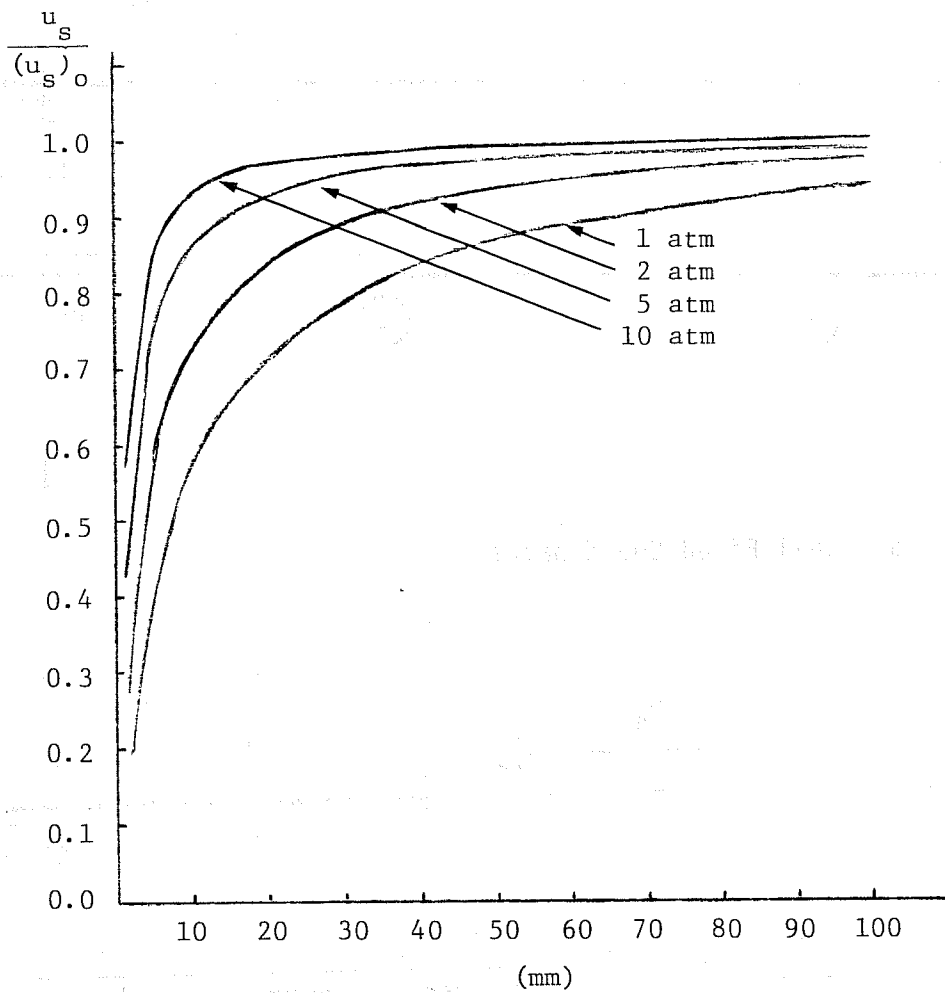


Fig. 65 Theoretical curve of  $u_s / (u_s)_0$  vs. sphere diameter and initial pressure of mixture.

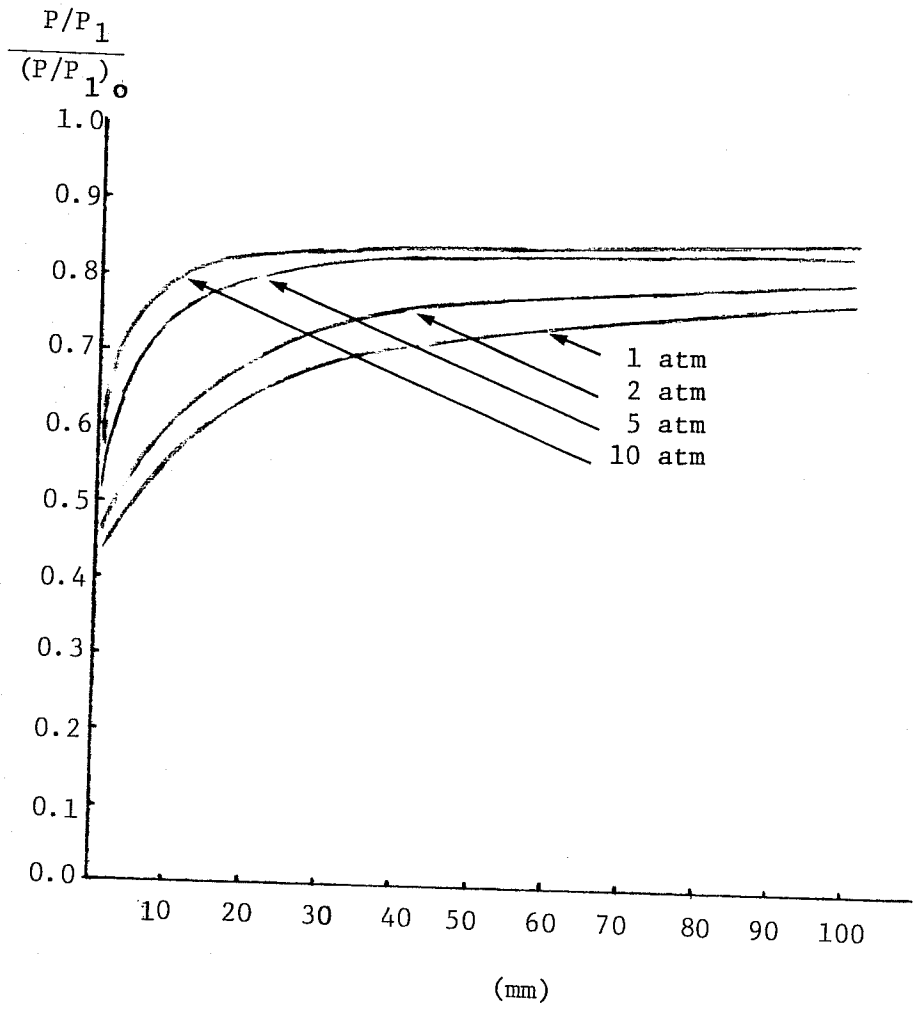


Fig. 66 Theoretical curve of  $p/p_1 / (p/p_1)_0$  vs. sphere diameter and initial pressure of mixture.

